CARBON DIOXIDE IN SYNTHETIC AND NATURAL SILICATE GLASSES

Thesis by

Gerald Jonathan Fine

In Partial Fulfillment of the Requirements

for the Degree of

Doctor of Philosophy

California Institute of Technology

Pasadena, California

1986

(Submitted November 15, 1985)

Acknowledgments

The research presented in this thesis was completed in collaboration with Professor Tom Tombrello, Dr. Marcus Mendenhall, Dr. Rogerio Livi, and Thomas Johnson. Their help is appreciated.

I have benefitted from the support and cooperation of many people while at Caltech. I am especially grateful to Roger Aines, Professor Art Boettcher of U.C.L.A., Professor Don Burnett, Phil Ihinger, Stephanie Mattson, Paula Rosener, Martin Ruzek, Henry Shaw, and Lynn Silver.

Professor George Rossman has been a continual source of both knowledge and advice. I sincerely thank him for his time and energies.

Finally, I thank my thesis advisor, Professor Edward Stolper, who has been a good advisor, a good teacher, and a good friend.

This research was supported by NSF grants EAR-8212765 and EAR-8417434.

Abstract

Infrared spectroscopy has been used to study the speciation of CO_2 in both synthetic silicate glasses quenched from melts held at high temperatures and pressures and in natural basaltic glasses. In glasses near the $NaAlO_2$-SiO_2 join, absorption bands resulting from the antisymmetric stretches of both molecular CO_2 (2352 cm^{-1}) and CO_3^{2-} (1610 cm^{-1} and 1375 cm^{-1}) are observed. The latter are attributed to distorted Na-carbonate ionic-complexes. Molar absorptivities for each of the absorption bands have been determined; these molar absorptivities allow the quantitative determination of species concentrations in sodium aluminosilicate glasses with a precision on the order of several percent of the amount present. The accuracy of the method is estimated to be ±15-20% at present.

The ratio of molecular CO_2 to CO_3^{2-} in sodium aluminosilicate glasses varies little for each silicate composition over the range of total dissolved CO_2 contents (0-1.5%), pressures (15-33 kbar) and temperatures (1400-1560°C) studied. This ratio is, however, a strong function of silicate composition, increasing both with decreasing Na_2O content along the $NaAlO_2$-SiO_2 join and with decreasing Na_2O content in peraluminous compositions off the join.

The molar absorptivities determined for sodium aluminosilicate glasses have also been used to measure the concentrations of CO_2 in albitic ($NaAlSi_3O_8$) glasses quenched from melts equilibrated with CO_2 vapor at high pressures (15-30 kbar) and temperatures (1450-1625°C). The results show that total CO_2 solubility increases with increasing pressure at constant temperature. Both molecular CO_2 and CO_3^{2-}

concentrations increase with pressure. At constant pressure, the solubility of molecular CO_2 decreases with temperature while the concentration of CO_3^{2-} increases. The net effect is that total CO_2 solubility is not significantly dependent on temperature, decreasing slightly with increasing temperature at constant pressure.

The speciation of CO_2 in both synthetic Ca ± Mg-composition glasses and natural basaltic glasses contrasts with the case of CO_2-bearing sodium aluminosilicate glasses. CO_2 is inferred to be dissolved in these glasses as distorted Ca- or Mg-carbonate ionic-complexes that result in unique infrared absorption bands at 1515 cm^{-1} and 1435 cm^{-1}. The molar absorptivities for each of these absorption bands were also determined. No detectable molecular CO_2 is dissolved in these glasses.

Infrared spectroscopic measurements of species concentrations in glasses provide insights into the molecular level processes accompanying CO_2 solution in melts and can be used to test and constrain thermodynamic models of CO_2-bearing melts. CO_2 speciation in silicate melts can be modelled by equilibria between molecular CO_2, CO_3^{2-}, and oxygen species in the melts. Consideration of the thermodynamics of such equilibria can account for the observed linear relationship between molecular CO_2 and carbonate concentrations in sodium aluminosilicate glasses, the absence of molecular CO_2 in Ca ± Mg silicate glasses, the proposed linear relationship between total dissolved CO_2 content and the activity of CO_2 in melts, and observed variations in CO_2 solubility in melts.

Dissolved CO_2 contents of natural basaltic glasses can also be determined from the intensities of the carbonate absorption bands at 1515 cm^{-1} and 1435 cm^{-1}. The uncertainty of the method is estimated to be ±15% of the amount present. The infrared technique is a powerful tool for the measurement of dissolved CO_2 contents in natural basaltic glasses since it is nondestructive, can be aimed at regions of glass a few tens of micrometers in size, and discriminates between dissolved carbonate and carbon present as carbonate alteration, contained in fluid inclusions or adsorbed on the glass.

A set of submarine basaltic glasses dredged from a variety of locations contain 0-400 ppm dissolved CO_2, measured using the infrared technique. These concentrations are lower than most previous reports for similar basaltic glasses. No general relationship is observed between dissolved CO_2 content and depth of magmatic eruption.

Preface

This thesis includes condensed versions of four published or soon-to-be published papers listed in the references: Fine and Stolper (1985ab) and Fine et al. (1985ab). Some revision or rewriting of each manuscript has occurred and new text has been added.

Table of Contents

Acknowledgments.....ii

Abstract.....iii

Preface.....vi

Introduction.....1

Chapter 1. The Speciation of Carbon Dioxide in Sodium Aluminosilicate Glasses.....6

Experimental Techniques.....7

Experimental Results.....17

Band Assignments.....17

Calibration of Band Intensities Versus Species Concentrations.....36

Precision and Accuracy.....42

Speciation of Carbon Dioxide in Sodium Aluminosilicate Glasses.....50

Discussion.....63

Comparison with Previous Spectroscopic Investigations.....63

Solubility Mechanisms of Carbon Dioxide in Sodium Aluminosilicate Melts.....69

Conclusions.....72

Chapter 2. The Solubility of Carbon Dioxide in Molten Albite.....74

Experimental Techniques.....76

Sample Synthesis.....76

Infrared Spectroscopy of CO_2-Saturated Glasses.....80

Results.....86

Comparison with Previous Results.....98

Conclusions.....99

Chapter 3. The Speciation of Carbon Dioxide in Ca ± Mg Silicate Glasses.....100

Synthesis of CO_2-Bearing Glass Standards.....101

Results.....109

Band Assignments and Intensities.....109

Band Intensity Calibrations.....125

Conclusions.....132

Chapter 4. Thermodynamic Considerations.....134

Speciation of CO_2 in Silicate Melts.....135

Solubility of CO_2 in Silicate Melts.....145

Water Versus CO_2 Speciation.....149

Conclusions.....151

Chapter 5. The Concentration of Carbon Dioxide in Natural Basaltic Glasses.....153

Results.....160

Conclusions.....172

Conclusions.....173

Appendix 1. Measurement of the Carbon Content of Silicate Glasses Using the $^{12}C(d,p_0)^{13}C$ Nuclear Reaction.....176

Experimental Procedure.....178

Results.....184

Conclusions.....193

References.....194

Introduction

Stimulated by the important role played by carbon dioxide in the petrogenesis of a wide range of igneous rocks, particularly alkaline basic magmas (e.g., Eggler, 1973; Wyllie, 1979), there has been considerable recent interest in the solubility mechanisms of CO_2 in silicate melts. Two contrasting approaches to understanding these solution mechanisms have been pursued. The first is an indirect approach that uses systematic variations in solid-liquid phase equilibria to infer structural changes that occur in melts when they dissolve CO_2. For example, the liquidus volume of pyroxene, a polymerized phase, enlarges relative to that of olivine, an unpolymerized phase, when CO_2 is added to melts. This has been used to infer that addition of CO_2 results in increased polymerization of melts (Eggler, 1974, 1978; Kushiro, 1975). Unfortunately, this intuitively satisfying line of reasoning has given, at best, only qualitative insights.

The second approach used to understand CO_2 solution mechanisms involves spectroscopic techniques. Both infrared (Mysen et al., 1975; Brey and Green, 1975, 1976; Mysen, 1976; Brey, 1976; Mysen et al., 1976; Eggler et al., 1979) and Raman (Verweij et al., 1977; Sharma, 1979; Sharma et al., 1979; Mysen and Virgo, 1980ab; Rai et al., 1983) spectroscopy have been used to study CO_2-bearing silicate glasses quenched from melts to elucidate aspects of the speciation of CO_2-bearing melts. These spectroscopic techniques can provide direct, quantitative information on how, at a molecular level, carbon dioxide is dissolved in silicate glasses and how it influences the structure of the silicate framework. In particular, infrared and Raman spectroscopy can

be used to distinguish between carbon dioxide that is dissolved as carbonate (CO_3^{2-}) ions and that which is dissolved as molecules of CO_2.

Dissolved molecular CO_2 and CO_3^{2-} each have unique infrared signatures, distinct from CO_2 contained in vesicles, carbonate occurring in any crystalline form, or other carbonaceous material. Infrared spectroscopy can thus discriminate between dissolved and extraneous forms of CO_2 and allow the accurate identification and measurement of the concentrations of dissolved species in both natural and synthetic glasses. Spectroscopy is also a non-destructive technique that does not require fusion of the glass being analyzed, eliminating the possibility of reactions between C species during heating. An infrared beam can be directed at spots as small as tens of microns, avoiding crystals and vesicles, and can be used to examine sample homogeneity. These qualities make infrared spectroscopy a potentially powerful tool for the investigation of dissolved CO_2 in natural and synthetic glasses.

Most recent spectroscopic investigations have not taken full advantage of the quantitative potential of either infrared or Raman spectroscopy. Most investigators have simply noted the existence of absorption or emission bands and thus of particular species in the glasses; the intensities of the bands have not generally been used to determine the concentrations of the absorbing or emitting species. Exceptions include the work of Verweij et al. (1977) in which the potential for using Raman spectroscopy to determine the concentrations of CO_3^{2-} groups in K_2O-SiO_2-CO_2 glasses was discussed and the work of Sharma and co-workers in which Raman spectroscopy was used to determine relative concentrations of CO_3^{2-} ions as a function of pressure and

temperature in glasses of sodium melilite, diopside, and akermanite composition (Sharma, 1979; Sharma et al., 1979). In addition, Mysen (1976) used infrared spectroscopy to estimate CO_3^{2-} concentrations in glasses on the $NaAlO_2$-SiO_2-CO_2 join. In that study, Mysen concluded that the relative proportions of molecular CO_2 groups and carbonate groups in CO_2-bearing glasses are strong functions of silicate composition and of the pressures and temperatures from which melts are quenched to glasses.

In this thesis, I report the results of experiments designed to develop more fully the potential of infrared spectroscopy for quantitative determinations of the concentrations of carbon-bearing species in silicate glasses. In Chapter 1, molar absorptivities (or extinction coefficients) are determined for absorption bands due to molecular CO_2 and carbonate in glasses near the $NaAlO_2$-SiO_2-CO_2 join. These molar absorptivities are used to measure the concentrations of molecular CO_2 and carbonate in sodium aluminosilicate glasses. Using this information, the dependence of the speciation of CO_2 on sodium aluminosilicate glass composition, on total dissolved CO_2 content, and on the pressure and temperature of equilibration of the melt from which the glass was quenched is investigated. In Chapter 2, infrared spectroscopy is used to determine the concentrations of total dissolved CO_2 in albitic ($NaAlSi_3O_8$) glasses quenched from melts equilibrated with CO_2 vapor at a variety of pressures and temperatures. In the next chapter, it is demonstrated that infrared spectroscopy is also a useful tool for the identification and measurement of dissolved CO_2 species in a variety of synthetic Ca ± Mg silicate glasses, including basaltic

compositions. I show that the speciation of CO_2 in these glasses is similar over a wide range of glass compositions, yet different from the speciation of CO_2 in $NaAlSi_2O_6$-SiO_2-CO_2 glasses.

Chapter 4 presents a simple thermodynamic treatment to guide thinking about the dependence of CO_2 speciation and solubility on melt composition. This treatment provides insights into the solubility mechanisms of CO_2 in silicate melts, into the thermodynamics of CO_2-bearing silicate melts, and into the effects of dissolved CO_2 on the phase equilibria of silicate melts.

Finally, in Chapter 5, the applicability of these results to the study of natural basaltic glasses is demonstrated and the concentration of total dissolved CO_2 in a variety of ocean floor basalts is measured.

Chapter 1. The Speciation of Carbon Dioxide in Sodium Aluminosilicate Glasses

The experiments described in this chapter were designed with three immediate goals: first, to develop infrared spectroscopy as a quantitative analytic tool for the measurement of the concentrations of CO_2 species in $NaAlSi_2O_6$-SiO_2-CO_2 glasses; second, to understand both the nature of CO_2 solution in fully or nearly-fully polymerized glasses and the effects of changing silicate composition on the speciation of CO_2; third, to establish a framework for the thermodynamic model of CO_2 solution discussed in Chapter 4.

Experimental Techniques

Powdered silicate starting materials were prepared at three compositions along the $NaAlO_2$-SiO_2 join: $NaAlSi_2O_6$ (jd), $NaAlSi_3O_8$ (ab) and $NaAlSi_4O_{10}$ (a composition close to the 1 atm. albite-silica eutectic designated as eu). Glasses of jd composition (batches jd-D and jd-E) were synthesized by grinding Na_2CO_3, Al_2O_3 and SiO_2 (Johnson-Matthey SpecPure reagents) in agate under ethanol for 6 hours followed by melting at 1580°C for 12 hours in air at 1 atm. Appropriate amounts of SiO_2 glass were then added to jd-E to prepare batches ab-E and eu-E. These decarbonated mixtures were ground under ethanol for 6 hours and dried at 850°C in air at 1 atm. for 2 days to remove any hydrocarbon residue or adsorbed CO_2. When mixtures not dried in this fashion were used as starting materials for high pressure experiments, CO_2 was detected spectroscopically in the run products even when no CO_2 was loaded into the charges. Drying times of more than 1 week resulted in significant Na-loss. Some Na-depleted compositions were used as

starting materials; these are designated jd-X, ab-X, and eu-X. All starting materials were stored over dessicant after drying.

Selected glasses of each composition were analyzed for major elements in order to verify glass homogeneity and to determine the extent of Na-loss during the drying process. Analyses were obtained using an automated MAC-5 electron microprobe with a 15 KV operating voltage, a sample current of 5 nA on brass and a 40-45 micron spot size (Table 1). The results of these analyses are shown graphically in Figure 1.

The starting materials were loaded along with known amounts of silver oxalate ($Ag_2C_2O_4$) into Pt capsules, which were then sealed by arc-welding. These Pt capsules were then loaded into larger Pt capsules containing a dry hematite-magnetite buffer or sintered hematite. The amounts of silver oxalate and silicate were weighed on a Cahn electrobalance to 0.0005 mg precision out of 0.0750-20.0000 mg total and were chosen to produce vapor-undersaturated melts. The silver oxalate was analyzed by gas manometry in the laboratory of Professor S. Epstein and found to be stoichiometric to within 5% of its nominal total CO_2 content. It was stored in a light-proof container over dessicant to minimize decomposition and H_2O-adsorption.

The double capsules were held at constant pressure (15-33 kbar) and temperature (1400-1560°C) in a 0.5 inch solid media piston-cylinder apparatus using a NaCl and pyrex cell. A hot piston-in technique was used: runs were brought cold to a pressure 5 kbar below the desired pressure, the temperature was raised to the final temperature and then the final pressure was applied. Temperature was monitored using W3%Re -

Table 1- Analyses of glass compositions used. Microprobe techniques are described within the text.

Starting Batch	jd ideal	jd-D	jd-E	jd-X	ab ideal	ab-E	ab-X	eu ideal	eu-E	eu-X
Na_2O	15.33	14.52	13.81	12.66	11.82	11.28	10.80	9.62	9.80	9.25
Al_2O_3	25.22	25.47	24.85	24.80	19.44	19.34	19.28	15.83	15.07	15.93
SiO_2	59.45	60.10	61.43	62.42	68.74	69.66	69.81	74.55	74.80	75.46
TOTAL	100.00	100.09	100.09	99.88	100.00	100.38	99.89	100.00	99.67	100.64
# of analyses		12	4	6		7	7		6	3

Figure 1- Graphical representation of the starting compostions used in this chapter. Ideal stoichiometric compositions are marked by X. The fields show the range of microprobe analyses, while the solid circles show the average of all analyses for each sample.

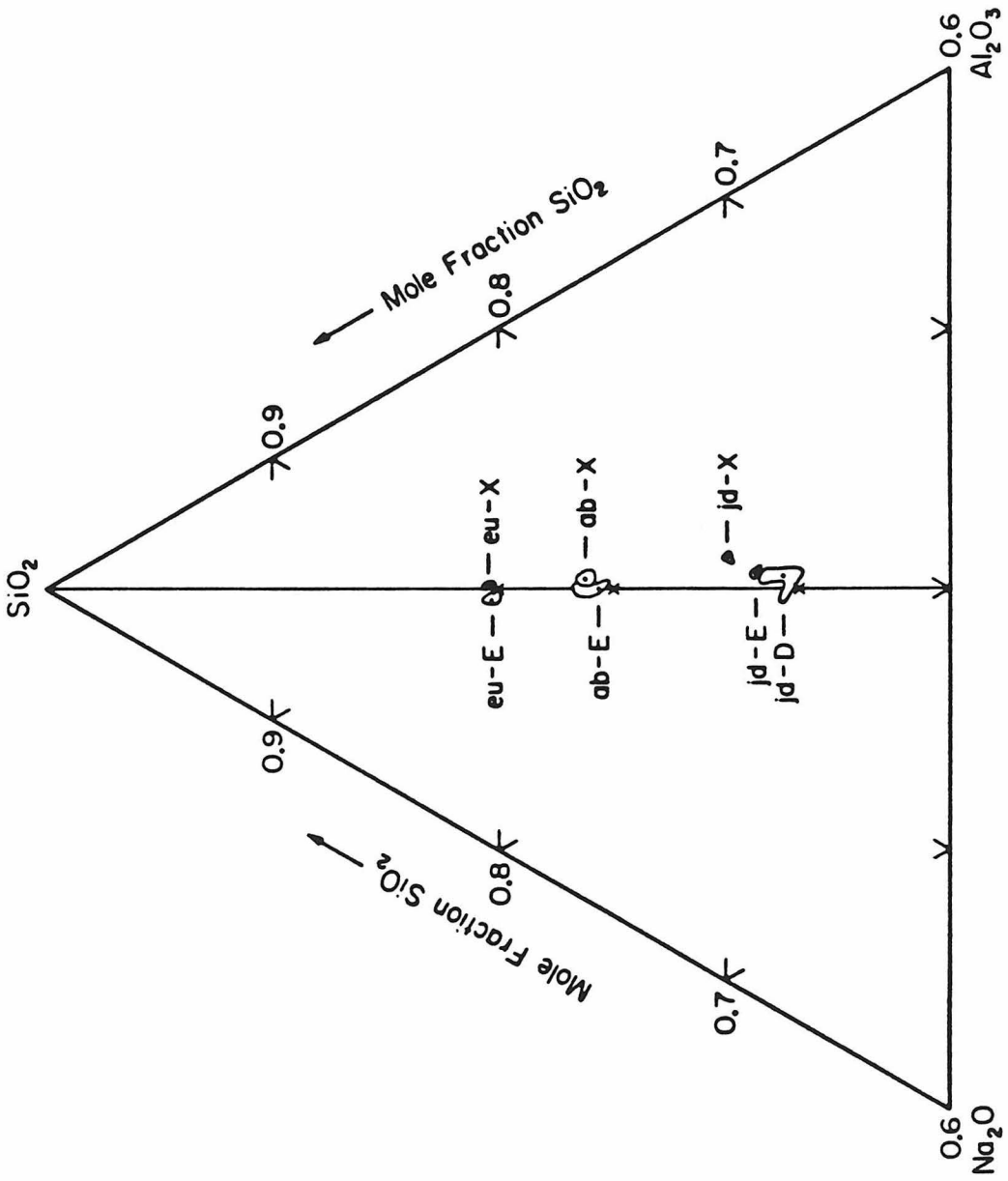
SiO2
0.6
Al2O3
0.6
Na2O
Mole Fraction SiO2
0.9
0.8
0.7
Mole Fraction SiO2
0.9
0.8
0.7
eu-E
eu-X
ab-E
ab-X
jd-E
jd-D
jd-X

W25%Re thermocouples. Pressure was calibrated against the reaction: ab = jd + qz at 29.5 kbar and 1100°C (Holland, 1980) and a -7% correction applied.

Upon heating, silver oxalate is presumed to decompose according to the reaction: $Ag_2C_2O_4 = 2Ag + 2CO_2$. This results in melts containing disseminated Ag and dissolved CO_2. Run times of 1 hour or more were needed to produce CO_2 homogeneity and uniform species concentrations in the glass run products. Runs were quenched by turning off the power to the furnace; quench rates were 150-200°C/sec. At the end of most runs, the contents of the outer capsule were examined and both hematite and magnetite found to be present. CO_2-free glasses of each composition were synthesized at high pressures by running both unwelded and welded silver oxalate-free inner capsules. Infrared spectra of these glasses did not differ from the infrared spectra of glasses of the same compositions prepared at 1 atm. in air.

After quenching, the inner capsules were sectioned and doubly-polished plates of the glasses were prepared. In most samples disseminated Ag metal gave the glass in the bottom of the capsule an orange color or blueish-orange streaked appearance. The thickness of each glass plate was measured using a micrometer or dial indicator. The plates were then placed over metal apertures 150-1000 microns in diameter and their transmission infrared spectra were obtained. Spectra discussed in this chapter were gathered on a Perkin-Elmer 180 infrared spectrophotometer in the linear absorbance mode (base ten logarithm) over the frequency range 4000 cm^{-1} to 1200 cm^{-1}. The sample chamber was purged with high purity N_2 while each spectrum was recorded. Spectra

were recorded on chart paper and digitized with a Tektronix 4052 computer. The spectra of anhydrous, decarbonated glasses of each composition were then computer-subtracted from these spectra. Both absorption intensities and integrated absorption intensities were determined from the background-subtracted digital data. The precision of absorbance data obtained from the PE 180 is estimated to be about 0.01 (1σ) at an absorbance of 0.5 (Stolper, 1982a).

Many of the glasses synthesized early in this study were not suitable for calibration of absorption band intensities versus species concentration because the final step in the drying procedure was not performed and the glasses were dark, presumably containing either graphite or a hydrocarbon residue. In these instances, total dissolved carbon contents were presumed not to be accurately known. The infrared spectra of all these glasses were still taken and data obtained from these samples, discussed below, were still useful.

After infrared spectra were taken, some sodium aluminosilicate glasses were independently analyzed for total carbon using the $^{12}C(d,p_0)^{13}C$ nuclear reaction. This technique, used by Filleux et al. (1977), Oberheuser et al. (1983), and Mathez et al. (1984), is discussed more fully in Appendix 1. It allowed the independent determination of total C contents (within 5% relative certainty) of the same pieces of glass on which spectra were taken. These analyses show that after 1 hour long runs, the amount of C analyzed after the run was generally within 10% of the amount loaded into the capsule (Table 2).

Two glasses compositionally off the $NaAlSi_2O_6$-SiO_2 join were also used in this study. The first,a 56% Na_2O, 43% SiO_2 (wt.%) glass was

Table 2- Comparison of wt. % CO_2 loaded into Pt capsules containing sodium aluminosilicate glass with total carbon (reported as wt.% CO_2) analyzed using the $^{12}C(d,p_0)^{13}C$ nuclear reaction. Run conditions are given in Appendix 1.

Sample #	CO_2 Loaded (wt. %)	CO_2 Analyzed (wt. %)
ABC-53	0.67	0.69
ABC-54	0.38	0.32
ABC-55	0.20	0.19
ABC-58	0.40	0.36
ABC-62	0.94	0.88
ABC-63	0.00	0.07
ABC-64	0.75	0.77
JDC-111	0.17	0.20
JDC-112	0.54	0.55
JDC-116	0.56	0.55
NC-15	0.55	0.52
NC-17	0.25	0.28
NC-19	0.43	0.47

equilibrated with CO_2 vapor at 1 atm., 1100°C for 24 hours. The second, a 30% Na_2O, 10% Al_2O_3, 60% SiO_2 glass was equilibrated with 0.31 wt.% CO_2 at 1450°C, 25 kbar for 1 hour.

A few glasses were prepared using starting materials consisting of CO_2-free glass and Na_2CO_3 enriched with 90% ^{13}C as a CO_2 source rather than $Ag_2C_2O_4$. These glasses were enriched in Na and compositionally not on the $NaAlO_2$-SiO_2 join. CO_2-bearing ab and jd glasses prepared in the laboratory of Professor A. Boettcher were also used in the study. They were prepared using Na_2CO_3 or $Ag_2C_2O_4$ as CO_2 sources and were run at a variety of pressures and temperatures.

Densities used in this study were estimated from the data of Kushiro (1978); the presence of disseminated Ag or bubbles (Chapter 2) in the run products precluded direct density measurements of most glasses. It is assumed that the effect of dissolved CO_2 on glass density is not significant.

Experimental Results

Band Assignments

The spectra of a CO_2-free and a CO_2-bearing jadeite glass are shown in Figure 2. Four strong absorption bands are present in the CO_2-bearing glass at frequencies of higher than 1200 cm^{-1} that are not present in the CO_2-free glass. Although their relative intensities vary with CO_2 content and glass composition (Figures 3, 4, and 5 and Table 3) the locations of these four bands are essentially identical in all of the CO_2-bearing $NaAlO_2$-SiO_2 glasses examined. At wavenumbers lower than

Figure 2- Infrared spectrum (solid line) of a jadeite glass (JDC-84) containing 0.80 wt. % total dissolved CO_2 as measured by infrared spectroscopy. Band assignments are given. The dashed line is the spectrum of a CO_2-free jadeite glass synthesized at 1 atm. The silicate background has not been subtracted from either spectrum, hence the spectra go offscale at approximately 1200 cm^{-1} due to aluminosilicate vibrations.

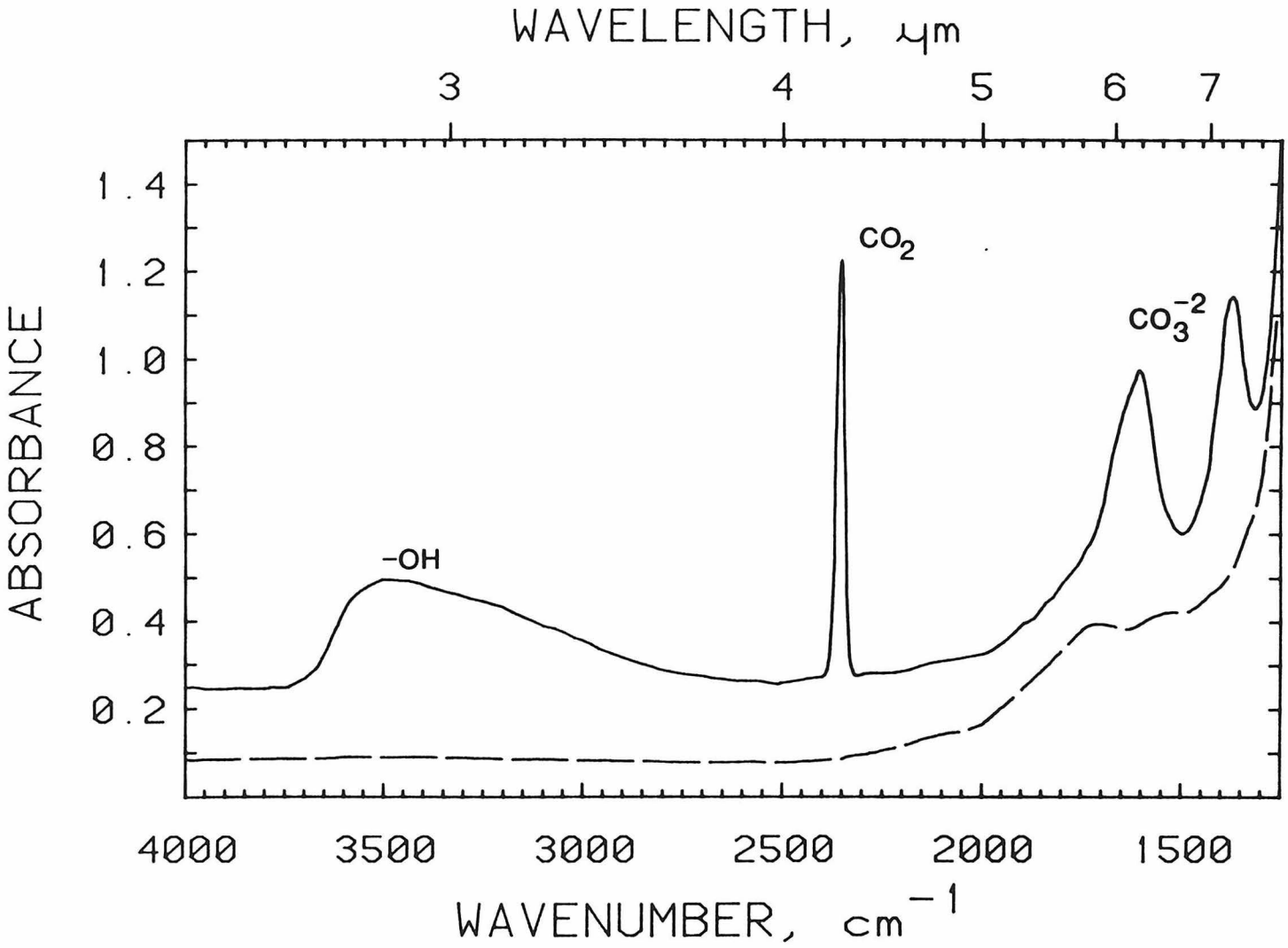
WAVELENGTH, μm
3
4
5
6
7
ABSORBANCE
1.4
1.2
1.0
0.8
0.6
0.4
0.2
CO_2
CO_3^{-2}
-OH
4000
3500
3000
2500
2000
1500
WAVENUMBER, cm^{-1}

Figure 3- Background subtracted spectra, from 2500 - 2200 cm^{-1} and all normalized to 100 microns sample thickness, of four jadeite composition glasses containing variable amounts of total dissolved CO_2. Sample numbers and total dissolved CO_2 contents are shown. The band at 2352 cm^{-1} increases in a regular fashion with increasing total dissolved CO_2.

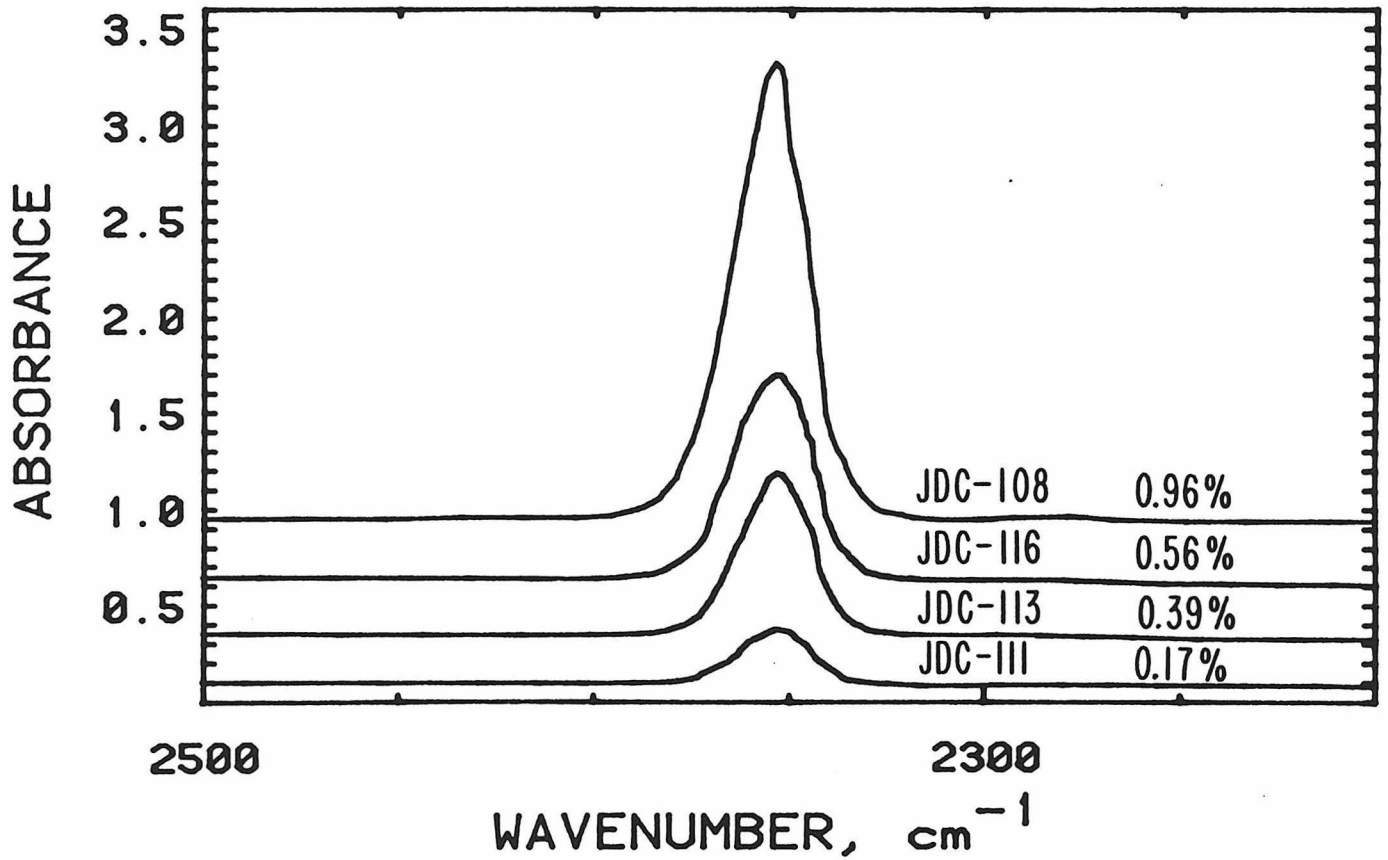
ABSORBANCE
3.5
3.0
2.5
2.0
1.5
1.0
0.5
JDC-108 0.96%
JDC-116 0.56%
JDC-113 0.39%
JDC-111 0.17%
2500
2300
WAVENUMBER, cm-1

Figure 4- Background subtracted spectra, from 1800 - 1200 cm^{-1} and normalized to sample thicknesses of 100 microns, of the same jadeite glasses shown in Figure 3. Sample numbers and total dissolved CO_2 contents are shown. The bands at both 1610 and 1375 cm^{-1} increase with increasing total dissolved CO_2, yet their intensities are always approximately equal (1.17 $absorbance_{1610}$ = $absorbance_{1375}$).

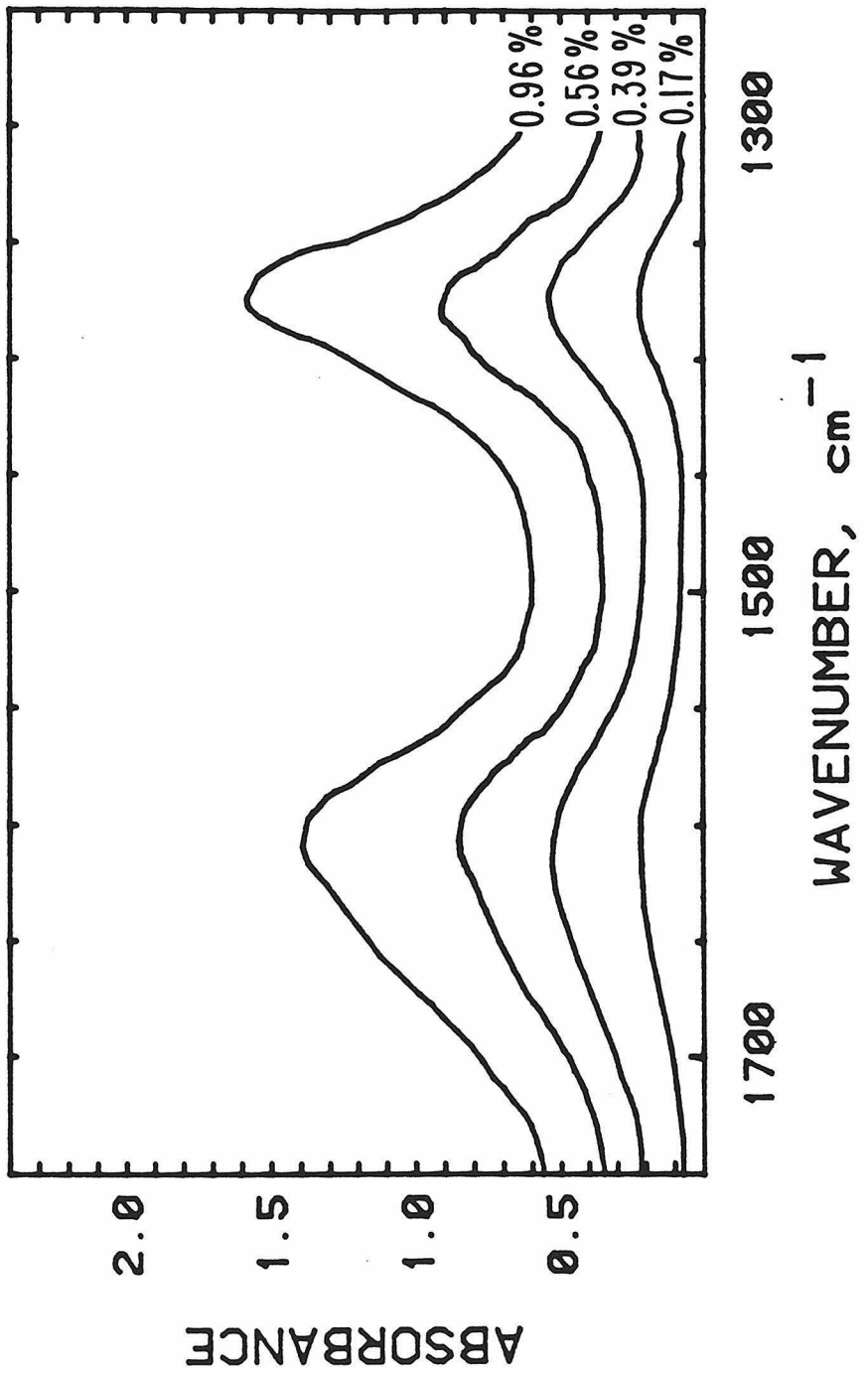
0.96 %
0.56 %
0.39 %
0.17 %
2.0
1.5
1.0
0.5
ABSORBANCE
1700
1500
1300
WAVENUMBER, cm^{-1}

Figure 5- Background subtracted spectra, from 2600 to 1200 cm^{-1}, of CO_2-bearing silicate glasses of four different compositions, jd-E, ab-E, eu-E, and eu-X. All of the spectra are normalized to constant intensity of the 2352 cm^{-1} band. The intensities of the carbonate absorption bands increase with increasing Na content and decreasing silica content. (Samples shown are NC-10, NC-19, ABC-53, and JDC-108.)

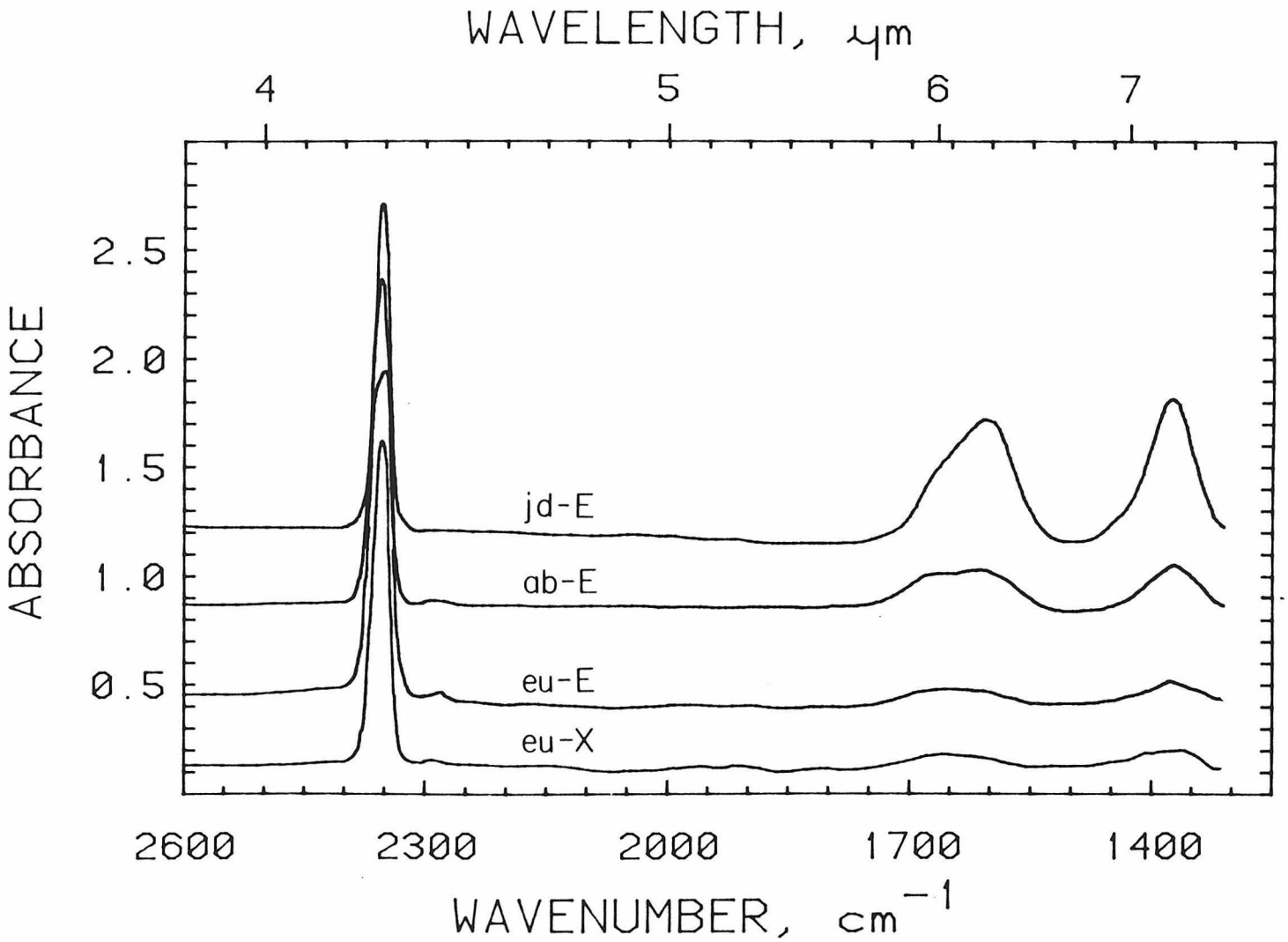
WAVELENGTH, μm
4
5
6
7
ABSORBANCE
2.5
2.0
1.5
1.0
0.5
jd-E
ab-E
eu-E
eu-X
2600
2300
2000
1700
1400
WAVENUMBER, cm⁻¹

Table 3- Data obtained for Chapter 1.

Sample	#	Starting Comp.	P (kbar)	T (°C)	duration (min.)	CO_2 Loaded (wt. %)	H_2O[a] (wt. %)	Density[b] (g/l)	Thickness (cm)	Band Location	Abs.	Integr. Abs.	Band Location	Abs.	Integr. Abs.	Band Location	Abs.	Integr. Abs.
NC	2	eu-E	25	1450	30	1.81 [c]	0.37	2440	0.0055	2350	1.80	67.96	1657	0.09	11.17	1379	0.11	6.60
NC	3	eu-E	25	1450	60	1.35 [c]	0.41	2440	0.0043	2353	0.11	4.19	1650	0.01	1.44	1424	0.02	2.41
NC	4	eu-E	25	1450	60	0.45 [c]	0.29	2440	0.0058	2353	0.88	24.84	1656	0.04	4.02	1358	0.04	4.42
NC	6	eu-E	25	1450	60	0.90 [c]	0.42	2440	0.0063	2355	0.96	35.03	1650	0.07	8.26	1361	0.08	7.55
NC	7	eu-E	25	1450	60	0.60 [c]	0.26	2440	0.0067	2352	1.06	30.92	1660	0.05	5.00	1407	0.07	7.00
NC	10	eu-E	25	1450	67	1.25 [c]	0.39	2440	0.0043	2353	1.30	38.01	1652	0.06	6.93	1370	0.05	5.06
NC	13	eu-X	25	1450	60	0.00	0.14	2440	0.0167	2354	0.19	4.11	d			d		
NC	15	eu-X	25	1450	60	0.55	0.24	2440	0.0074	2354	1.33	38.18	d			d		
NC	17	eu-X	25	1450	60	0.25	0.18	2440	0.0083	2353	1.08	29.58	d			d		
NC	19	eu-X	25	1450	60	0.43	0.27	2440	0.0044	2355	1.04	27.79	d			d		
NC	20	eu-X	25	1450	60	0.20	0.38	2440	0.0073	2354	0.85	22.28	d			d		
NC	21	eu-X	25	1450	60	0.36	0.39	2440	0.0075	2353	1.46	38.92	d			d		
ABC	14	ab-E	25	1450	30	c	0.10	2530	0.0200	2355	0.03	0.14	d			d		
ABC	22	ab-E	25	1450	60	0.65 [c]	0.21	2530	0.0060	2356	1.38	44.70	1620	0.14	17.98	1383	0.16	10.90
ABC	23	ab-E	33	1450	60	1.83 [c]	0.65	2530	0.0026	2354	1.29	37.18	1614	0.16	21.22	1372	0.16	11.57
ABC	24	ab-E	33	1450	60	0.52 [c]	0.22	2530	0.0056	2355	0.72	21.18	1620	0.09	11.70	1372	0.12	8.58
ABC	25	ab-E	33	1450	60	1.03 [c]	0.39	2530	0.0037	2355	1.17	36.34	1618	0.15	20.13	1377	0.17	11.27
ABC	27	ab-E	27	1450	60	0.64 [c]	0.39	2530	0.0046	2353	0.41	10.63	1619	0.05	6.16	1373	0.05	3.83
ABC	29	ab-E	15	1450	60	1.02 [c]	0.86	2440	0.0030	2354	0.38	8.72	1606	0.05	5.30	1377	0.03	1.80
ABC	30	ab-E	15	1450	60	0.78 [c]	0.49	2440	0.0036	2352	0.41	11.17	1611	0.04	4.15	1382	0.05	4.13
ABC	33	ab-E	25	1560	30	0.65 [c]	0.27	2530	0.0046	2354	0.78	21.97	1618	0.06	7.54	1374	0.09	6.92
ABC	35	ab-E	25	1560	30	0.44 [c]	0.21	2530	0.0067	2354	0.83	23.17	1622	0.07	8.59	1376	0.13	11.41
ABC	53	ab-E	25	1450	60	0.67	0.14	2510	0.0045	2353	1.43	36.60	1625	0.07	9.29	1374	0.13	10.36
ABC	54	ab-X	20	1450	60	0.38	0.16	2510	0.0055	2353	0.75	18.91	1626	0.04	4.42	1377	0.07	5.27
ABC	55	ab-X	20	1450	60	0.20	0.16	2510	0.0081	2353	0.48	11.63	1622	0.02	2.41	1380	0.10	9.62
ABC	56	ab-X	20	1450	60	0.49	0.30	2510	0.0051	2356	1.06	28.33	1619	0.04	3.87	1378	0.06	5.28
ABC	57	ab-X	20	1450	60	0.97	0.29	2510	0.0040	2354	0.97	25.21	1663	0.06	7.85	1384	0.09	6.87
ABC	58	ab-X	20	1450	60	0.40	0.18	2510	0.0070	2352	1.07	28.46	1610	0.06	8.94	1374	0.09	6.83
ABC	62	ab-X	20	1450	60	0.94 [e]	0.35	2510	0.0036	2353	1.37	36.49	1606	0.08	10.50	1375	0.10	6.51
ABC	64	ab-X	20	1450	60	0.75	0.15	2510	0.0058	2352	1.85	49.55	1616	0.13	19.18	1379	0.17	11.22
JDC	67	jd-D	25	1400	30	0.99 [c]	0.26	2600	0.0053	2353	0.76	19.52	1605	0.24	27.92	1377	0.27	20.05
JDC	68	jd-D	25	1400	30	0.58 [c]	0.39	2600	0.0073	2353	0.57	13.56	1605	0.29	30.00	1378	0.32	22.54
JDC	69	jd-D	25	1400	30	1.64 [c]	0.42	2600	0.0033	2353	0.86	20.92	1607	0.32	35.38	1375	0.35	24.39
JDC	72	jd-D	25	1400	30	0.33 [c]	0.37	2600	0.0080	2353	0.44	9.61	1604	0.21	21.68	1378	0.24	16.60
JDC	73	jd-D	25	1400	30	0.26 [c]	0.50	2600	0.0062	2352	0.34	8.10	1603	0.21	21.22	1388	0.24	17.40
JDC	74	jd-D	25	1400	30	0.13 [c]	0.60	2600	0.0071	2353	0.26	7.16	1606	0.15	16.35	1384	0.19	14.36

Sample	#	Starting Comp.	P (kbar)	T (°C)	duration (min.)	CO_2 Loaded (wt. %)	H_2O[a] (wt. %)	Density[b] (g/l)	Thickness (cm)	Band Location	Abs.	Integr. Abs.	Band Location	Abs.	Integr. Abs.	Band Location	Abs.	Integr. Abs.
JDC	76	jd-D	25	1400	30	0.00 [c]	0.65	2600	0.0049	2352	0.23	4.66	1643	0.05	4.83	1397	0.12	7.83
JDC	84	jd-D	25	1450	30	1.56 [c]	0.35	2600	0.0044	2352	0.71	19.64	1611	0.30	33.56	1380	0.31	23.28
JDC	85	jd-D	25	1450	30	0.34 [c]	0.24	2600	0.0089	2352	0.31	10.13	1612	0.18	18.95	1378	0.17	11.54
JDC	86	jd-D	25	1450	30	1.11 [c]	0.30	2600	0.0055	2353	0.79	22.07	1610	0.36	38.19	1382	0.38	26.28
JDC	89	jd-D	25	1450	30	0.72 [c]	0.32	2600	0.0027	2355	0.38	10.64	1612	0.18	21.49	1376	0.18	13.87
JDC	90	jd-D	25	1450	30	1.21 [c]	0.33	2600	0.0052	2353	0.66	16.76	1613	0.28	31.42	1381	0.26	20.26
JDC	91	jd-D	25	1450	30	0.12 [c]	0.30	2600	0.0041	2348	0.05	1.80	1625	0.04	5.05	1378	0.04	2.70
JDC	103	jd-X	25	1450	60	0.33	0.28	2600	0.0066	2353	0.65	17.62	1623	0.08	8.57	1383	0.05	2.79
JDC	108	jd-E	25	1450	60	0.96	0.13	2600	0.0041	2354	0.98	24.81	1609	0.33	37.52	1374	0.39	27.99
JDC	110	jd-E	25	1450	60	0.00	0.11	2600	0.0104	[d]			[d]			[d]		
JDC	111	jd-E	25	1450	60	0.17	0.12	2600	0.0115	2354	0.34	9.16	1607	0.16	19.44	1378	0.17	10.45
JDC	112	jd-E	25	1450	60	0.54	0.14	2600	0.0139	2354	1.23	36.61	1603	0.60	69.58	1380	0.64	43.98
JDC	113	jd-E	25	1450	60	0.39	0.18	2600	0.0059	2353	0.51	12.90	1617	0.19	21.71	1372	0.19	12.94
JDC	114	jd-E	25	1450	60	0.66	0.16	2600	0.0072	2354	0.46	11.47	1622	0.20	25.60	1371	0.25	18.58
JDC	116	jd-E	25	1450	60	0.56	0.12	2600	0.0109	2353	1.17	33.11	1607	0.54	61.82	1380	0.60	42.42
BOET2582 [f]		jd	20	1450	15	SAT. [g]	0.43	2600	0.0018	2354	0.63	14.05	1595	0.33	36.05	1379	0.32	20.95
BOET2990 [f]		ab	20	1450	360	1.00 [h]	0.49	2510	0.0053	2354	1.12	28.76	1631	0.08	12.57	1363	0.09	6.42
BOET2995 [f]		ab	20	1450	60	1.00	0.20	2510	0.0032	2355	1.22	35.21	1612	0.08	10.61	1369	0.09	6.11

[a] H_2O contents determined using the method of Stolper (1982a) and an extinction coefficient of 80 liters/mole-cm.
[b] Densities either obtained or extrapolated from Kushiro (1978).
[c] Glasses were dark, presumably containing graphite and other reduced carbon species, so that total CO_2 contents are unknown.
[d] Band intensity too low to characterize.
[e] Glass contains a few small bubbles.
[f] Samples provided by Professor A. Boettcher.
[g] Vapor saturated, Na_2CO_3 used as a CO_2 source rather than $Ag_2C_2O_4$.
[h] Total loaded CO_2 content believed unknown due to long run length (see text).

1200 cm^{-1}, the vibrations of the aluminosilicate networks comprising these glasses result in absorption bands that go offscale.

The broad band at approximately 3550 cm^{-1} is due to the stretching of -OH groups (Stolper, 1982a) and was used to quantitatively measure the amount of H_2O dissolved in each sodium aluminosilicate glass using a molar absorptivity of 80 liters/mole-cm. Water contents of the CO_2-bearing glasses quenched from melts at high pressure typically range from 0.2 wt. % to 0.5 wt. % H_2O. These levels of dissolved water are believed unavoidable in experiments of this type, independent of drying procedure or the use of a double-capsule, buffered assembly. Water concentrations are higher in CO_2-bearing glasses than in those without CO_2. This suggests that adsorbed H_2O on the silver oxalate and/or hydrogen that diffuses through both the buffer and Pt capsule wall and reacts with CO_2 to produce H_2O and reduced carbon species during the experiments are responsible for most of the water in these nominally anhydrous runs. Absorptions due to dissolved hydrocarbons or CO were not observed in any spectra. If reduced carbon is produced by reaction of hydrogen and dissolved CO_2 in the experiments, it is either not detectable via infrared spectroscopy (e.g., graphite) or diffuses out of the Pt capsules (Watson et al., 1982).

Preliminary experiments conducted in our laboratory and in the laboratory of Professor Boettcher have indicated that run lengths of 3 or more hours are necessary to result in significant depletions in spectroscopically measured total dissolved CO_2. If substantial carbon is lost or substantial reduced carbon is produced in shorter runs, it could modify some of the conclusions presented here. However, graphite is not

observed in the run products and both the hydration of the glasses and obvious depletions of the glasses in spectroscopically observable carbon have been minimized by run lengths of only 1 hour. It is emphasized that despite the most rigorous precautions, water seems to be unavoidable in these piston-cylinder experiments. In fact, water contents seem to be largely independent of drying procedures and even the experiments conducted by Professor Boettcher using special precautions to ensure dry conditions (Boettcher et al., 1981) contain dissolved water. Even C-free runs contain water. The only consolation is that our laboratory is able to precisely measure water concentrations.

The sharp band at 2352 cm^{-1} is attributed to the ν_3 antisymmetric stretch of molecular $^{12}CO_2$ (Mysen et al., 1975; Mysen et al., 1976; Mysen, 1976; Brey, 1976). For several reasons it appears that this molecular CO_2 is homogeneously dissolved at molecular scale, probably as weakly bound units located in holes or cages in the overall melt structure, rather than present as trapped fluid inclusions. The intensity of this band increases in a regular fashion with increasing total CO_2 content (Figure 3). Most glasses are bubble free when viewed at high power (500X) with an optical microscope and their total dissolved CO_2 contents are generally much lower than published CO_2 solubilities (Mysen, 1976). Finally, the location of the band is slightly shifted from that of gaseous CO_2 at 2349 cm^{-1} (Nakamoto, 1978). When bubbled glasses are intentionally prepared and run, a double band suggestive of both gaseous CO_2 in bubbles and dissolved CO_2

is observed. Other arguments suggesting structurally bound CO_2, including SEM observations, are presented by Mysen et al. (1976).

The ν_3 antisymmetric stretch of a free, undistorted carbonate group (D_{3h} symmetry) results in a degenerate absorption band at ~1415 cm^{-1}. Distortion of the CO_3^{2-} group (to C_{2v} on C_s symmetry) results in a loss of the degeneracy and the appearance of two bands (White, 1974; Nakamoto, 1978). Following Brey and Green (1975), the broad bands at 1610 cm^{-1} and 1375 cm^{-1} are attributed to the ν_3 stretch of distorted carbonate groups. Sharma (1979), Sharma et al. (1979), and Mysen and Virgo (1980a) assigned analogous bands in other glass compositions the same way.

The constancy of the splitting of the ν_3 mode (~235 cm^{-1}) of carbonate ions in the glasses studied suggests that the local environment of the carbonate group does not vary much over the range of Na_2O, Al_2O_3, SiO_2, and CO_2 contents of the glasses. The degree of splitting observed is much larger than that generally caused by symmetry lowering in crystalline carbonates (White, 1974), but Nakamoto (1978) notes that either a unidentate (C_s) or bidentate (C_{2v}) carbonate complex (a carbonate ion coordinated to a metal atom) could have approximately the required splitting. The details of the observed splitting presumably provide important information on the local environment of CO_3^{2-} ions in the glasses, but I am unable to completely decipher these details at this time. Nevertheless, the large splitting is consistent with previous suggestions that carbonate ions are coordinated with sodium atoms in sodium aluminosilicate glasses (Mysen and Virgo, 1980b). That the local carbonate environment is almost certainly

dependent upon, if not dominated by, the charge-balancing or network modifying cations of the melt (Holloway et al., 1976) is confirmed by the fact that the ν_3 bands of CO_3^{2-} groups in a wide range of CO_2-bearing glasses with dominantly divalent network modifying cations, including basaltic glasses, glasses in the system $CaO-Al_2O_3-SiO_2$, and diopside and akermanite glasses (Rai et al., 1983; Sharma, 1979; and Sharma et al., 1979; Chapter 3) are split almost identically, but quite differently from the Na-bearing aluminosilicate glasses.

Although it is suggested that carbonate is present in the glasses as distorted sodium carbonate ionic-complexes, aluminum probably plays an important role in the local environment of carbonate groups. This is suggested by the fact that the ν_3 carbonate bands of the Al-poor $Na_2O-Al_2O_3-SiO_2$ and Na_2O-SiO_2 glasses examined are, as in crystalline Na_2CO_3, not split to the extent observed in this study, if at all. One extremely intense band attributed to dissolved CO_3^{2-} is observed at ~1400 cm^{-1} in the spectra of these glasses. The precise nature of the interaction between aluminum and sodium in the distortion of carbonate complexes and in influencing the relative proportions of molecular CO_2 and carbonate in our glasses cannot be addressed with these results and will require study of a wider range of silicate compositions on the $Na_2O-Al_2O_3-SiO_2-CO_2$ join.

Other interpretations of the bands at 1610 cm^{-1} and 1375 cm^{-1} can be found in the literature. Often, the high energy band has either not been recognized or not assigned to any C-bearing species (Mysen et al., 1975; Mysen, 1976; Mysen et al., 1976). Mysen (1976) and Mysen et al. (1976) also suggest that in some instances, these bands may be due to

HCO_3^-. Rai et al. (1983) conclude that the analogous doublet in CO_2-bearing diopside glass is due to two distinct carbonate sites in the glass. None of these suggestions can be readily reconciled with the observations that although the intensities of both bands increase with increasing total dissolved CO_2 (Figure 4), their intensities are approximately equal to each other (1.17 $absorbance_{1610}$ = $absorbance_{1375}$) regardless of total dissolved CO_2 content, silicate composition, or total dissolved H_2O (Figure 6). It is also noted that the doublets in the diopsidic glasses of Rai et al. (1983), in the akermanite glasses of Sharma et al. (1979), and in basaltic glasses and glasses in the system $CaO-Al_2O_3-SiO_2-CO_2$ (Chapter 3) mimic to within a few wavenumbers the splitting observed in the infrared spectrum of distorted CO_3^{2-} groups in scapolite. Scapolite contains only a single carbonate site (Papike and Stephenson, 1966; Chamberlain et al., 1985), rather than two carbonate sites or HCO_3^- groups.

Table 3 presents the quantitative results obtained during this study, including the run conditions of all syntheses, the exact locations, intensities and integrated intensities of all of the aforementioned absorption bands, and the thickness and density of each sample studied.

Three other bands of low intensity were also observed during the course of this study. The band at 1610 cm^{-1} is distorted due to the presence of an unassigned, broad, low intensity absorption band centered at ~1680 cm^{-1}. Another band, at approximately 3710 cm^{-1}, appears to vary directly with the intensity of the 2352 cm^{-1} band. It is tentatively attributed to a combination of the ν_1 (Raman active only) +

Figure 6- Intensity of the carbonate absorption band at 1375 cm^{-1} versus the intensity of the carbonate absorption band at 1610 cm^{-1}, both normalized to 100 micron sample thickness, for all of the samples studied. The silicate composition of each glass is indicated. The intensities of both bands are approximately equal (1.17 $absorbance_{1610}$ = $absorbance_{1375}$) regardless of silicate composition, total CO_2 concentration, dissolved H_2O content, or the pressure and temperature from where the glass was quenched.

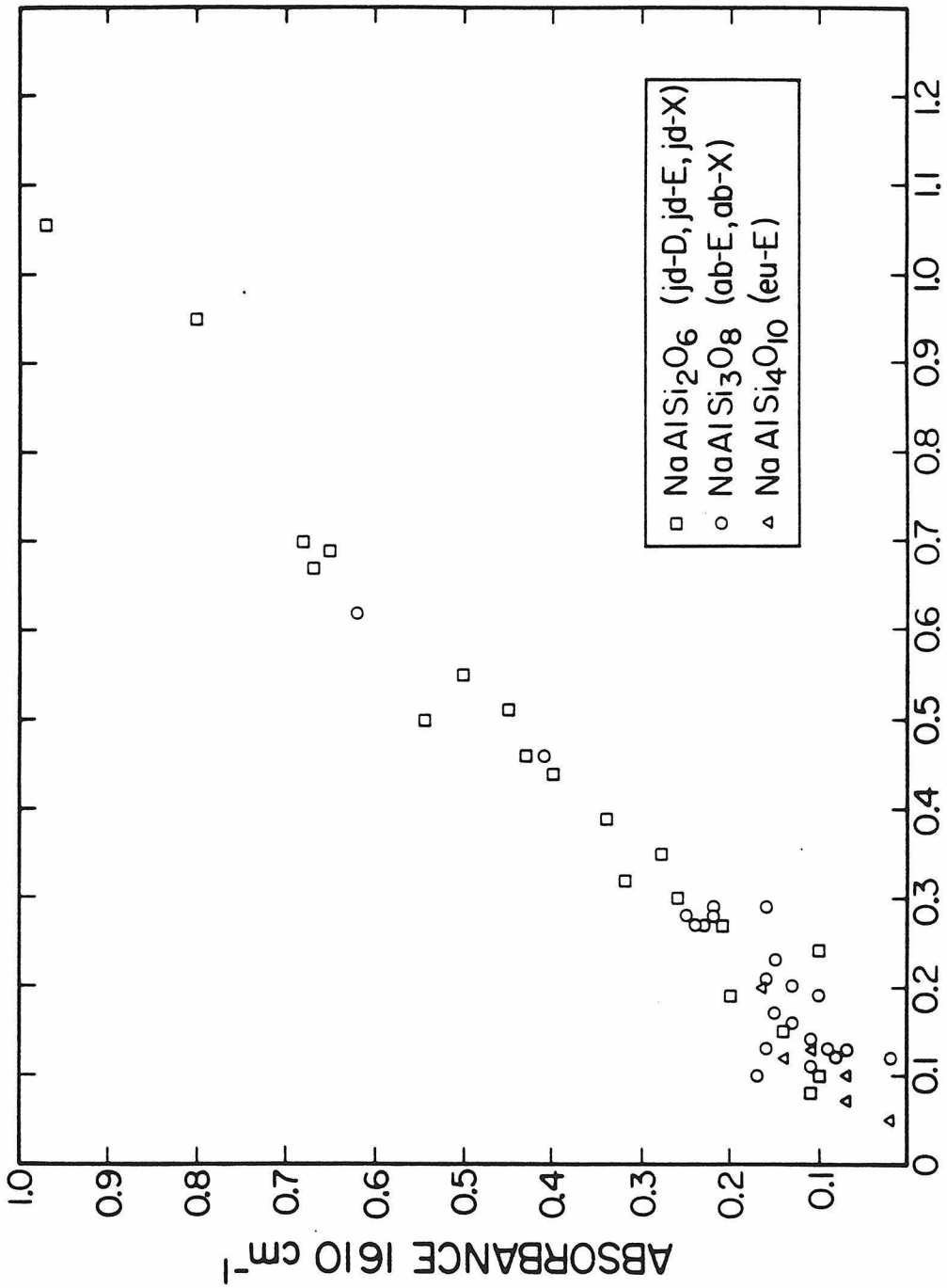
ABSORBANCE 1610 cm⁻¹
ABSORBANCE 1375 cm⁻¹
0
0.1
0.2
0.3
0.4
0.5
0.6
0.7
0.8
0.9
1.0
1.1
1.2
NaAlSi2O6 (jd-D, jd-E, jd-X)
NaAlSi3O8 (ab-E, ab-X)
NaAlSi4O10 (eu-E)

ν_3 modes of molecular CO_2. The intensity of a small band at 2287 cm^{-1} also varies directly with the intensity of the 2352 cm^{-1} band. This band is assigned to the ν_3 antisymmetric stretch of molecular $^{13}CO_2$. Both of these bands are used in Chapter 2 for the determination of molecular CO_2 concentrations in glasses enriched in this component.

All of the band assignments attributed to C-bearing species are consistent with the spectra of $^{13}CO_2$-enriched glasses (Figure 7). The band at 2352 cm^{-1} is offset to 2287 cm^{-1} as expected (Nakamoto, 1978, p. 116), and the bands at 1610 cm^{-1} and 1375 cm^{-1} are lowered in frequency 50 cm^{-1} and 35 cm^{-1} respectively. The unassigned band at 1680 cm^{-1} is also offset ~50 cm^{-1}, indicating that it too is due to a C-bearing species.

Calibration of Band Intensities Versus Species Concentrations

The Beer-Lambert law expresses the relationship between absorption band intensity and the concentration of either CO_2 or CO_3^{2-}:

$$C = \frac{44.01 \text{ x absorbance}}{d \text{ x } \rho} \text{ x } \frac{1}{\varepsilon} \quad , \qquad (1)$$

where C is the weight fraction of either CO_2 or CO_3^{2-} (expressed as a weight fraction of CO_2), 44.01 is the molecular weight of CO_2 in g/mole, absorbance (base ten logarithm) is expressed in absorbance units, d is the sample thickness in cm, ρ is the sample density in g/liter, and ε is the molar absorptivity (or extinction coefficient) in liters/mole-cm. If integrated absorbances are measured instead of absorbances, the integrated molar absorptivity (ε^* in liters/mole-cm^2) is substituted for

Figure 7- Spectra of ^{12}C- (top) and 90% ^{13}C- (bottom) enriched jadeite glasses. The lowered ratios of the intensities of the molecular CO_2 bands to the intensities of the carbonate bands in the ^{13}C enriched glass are due to the additional Na_2O added to the glass.

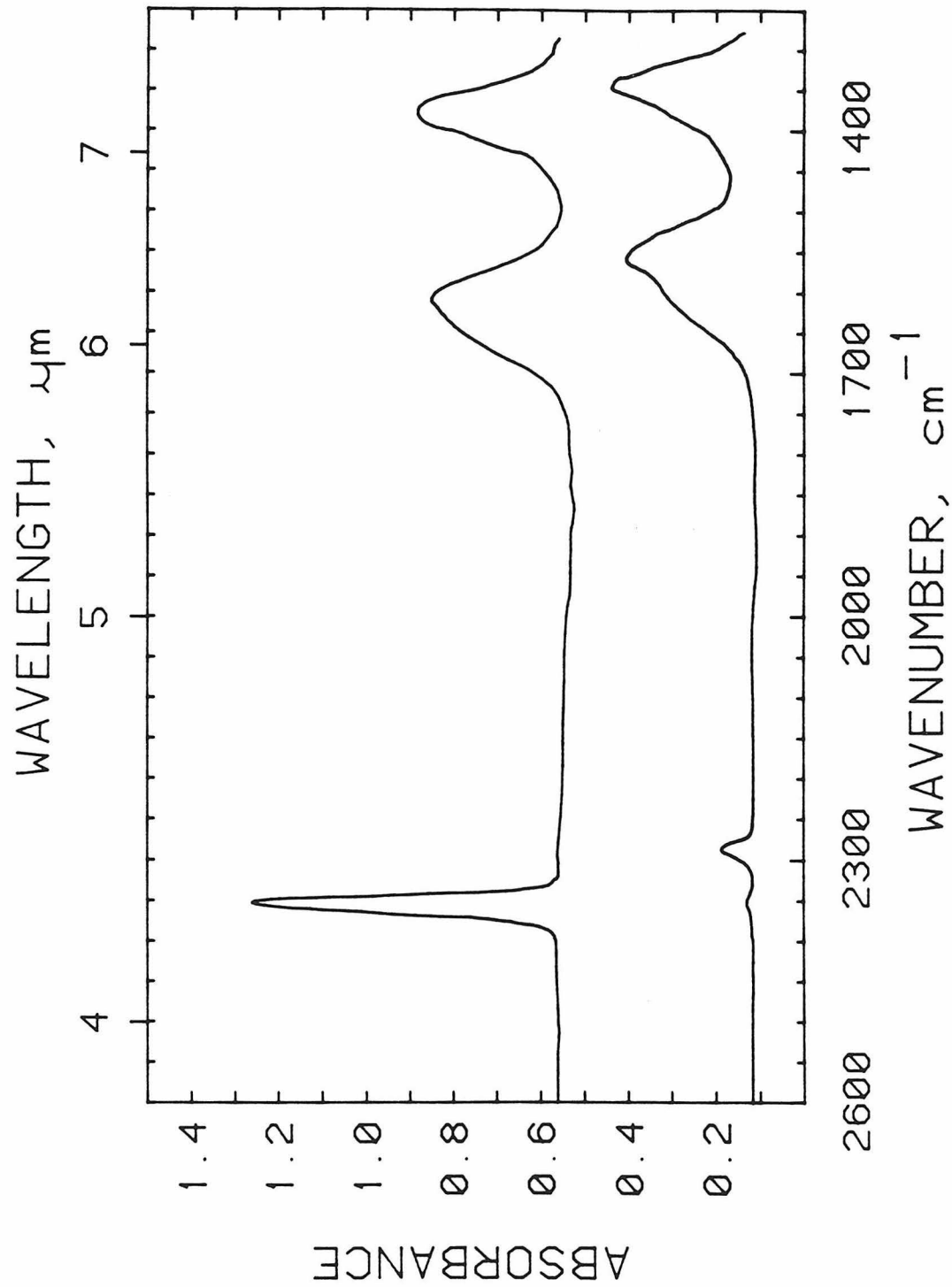
WAVELENGTH, μm
4
5
6
7
ABSORBANCE
1.4
1.2
1.0
0.8
0.6
0.4
0.2
2600
2300
2000
1700
1400
WAVENUMBER, cm⁻¹

molar absorptivity in equation (1). The total amount of carbon dissolved in a glass as molecular carbon dioxide and carbonate can be readily determined via infrared spectroscopy using equation (1) provided that the molar absorptivities of the band due to molecular CO_2 and one of the carbonate bands are known.

Molar absorptivities (and integrated molar absorptivities) for the 2352 cm^{-1}, 1610 cm^{-1}, and 1375 cm^{-1} bands are listed in Table 4 and were determined by the following procedure: An equation was written giving total dissolved CO_2 as the sum of dissolved molecular CO_2, based on the absorbance of the 2352 cm^{-1} band, and of CO_2 dissolved as carbonate, based on the absorbance of the 1610 cm^{-1} band, for each of the 20 sodium aluminosilicate glasses for which total CO_2 contents were believed to be accurately known (see Table 3). The molar absorptivities of the 2352 cm^{-1} and 1610 cm^{-1} bands were then determined based on these 20 equations using a least-squares method similar to that given by Albarede and Provost (1977) by which errors could be assigned to all of the parameters given in equation (1) and to the best fit molar absorptivities. Three glasses (NC-15, ABC-57, and JDC-114) were anomalous, probably due to either errors in sample weighing or CO_2 loss during synthesis, and were ultimately rejected from the fitting procedure. The best fit value of the ratio of the extinction coefficients of the 1610 cm^{-1} and 1375 cm^{-1} bands was determined from the data shown in Figure 6 and the molar absorptivity of the 1375 cm^{-1} band given in Table 4 is based on this ratio. The ratios of the integrated absorbances to absorbances for each of these bands were also

Table 4- Calculated molar absorptivities and integrated molar absorptivities for infrared absorption bands due to C-bearing species.

Band (cm^{-1})	Assignment	Molar Absorptivity[a] (liters/mole-cm)	Integrated Molar Absorptivity[a] (liters/mole-cm^2)
2352	molecular CO_2	945 ± 45	25200 ± 1200
1610	CO_3^{2-}	200 ± 15	24100 ± 1900
1375	CO_3^{2-}	235 ± 20	16800 ± 1500

[a] Errors in these reported values were calculated assuming uncertainties of ±10% total loaded CO_2, of ±2% estimated density, of ±0.02 absorbance units, and of ±3 microns sample thickness. To the extent that reduced carbon species are present in these glasses, these absorptivities have been underestimated.

determined by least squares and the integrated molar absorptivities listed in Table 4 are based on these ratios.

The procedure for determining molar absorptivities is based on two critical assumptions. First, molar absorptivities are assumed to be constant over the range of compositions studied, and second, all dissolved CO_2 is assumed to be present as either molecular CO_2 or carbonate. The internal consistency of these assumptions can be tested by comparing total CO_2 concentrations, obtained by summing spectroscopically determined molecular CO_2 and carbonate concentrations, with the amounts of CO_2 originally loaded into the capsules. Figure 8 shows that the spectroscopically determined values adequately reproduce the total amount of CO_2 originally added to these glasses over the range of silicate compositions studied.

Precision and Accuracy

From these results, infrared spectroscopy appears to be a useful tool for the measurement of CO_2 concentrations in glasses along the $NaAlO_2$-SiO_2 join to low levels of total dissolved carbon. Estimated detection limits are 25 ppm molecular CO_2 and 75 ppm CO_3^{2-} for 200 micron thick pieces of glass. Thicker samples would, from equation (1), have lower detection limits, but absorption bands due to aluminosilicate vibrations would tend to overwhelm the bands at both 1610 cm^{-1} and 1375 cm^{-1} in thicker specimens.

The precision of the infrared technique for measuring CO_2 concentrations in sodium aluminosilicate glasses is assessed to be on the order of several percent and no worse than ±5-6%. This estimate is

Figure 8- Comparison of total CO_2 contents based on amount of silver oxalate loaded into the capsule and based on summing spectroscopically determined molecular CO_2 and CO_3^{2-} concentrations using the bands at 2352 cm^{-1} and 1375 cm^{-1}. Molar absorptivities are from Table 4. A line of loaded CO_2 = measured CO_2 is shown for reference. Samples shown are those used to determine molar absorptivities by least squares; the close correspondence of the data to a 45° line reflects the internal consistency of the calibration procedure. (Samples shown are NC-13, 17, 19, 20, 21; ABC-53, 54, 55, 56, 58, 62, 64; JDC-103, 108, 110, 111, 112, 113, 116, and BOET-2295.)

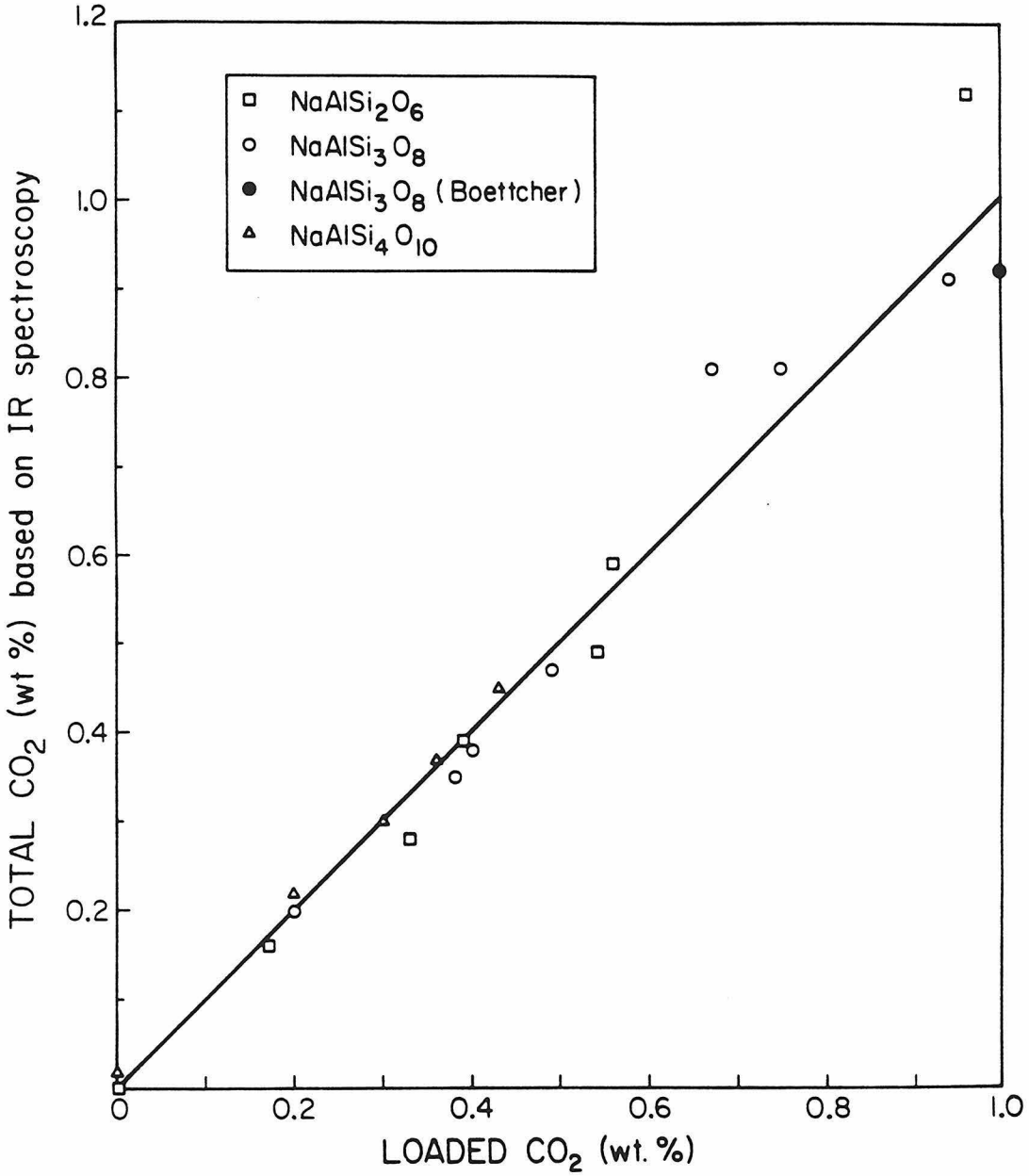
NaAlSi2O6
NaAlSi3O8
NaAlSi3O8 (Boettcher)
NaAlSi4O10
TOTAL CO2 (wt %) based on IR spectroscopy
LOADED CO2 (wt. %)
0
0.2
0.4
0.6
0.8
1.0
1.2

based on potential uncertainties in absorbance (0.01 for an absorbance of 0.5 with the PE 180, based on the reproducibility of individual measurements from Stolper, 1982a), estimated density (±2%), and sample thickness (±3 μm) measurements and varies from sample to sample. Infrared spectroscopy can thus precisely measure the relative amounts of CO_2 dissolve in sodium aluminosilicate glasses. On the other hand, the accuracy of the technique for sodium aluminosilicate glasses, as reflected by Figure 8, is estimated to be ±15-20% of the amount present due to uncertainties in both the molar absorptivities that have been determined and in the CO_2 contents of the standard glasses.

It has already been suggested that possible causes of these uncertainties include minor loss of CO_2 during the piston-cylinder experiments and some heterogeneities in CO_2 within individual glasses. These hypotheses were not originally testable with the PE 180 spectrophotometer, but with the acquisition of a Nicolet Instruments 60SX FTIR, I was able to use smaller beam sizes and discovered that both suspicions are probably correct. Figures 9 and 10 demonstrate that a typical undersaturated CO_2-bearing glass is zoned, with higher CO_2 and lower H_2O contents in the core of the glass than in the rim next to the Pt capsule enclosing the sample. This profile again suggests that H_2 enters the capsule and reacts with CO_2 to form water and reduced carbon species. These species either then diffuse through the Pt wall, as originally suggested by Watson et al. (1982), or concentrate at the rim of the glass. Again, no evidence for reduced carbon species in the glasses has been found. While the nuclear microprobe apparently verified that total C contents integrated over a substantial area of a glass plate (from

Figure 9- Concentration profiles for dissolved CO_3^{2-}, molecular CO_2, and total CO_2 in sample ABC-58. A map showing the approximate location of each measurement is also shown. The glass used is a horizontal section of a piston-cylinder run.

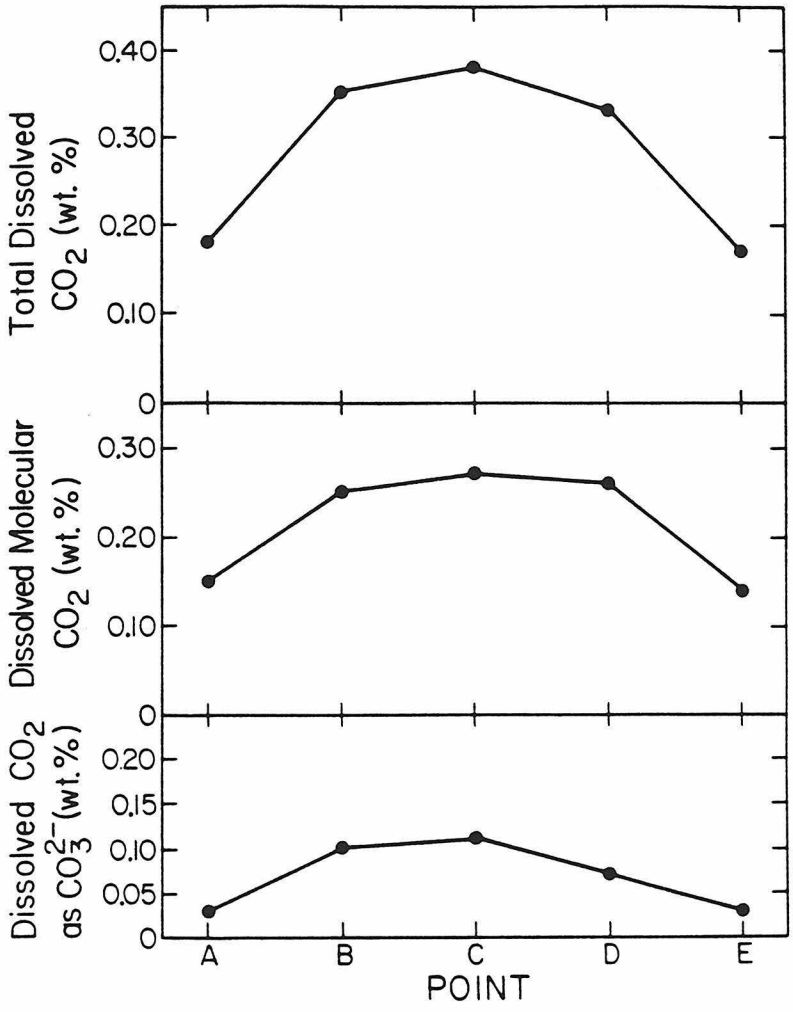
Total Dissolved CO_2 (wt. %)
0.40
0.30
0.20
0.10
0
Dissolved Molecular CO_2 (wt. %)
0.30
0.20
0.10
0
Dissolved CO_2 as CO_3^{2-} (wt. %)
0.20
0.15
0.10
0.05
0
A
B
C
D
E
POINT

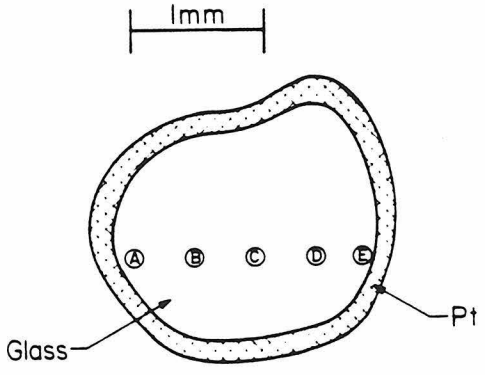
1mm
A
B
C
D
E
Pt
Glass

Figure 10- Concentration profile for total dissolved H_2O in sample # ABC-58. The location of each measurement is the same as shown in Figure 9.

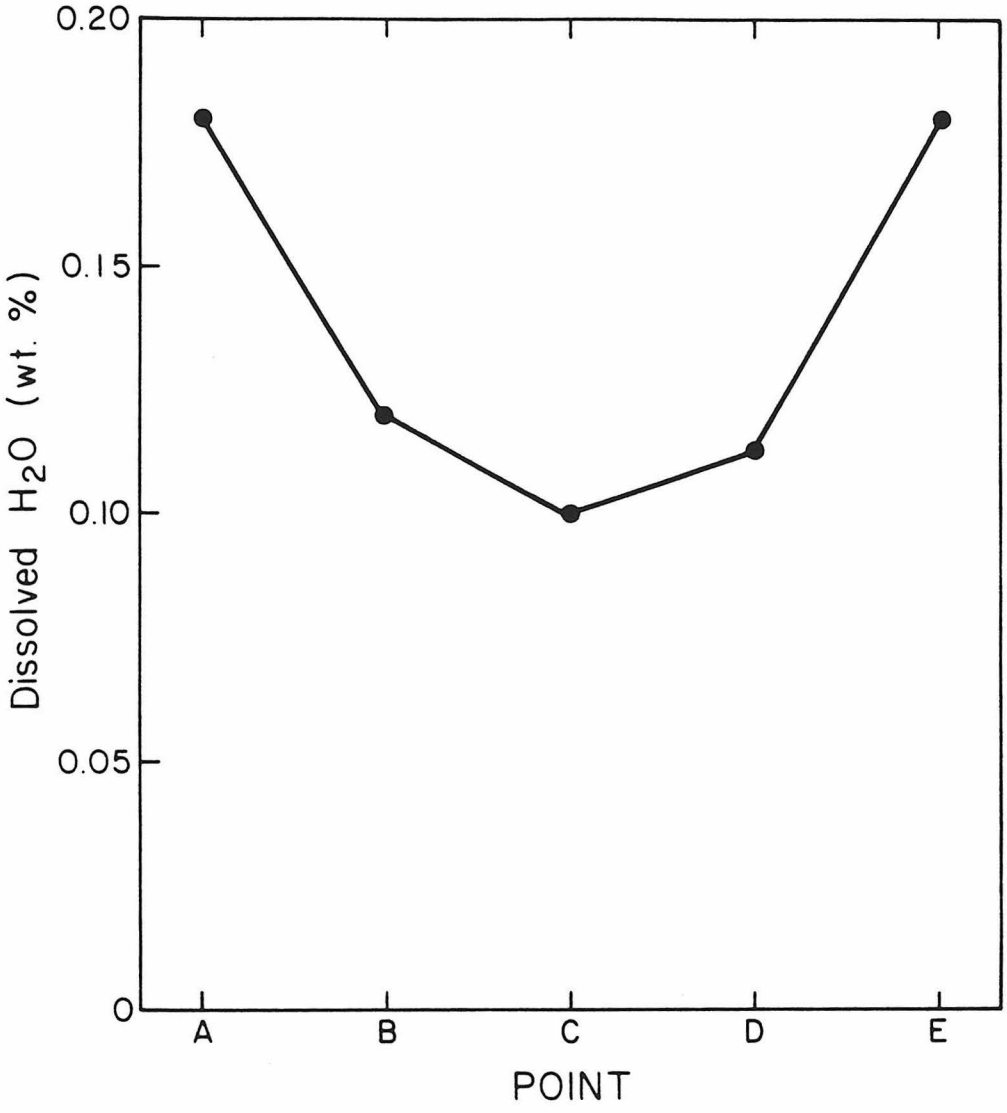
0.20
0.15
0.10
0.05
0
Dissolved H_2O (wt. %)
A
B
C
D
E
POINT

~0.25 mm^2 to ~0.50 mm^2, generally in the center of the glass plate) did not significantly decrease (Table 2), the scatter to the data was probably introduced by making infrared measurements near the rims of some glass samples rather than at their cores. I note that improved accuracy of the technique might be possible given this information.

Speciation of Carbon Dioxide in Sodium Aluminosilicate Glasses

The extinction coefficients given in Table 4 have been used to obtain the amounts of molecular CO_2 and CO_3^{2-} dissolved in each of the glasses synthesized in this study. The results are presented in Table 5.

Figure 11 shows molecular CO_2 versus carbonate concentrations for jd-E, ab-E, and eu-E glasses synthesized at 1450°C and 25 kbar with up to 1.1 wt.% total dissolved CO_2. For each silicate composition, the ratio of molecular CO_2 to CO_3^{2-} dissolved in the glasses varies little over the range of total CO_2 contents studied. The ratio is, however, a strong function of silicate composition, increasing with increasing silica and decreasing soda and alumina content along the $NaAlO_2$-SiO_2 join. CO_2 dissolves in jd glass predominately as CO_3^{2-}, the ratio of molecular CO_2 to CO_2 dissolved as CO_3^{2-} is approximately 0.6. In ab and eu glasses, molecular CO_2 predominates; the ratios are approximately 2.3 and 5, respectively. Glasses prepared from compositions that lost Na during the initial drying process (jd-X, ab-X, eu-X) have higher, but still constant molecular CO_2 to CO_3^{2-} ratios. The ratio is 3.4 in jd-X glasses and 2.7 in ab-X glasses. Eu-X glasses contain negligible CO_3^{2-}.

Table 5- Concentrations (in wt. %) of molecular CO_2, CO_3^{2-}, and total CO_2 based on spectroscopic measurements. CO_3^{2-} concentrations are given as wt. % CO_2 dissolved as CO_3^{2-} and are based on the intensity of the 1375 cm^{-1} band. The mole fractions of molecular CO_2 and CO_3^{2-} are also given. Mole fractions are computed on the basis of moles of assumed mixing species (i.e. $CO_{2,mol}$, CO_3^{2-}, and O).

Sample	#	P (kbar)	T (°C)	CO_2 (mol.)	CO_3^{2-}	CO_2(Tot.)	X_{CO_2}	$X_{CO_3^{2-}}$
NC	2	25	1450	0.62	0.15	0.78	0.0046	0.0011
NC	3	25	1450	0.05	0.04	0.08	0.0004	0.0003
NC	4	25	1450	0.29	0.05	0.34	0.0021	0.0004
NC	6	25	1450	0.29	0.10	0.39	0.0021	0.0007
NC	7	25	1450	0.30	0.08	0.38	0.0022	0.0006
NC	10	25	1450	0.58	0.09	0.67	0.0042	0.0007
NC	13	25	1450	0.02	0.00	0.02	0.0002	0.0000
NC	15	25	1450	0.34	0.00	0.34	0.0025	0.0000
NC	17	25	1450	0.25	0.00	0.25	0.0018	0.0000
NC	19	25	1450	0.45	0.00	0.45	0.0033	0.0000
NC	20	25	1450	0.22	0.00	0.22	0.0016	0.0000
NC	21	25	1450	0.37	0.00	0.37	0.0027	0.0000
ABC	14	25	1450	0.00	0.00	0.00	0.0000	0.0000
ABC	22	25	1450	0.42	0.20	0.62	0.0032	0.0015
ABC	23	33	1450	0.91	0.46	1.37	0.0068	0.0034
ABC	24	33	1450	0.24	0.16	0.40	0.0018	0.0012
ABC	25	33	1450	0.58	0.34	0.92	0.0043	0.0025
ABC	27	27	1450	0.16	0.08	0.24	0.0012	0.0006
ABC	29	15	1450	0.24	0.08	0.32	0.0018	0.0006
ABC	30	15	1450	0.22	0.11	0.32	0.0016	0.0008
ABC	33	25	1560	0.31	0.15	0.46	0.0023	0.0011
ABC	35	25	1560	0.23	0.14	0.37	0.0017	0.0011
ABC	53	25	1450	0.59	0.22	0.81	0.0044	0.0016
ABC	54	20	1450	0.25	0.10	0.35	0.0019	0.0007
ABC	55	20	1450	0.11	0.09	0.20	0.0008	0.0007
ABC	56	20	1450	0.39	0.09	0.47	0.0029	0.0006
ABC	57	20	1450	0.45	0.17	0.62	0.0034	0.0012
ABC	58	20	1450	0.28	0.10	0.38	0.0021	0.0007
ABC	62	20	1450	0.71	0.21	0.91	0.0053	0.0015
ABC	64	20	1450	0.59	0.22	0.81	0.0044	0.0016
JDC	67	25	1400	0.26	0.37	0.62	0.0020	0.0028
JDC	68	25	1400	0.14	0.32	0.46	0.0011	0.0024
JDC	69	25	1400	0.47	0.77	1.23	0.0036	0.0059
JDC	72	25	1400	0.10	0.22	0.32	0.0008	0.0017
JDC	73	25	1400	0.10	0.28	0.38	0.0008	0.0021
JDC	74	25	1400	0.07	0.19	0.26	0.0005	0.0015
JDC	76	25	1400	0.08	0.18	0.26	0.0006	0.0014
JDC	84	25	1450	0.29	0.51	0.80	0.0022	0.0039
JDC	85	25	1450	0.06	0.14	0.20	0.0005	0.0011
JDC	86	25	1450	0.26	0.50	0.76	0.0020	0.0038
JDC	89	25	1450	0.25	0.48	0.73	0.0019	0.0037
JDC	90	25	1450	0.23	0.36	0.59	0.0017	0.0028
JDC	91	25	1450	0.02	0.07	0.09	0.0002	0.0005
JDC	103	25	1450	0.18	0.05	0.23	0.0014	0.0004
JDC	108	25	1450	0.43	0.69	1.12	0.0033	0.0053
JDC	110	25	1450	0.00	0.00	0.00	0.0000	0.0000
JDC	111	25	1450	0.05	0.11	0.16	0.0004	0.0008

TABLE 5 (cont'd.)

Sample	#	P (kbar)	T (°C)	CO_2 (mol.)	CO_3^{2-}	CO_2 (tot.)	X_{CO_2}	$X_{CO_3^{2-}}$
JDC	112	25	1450	0.16	0.33	0.49	0.0012	0.0026
JDC	113	25	1450	0.15	0.23	0.39	0.0012	0.0018
JDC	114	25	1450	0.11	0.25	0.37	0.0009	0.0019
JDC	116	25	1450	0.19	0.40	0.59	0.0015	0.0031
BOET	2582	20	1450	0.63	1.29	1.91	0.0048	0.0099
BOET	2990	20	1450	0.39	0.13	0.52	0.0029	0.0009
BOET	2995	20	1450	0.71	0.21	0.92	0.0053	0.0016

Figure 11- CO_2 concentration versus the concentration of CO_2 dissolved as CO_3^{2-} for glasses on the $NaAlSi_2O_6$-SiO_2-CO_2 join quenched from melts held at 1450 ^oC and 25 kbar. Concentrations are spectroscopically determined. The trends defined by each composition as a function of total CO_2 content are outlined and reproduced in Figures 12-14. (Data points are for NC-2, 3, 4, 6, 7, 10, ABC-14, 22, 27, 53, and JDC- 84, 85, 86, 89, 90, 91, 108, 111, 112, 113, 114, 116.)

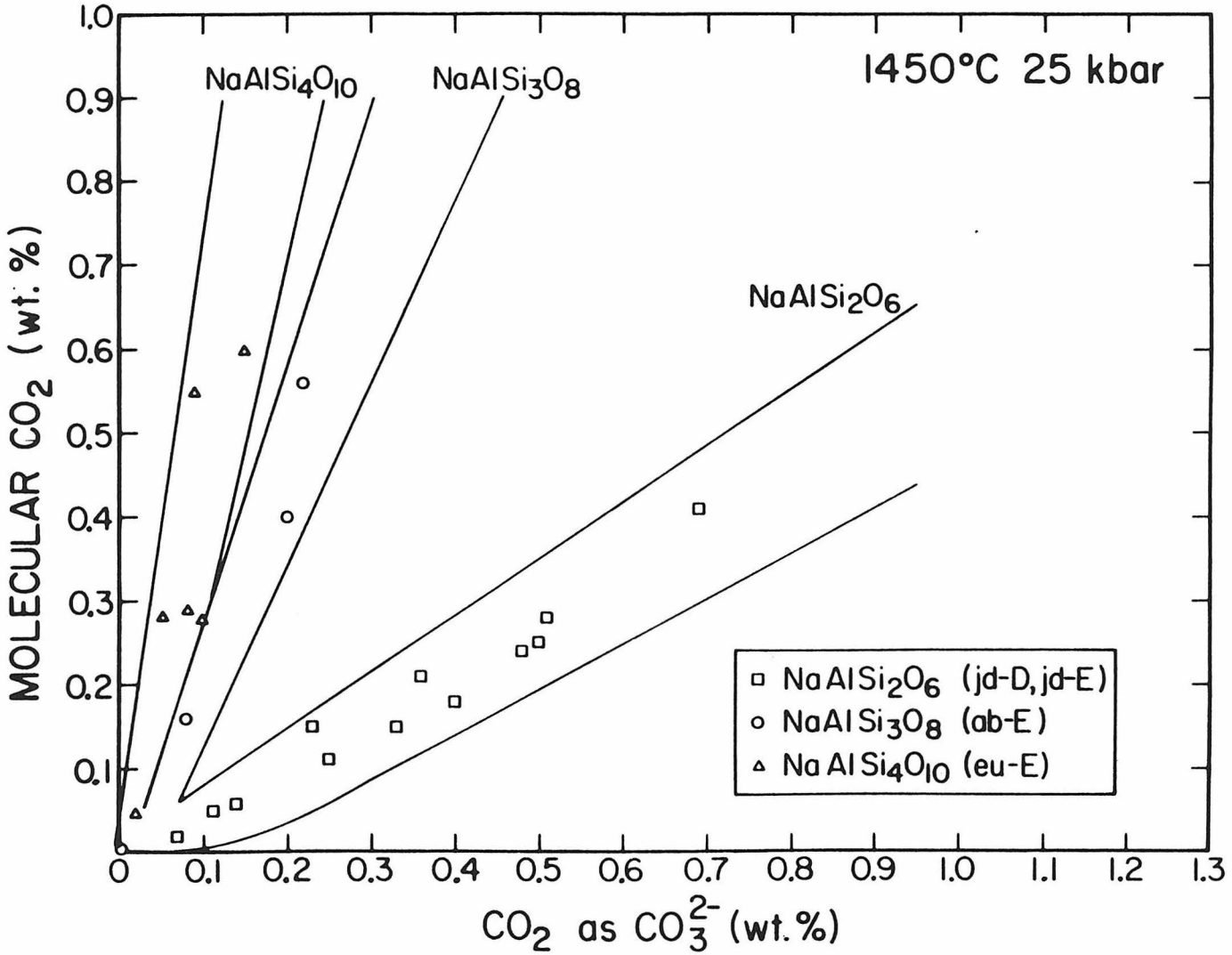
1450°C 25 kbar
NaAlSi4O10
NaAlSi3O8
NaAlSi2O6
MOLECULAR CO2 (wt. %)
CO2 as CO3 2- (wt. %)
NaAlSi2O6 (jd-D, jd-E)
NaAlSi3O8 (ab-E)
NaAlSi4O10 (eu-E)
0
0.1
0.2
0.3
0.4
0.5
0.6
0.7
0.8
0.9
1.0
1.1
1.2
1.3

I have also studied glasses of ab-E, ab-X and jd-E compositions quenched from melts held at pressures and temperatures other than 1450°C and 25 kbar. While there is some variation suggesting a slight increase in the ratio of molecular CO_2 to carbonate with decreasing temperature and pressure (Figures 12 and 13), the variations are minor for each of the compositions studied. The pressure and temperature dependence that is observed is small when compared to previously reported results (Mysen, 1976 and Figure 14). It is concluded that the speciation of CO_2 in glasses on the $NaAlO_2$-SiO_2 join is not strongly dependent on pressure and temperature over the 15-33 kbar, 1400-1560°C ranges.

The ratios of molecular CO_2 to CO_3^{2-} of the ab and jd CO_2-bearing glasses synthesized in the laboratory of Professor A. Boettcher are similar to those of our CO_2-bearing ab-E and jd-E glasses (Figure 12). Since these glasses were synthesized using both Na_2CO_3 and $Ag_2C_2O_4$ as CO_2 sources and were held at run conditions for a variety of run lengths, this correspondence is taken to be indicative of equilibrium between CO_2 species in the glasses we have studied.

Since none of the runs were anhydrous, it is difficult to assess the role of H_2O in the CO_2 speciation trends observed. Previous workers (Eggler and Rosenhauer, 1978) have stated that H_2O enhances the formation of CO_3^{2-}. There is no discernable relationship between the ratio of molecular CO_2 to CO_3^{2-} and the H_2O contents of the samples studied. However, the water contents of the glasses are low; higher water contents may well influence the speciation of CO_2.

Figure 12- Molecular CO_2 versus CO_2 dissolved as carbonate for glasses quenched from melts held at 1450°C and pressures other than 25 kbar. The pressure of each run is marked. Trends are for glasses equilibrated at 1450°C and 25 kbar (Figure 11). Filled data points are from samples synthesized in the laboratory of A. Boettcher. (Data points are for ABC-23, 24, 25, 29, 30, and BOET 2582, 2990, 2995.)

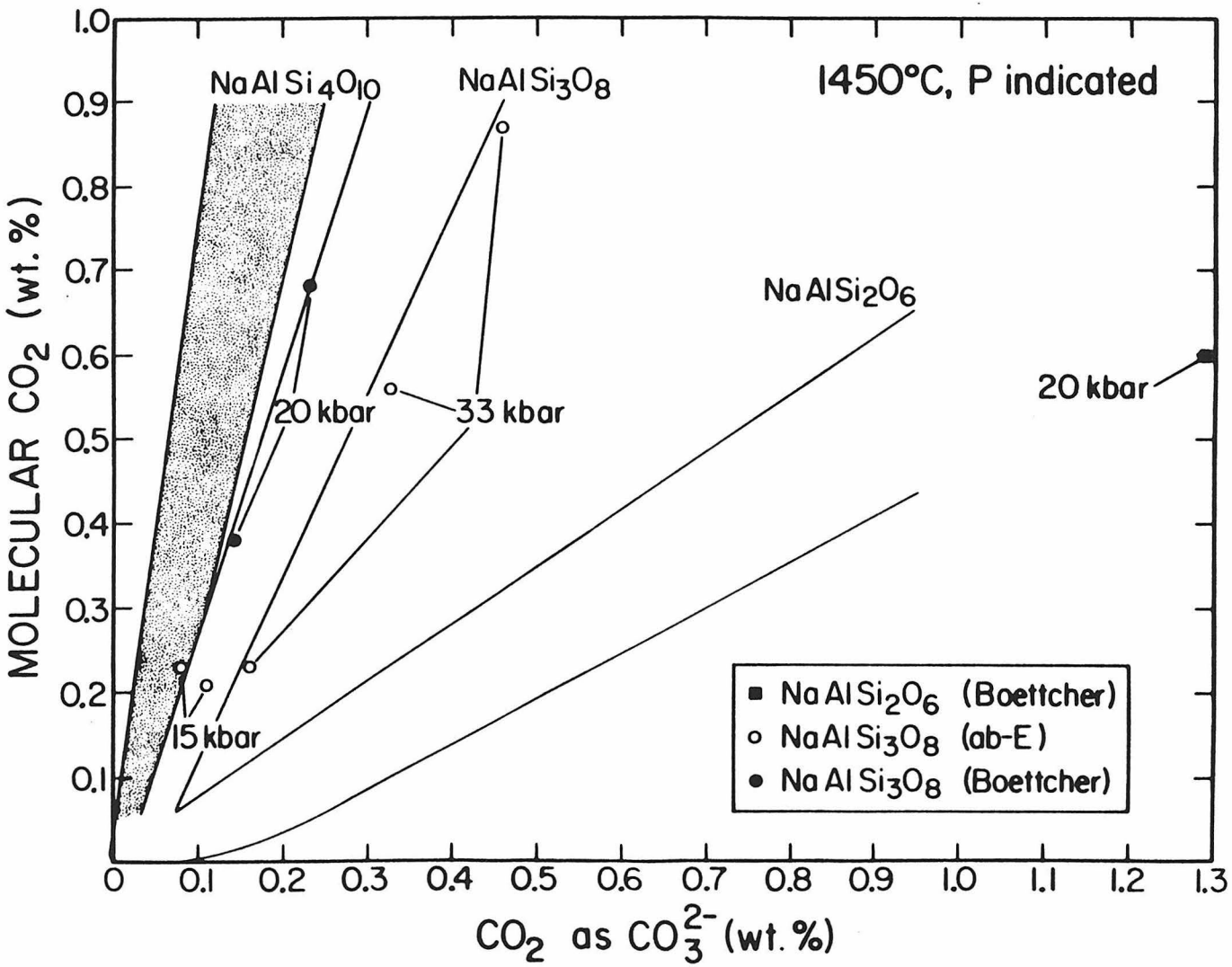
1450°C, P indicated
NaAlSi4O10
NaAlSi3O8
NaAlSi2O6
20 kbar
33 kbar
20 kbar
15 kbar
NaAlSi2O6 (Boettcher)
NaAlSi3O8 (ab-E)
NaAlSi3O8 (Boettcher)
MOLECULAR CO2 (wt.%)
CO2 as CO3 2- (wt.%)
0
0.1
0.2
0.3
0.4
0.5
0.6
0.7
0.8
0.9
1.0
1.1
1.2
1.3

Figure 13- Molecular CO_2 versus CO_2 dissolved as carbonate for glasses quenched from melts held at 25 kbar and temperatures other than 1450°C. The temperature of each run is marked. Trends are for glasses equilibrated at 1450°C and 25 kbar (Figure 11). (Data points are for ABC-33, 35, and JDC-68, 69, 72, 73,74, 76.)

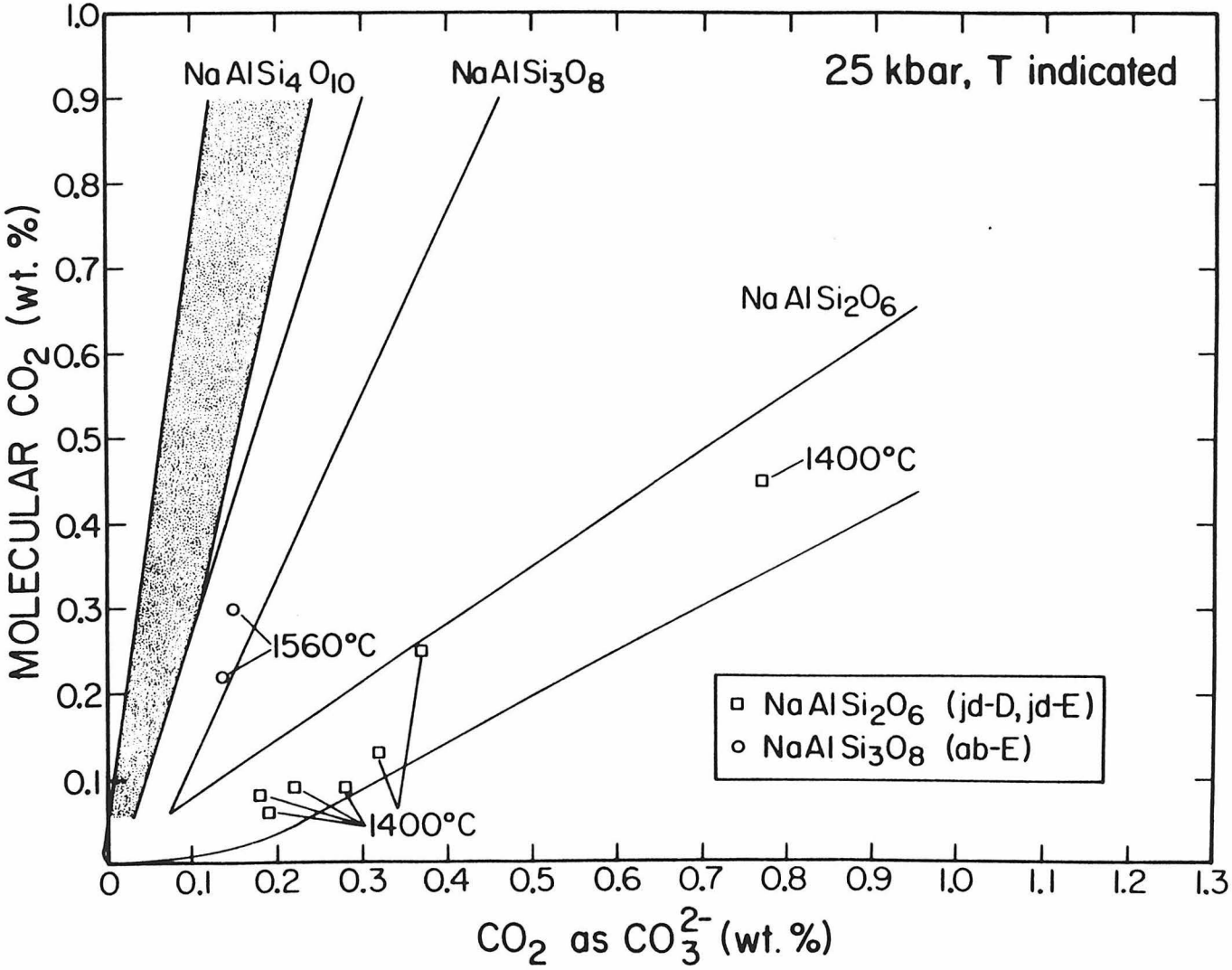
25 kbar, T indicated
NaAlSi4O10
NaAlSi3O8
NaAlSi2O6
1400°C
1560°C
1400°C
NaAlSi2O6 (jd-D, jd-E)
NaAlSi3O8 (ab-E)
MOLECULAR CO2 (wt. %)
CO2 as CO3 2- (wt. %)
0
0.1
0.2
0.3
0.4
0.5
0.6
0.7
0.8
0.9
1.0
1.1
1.2
1.3

Figure 14- Molecular CO_2 concentration versus the concentration of CO_2 dissolved as CO_3^{2-} for glasses on the $NaAlO_2$-SiO_2-CO_2 join comparing the data of Mysen (1976) with the results (shaded regions) presented in this study. Mysen's data points are labelled with the pressure and temperature of the melt prior to quenching. There is essentially no correlation between the two data sets.

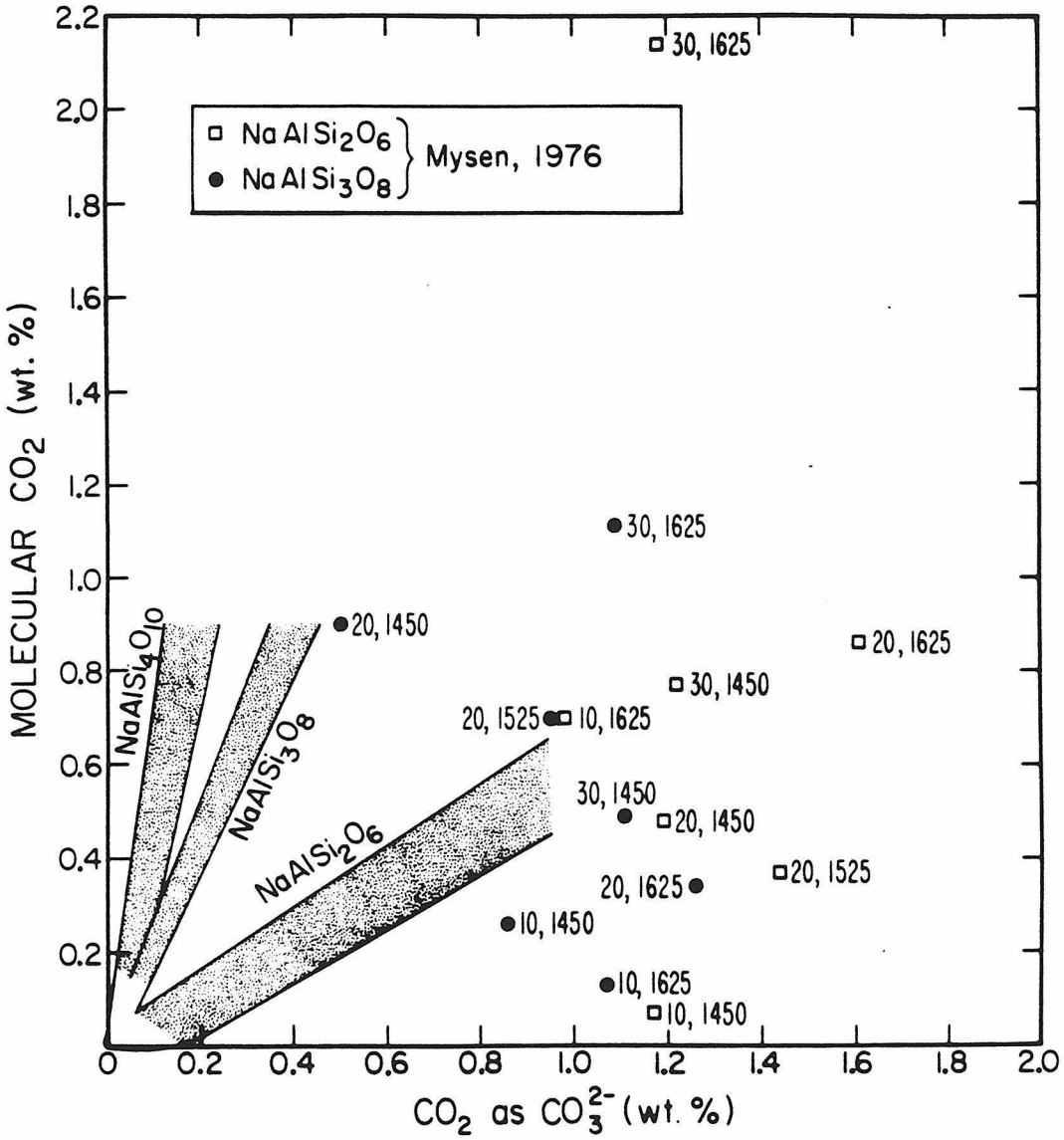
□ $NaAlSi_2O_6$
● $NaAlSi_3O_8$
Mysen, 1976
MOLECULAR CO_2 (wt. %)
CO_2 as CO_3^{2-} (wt. %)
$NaAlSi_4O_{10}$
$NaAlSi_3O_8$
$NaAlSi_2O_6$
30, 1625
20, 1450
30, 1625
20, 1625
30, 1450
20, 1525
10, 1625
30, 1450
20, 1450
20, 1525
20, 1625
10, 1450
10, 1625
10, 1450

Discussion

Comparison with Previous Spectroscopic Investigations

The results are comparable with those of Mysen (1976), who used infrared spectroscopy to investigate CO_2 dissolution in glasses quenched from vapor-saturated melts on the $NaAlO_2$-SiO_2-CO_2 join. Mysen et al. (1976) also reported infrared studies of CO_2-bearing $NaAlSi_3O_8$ glass. In addition, Brey (1976) studied CO_2-bearing glasses on the $NaAlSi_3O_8$-$CaAl_2Si_2O_8$ join with infrared spectroscopy, and Raman spectroscopy was used to investigate glasses in this system by Mysen and Virgo (1980b). In all of these studies, as in this study, glasses were synthesized by quenching from melts held at high pressures and temperatures in piston-cylinder apparatuses. The pressures and temperatures from which the melts were quenched were similar in all of these investigations. One difference between these previous studies and this study is that they focussed on vapor-saturated systems whereas most of the glasses examined here were quenched from vapor-undersaturated melts.

There is little disagreement about the existence of both molecular CO_2 and carbonate in CO_2-bearing sodium aluminosilicate glasses, although Brey (1976) states, without supporting evidence, that the molecular CO_2 is a quenching phenomenon. This study confirms the conclusion of Mysen (1976) that the speciation of CO_2 in silicate melts is strongly dependent on silicate composition, with the ratio of molecular CO_2 to carbonate increasing with increasing silica content on the $NaAlO_2$-SiO_2 join. There is, however, little quantitative correspondence between the measured molecular CO_2 and carbonate contents and those reported by Mysen (1976) (Figure 14). There is no evidence of

the strong pressure and temperature dependence of CO_2 speciation that Mysen (1976) reported. Finally, there are essentially constant carbonate to molecular CO_2 ratios for each silicate composition as total dissolved CO_2 content increases; Mysen and Virgo (1980b) reported that the CO_3^{2-} to molecular CO_2 ratio increases sharply with total dissolved CO_2 in albite glasses.

Why are these results so different from those of Mysen (1976)? The total CO_2 contents of the glasses studied by Mysen tend to be at the high end of those studied here, since his experiments were vapor-saturated while most of these were not. The P-T conditions and total CO_2 contents of these two studies overlap, however, and the results should be comparable. The explanation of the discrepancies between results probably lies principally in differences in analytic techniques. Mysen (1976) used a mixture of $Ba^{14}CO_3$ and Na_2CO_3 as a CO_2 source and measured the total dissolved carbon content of each of his glasses by β-track radiography. Then, using the intensity of the 7.2 micron (~1375 cm^{-1} in this study) carbonate band, which he calibrated using mixtures of powdered CO_2-free silicate glass and Na_2CO_3 embedded in KBr discs, he determined the concentration of CO_3^{2-} dissolved in each glass. Molecular CO_2 concentrations were determined by the difference between the total carbon content and the CO_3^{2-} content.

One limitation of the procedure employed by Mysen (1976) is that uncertainties in bulk CO_2 content determined by β-track mapping and in carbonate concentration determined by infrared spectroscopy propagate into estimations of molecular CO_2 content. One potential problem is that all of the carbon detected by β-tracking may not be dissolved or

present as oxidized species. Other possible uncertainties associated with the use of β-track mapping for bulk carbon analysis have been discussed by Brey (1976), Rai et al. (1983), and Tingle (1985).

There are also uncertainties associated with Mysen's (1976) determination of carbonate concentrations via infrared spectroscopy. Infrared spectra were obtained on discs of KBr in which powdered glasses were embedded. Numerous studies (Duyckaerts, 1959; Tuddenham and Lyon, 1970; Russell, 1974; Wong and Angell, 1976) have indicated that extreme care must be taken with KBr pellets and that quantitative results are difficult to obtain. Experience in our laboratory has confirmed that KBr spectra are often quite difficult to interpret, especially in the case of these CO_2-bearing glasses, in which relevant band intensities are quite low. Particle size has a large effect on absorption spectra and care must be taken to reproducibly grind samples. Grinding can, in some cases, structurally alter the material of interest. Adsorption of gases on both the KBr and the ground sample may also be significant (Barker and Torkelson, 1975). It is clear that many of the earlier studies that used infrared spectroscopy on KBr pellets to study volatile speciation in glasses suffered from these difficulties. Therefore, many of the conclusions drawn from them are suspect. In particular, the conclusions that molecular CO_2 is a detectable constituent of nearly all C-bearing glasses, including basic compositions such as diopside and several natural rock compositions (Mysen et al., 1975; Mysen et al., 1976), and that its concentration varies systematically with conditions of melt equilibration were almost certainly artifacts. In the case of diopside, molecular CO_2 has not been detected by Raman spectroscopy

(Sharma, 1979; Mysen and Virgo, 1980a; Rai et al., 1983). I have studied one of the glasses synthesized by Rai et al. (1983) [Di #89] and conclude, using a molar absorptivity for the 2352 cm^{-1} band of 945 liters/mole-cm, that the concentration of molecular CO_2 is less than 25 ppm by weight (Chapter 3). I have also failed to detect any molecular CO_2 in synthetic CO_2-rich basaltic glasses or in glasses in the system $CaO-Al_2O_3-SiO_2-CO_2$ (Chapter 3). A combination of adsorbed CO_2 and incomplete purging of the sample chamber (Brey, 1976) may have been responsible for the spurious molecular CO_2 observed in the spectra of Mysen et al. (1975, 1976). Examination of the spectra of Mysen et al. (1975), Mysen et al. (1976), and Mysen (1976) suggests that water adsorbed on the KBr was probably also a problem, resulting in major absorptions at ~3500 and ~1600 cm^{-1}. Eggler at al. (1979) also suggest that adsorbed acetone can produce significant absorptions in spectra of powdered materials.

There may also be problems with the procedure used by Mysen (1976) to calibrate the intensity of the ~1375 cm^{-1} carbonate band. The carbonate band is split by ~200 cm^{-1} in $NaAlO_2-SiO_2$ glasses and only slightly split in Na_2CO_3 (White, 1974), suggesting that caution should be used in equating the integrated molar absorptivities for the carbonate groups in these two systems. Indeed, my measured integrated molar absorptivity for the 1440 cm^{-1} (actual location) band in Na_2CO_3 (determined using KBr pellets) is ~36500 liters/mol-cm^2, more than twice the value obtained for the 1375 cm^{-1} band. Mysen's (1976) calibration curve for the ~1400 cm^{-1} carbonate band (his Figure 10) is also troublesome since it is not linear and does not pass through zero and

that the area he measures to determine concentration is described in his text as "transmittance", whereas absorbance would be the usual measurement used for determining the CO_3^{2-} concentration.

By taking spectra on doubly-polished glass plates, our laboratory has avoided the problems associated with KBr pellets. Most important, however, is the fact that molecular CO_2 and carbonate band intensities are measured simultaneously in each glass plate. Thus, even if determinations of molar absorptivities are in error, leading to inaccuracies in the measured concentrations of the various species, the ratios of band intensities, and thus variations in the relative proportions of dissolved C-bearing species, can be precisely determined. This contrasts with the approach used by Mysen (1976) in which the concentration of molecular CO_2 was determined by difference between independent determinations of total dissolved CO_2 and carbonate concentrations. Using Mysen's approach, meaningful determinations of the relative proportions of molecular CO_2 and carbonate depend on both the accuracy and precision of the total CO_2 and carbonate concentrations. These factors probably explain the differences between the two data sets in Figure 14.

The results presented in this chapter indicate that at the relatively low concentrations of CO_2 in silicate glasses, the ratio of molecular CO_2 to carbonate in a glass varies little with total dissolved CO_2 content. Using Raman spectroscopy, Mysen and Virgo (1980b) found that over a similar range of pressure, temperature and CO_2 content, the ratio of carbonate to molecular CO_2 increased sharply with increasing total CO_2 content for albite glasses. It is difficult to evaluate this

conclusion since Mysen and Virgo (1980b) give no quantitative details. There is neither a demonstration of a linear variation in band intensity with species concentration, nor a discussion of the precision and accuracy of their determinations of band intensities, nor a consideration of their detection limits for CO_2 and CO_3^{2-} in glasses. The band at ~1075 cm^{-1} that they use to infer CO_3^{2-} concentration is deeply buried among three silicate bands, and its intensity can only be determined by deconvolution procedures. This probably means that the detection limit and precision for CO_3^{2-} concentrations determined by this procedure are poor. Apparently confirming this, they saw no CO_3^{2-} in an albite glass containing 0.68 weight percent total CO_2, whereas in equivalent glasses studied here, carbonate is readily detected. It also appears from Figure 3 of Mysen and Virgo (1980b) that the intensity of the band at ~1378 cm^{-1} they have assigned to molecular CO_2 increases roughly in proportion to their CO_3^{2-} band between 2.05 wt.% and 3.20 wt.% total CO_2. Their data might be consistent with a roughly constant molecular CO_2 to carbonate ratio. Thus, the apparent discrepancy between the Raman spectroscopic results of Mysen and Virgo (1980b) and the infrared results may simply reflect the fact that infrared spectroscopy is, at this stage, more useful as a tool for measuring the concentrations of C-bearing species in silicate glasses. A similar conclusion was reached by Stolper (1982a) regarding measurement of the concentrations of water and hydroxyl groups in glasses.

Solubility Mechanisms of CO_2 in Sodium Aluminosilicate Melts

Silicate melts are dynamic, with the homogenous equilibria between oxygen species continually readjusting as they are perturbed by the addition of CO_2 or other components. Even if only a single kind of oxygen actually reacts with molecular CO_2 to form carbonate, the concentrations of other oxygen species will be affected as they act to buffer the single reactive oxygen species. Thus, if the concentrations of the different oxygen species could be determined, it may be extremely difficult to specify which classes of oxygen are directly involved in carbonate-producing reactions and which are passively responding to these reactions. There has, however, been considerable speculation about the structural role played by the oxygens that react with CO_2 molecules to produce carbonate groups and about the structural changes that occur in the silicate framework of these melts when carbonation reactions proceed.

It is widely believed, based on Raman spectra (Mysen and Virgo, 1980b), X-ray scattering data (Taylor et al., 1979), and thermochemical studies (e.g., Navrotsky et al., 1982), that $NaAlO_2$-SiO_2 glasses and melts are nearly fully polymerized in the sense that every oxygen is shared between two silicate and/or aluminate tetrahedra. It is difficult to envision how CO_2 molecules can react with a melt in which there are only bridging oxygens to produce carbonate. One possibility is for the resulting carbonate ion to participate in the bridge between adjacent tetrahedra by forming silicon- or aluminum-bearing carbonate complexes (Sharma et al., 1979). An example of such a structure might be:

$$CO_2 + [\equiv(Si,Al) - O - (Si,Al) \equiv]$$

$$= \equiv(Si,Al) - O - \underset{\underset{O}{\|}}{C} - O - (Si,Al)\equiv$$

Carbonate concentration decreases as silica is added to melts, suggesting that oxygens bridging two Si tetrahedra do not react with CO_2 molecules in this way. However, the formation of such structures between Al and Si tetrahedra or between two Al tetrahedra cannot be ruled out. In these cases, sodium atoms that provided charge-balance for the bridging oxygens prior to reaction with CO_2 molecules would probably be associated with the newly formed structure in some way. This study yields no data indicating if complexes like this are present in the glasses, but note that these CO_3^{2-} groups would undoubtedly be highly asymmetric and that this unusual environment could, in principle, account for the splitting of the ν_3 carbonate band that we observe.

Another possibility is that bridging oxygens are removed from the silicate-aluminate network when they react with CO_2 molecules to produce carbonate ions. In such cases, structural and charge balance considerations are usually taken to require local rearrangements in the silicate and aluminate framework. For example, Mysen and Virgo (1980b) suggested that reaction of CO_2 molecules with bridging oxygens to produce carbonate groups is accompanied by the generation of octahedrally-coordinated aluminum. Other configurations, such as five-fold or three-fold coordination of aluminum (McKeown et al., 1984) or

aluminum triclusters (Lacy, 1963) could also be generated by such reactions. None of these reaction products has been positively identified by spectroscopy in CO_2-free or CO_2-bearing glasses, although their concentration may be expected to be quite high in very carbonate-rich aluminosilicate glasses. Mysen and Virgo (1980b) include weak bands they interpret as reflecting the presence of octahedrally-coordinated aluminum in their deconvolutions of the Raman spectra of CO_2-rich glasses.

It is doubtful that CO_2-free melts on the join $NaAlO_2$-SiO_2 are fully polymerized. They undoubtedly contain non-bridging and even free oxygens at some concentration level, probably some non-tetrahedrally coordinated aluminum (Boettcher et al., 1982; 1984), and perhaps aluminum triclusters. It may be that molecules of CO_2 react with two non-bridging oxygens to produce a bridging oxygen and a carbonate group in much the same way that carbonate groups are thought to be produced in depolymerized melts such as diopside (Eggler and Rosenhauer, 1978). Alternatively, free oxygen could react with CO_2 to form carbonate complexes (Tomlinson, 1953; Pearce, 1964; Wagner, 1975). Only small amounts of non-tetrahedrally coordinated aluminum or of aluminum triclusters would be required to produce enough non-bridging or free oxygens to account for the observed concentrations of CO_3^{2-} groups in the glasses I have studied. In addition, as reactive oxygens are consumed and carbonate ions are generated, the concentrations of the reactive oxygens might be regenerated to some extent by the equilibria between these and the major oxygen species; relatively large amounts of carbonate could be produced by reaction of CO_2 molecules with non-

bridging or free oxygens even if the concentrations of these species in melts are small.

Most of these and the equivalent statements of previous workers are highly speculative. Reliable and sensitive techniques for quantitatively determining both the concentrations of different types of oxygens and local configurations in glasses are needed before statements about changes in melt structure that accompany carbonate formation can be made with confidence.

Conclusions

1. Infrared spectroscopy can be used to quantitatively determine the concentrations of molecular CO_2 and carbonate groups in sodium aluminosilicate glasses. If doubly-polished glass plates are used instead of powders embedded in KBr pellets, species concentrations can be measured with a precision on the order of several percent of the amount present. This technique has the potential for analyzing individual spots with diameters on the order of 10 μm. The accuracy of species concentrations measurements is currently limited to about ±15-20% in glasses studied due to heterogeneous glass standards, but this accuracy can be improved with suitable standards.
2. Glasses in the system Na_2O-Al_2O_3-SiO_2-CO_2 near the $NaAlSi_2O_6$-SiO_2-CO_2 join that have been quenched from melts at 15-33 kbar, 1400-1560°C contain both carbonate and CO_2 molecules. Carbonate groups are in distorted environments that are very different from those in crystalline carbonates. The carbonate groups may be in the form of Na-carbonate ionic-complexes.

3. There is an approximately linear relationship between molecular CO_2 and carbonate concentrations for each of the sodium aluminosilicate compositions studied, up to at least 1 wt.% total dissolved CO_2. The molecular CO_2 to carbonate ratio is strongly dependent on the silicate composition of the glass, with the proportion of molecular CO_2 increasing as silica is approached on the $NaAlSi_2O_6$-SiO_2 join. Compositions that differ only in their soda concentrations have different molecular CO_2 to carbonate ratios, with those that have lower Na_2O contents having higher ratios.
4. The speciation of CO_2 in glasses quenched from melts is only weakly dependent on the pressure or temperature at which the melt was equilibrated over the 15-33 kbar, 1400-1560°C range. This contrasts with previously reported results.

Chapter 2. The Solubility of Carbon Dioxide in Molten Albite

The solubility of CO_2 in both natural and synthetic silicate melts has been extensively studied and a large volume of data has been accumulated. Unfortunately, little of the data agree and no clear picture of the interactions between CO_2 vapor and molten silicates has emerged.

There have been a number of motivations behind obtaining data of this sort. First, solubility data ultimately provide upper limits to the amounts of carbon dioxide contained in evolving magmas. There is, however, little reason to suspect that magmas are ordinarily saturated with CO_2 vapor in the range of pressures and temperatures associated with most experimental studies (10-40 kbar, 1250-1750°C), although a saturated state is probably reached at pressures approaching 1 atm. (e.g., Moore, 1979). This minimizes the importance of the absolute values of carbon dioxide solubilities in melts equilibrated at high pressures. However, information on the dependence of carbon dioxide solubility on the pressure and temperature of melt equilibration may provide some insight into the mechanism of carbon dioxide dissolution, into the nature of carbon dioxide evolution and degassing during magmatic ascent, and into the structures and properties of silicate melts (e.g., Mysen, 1976, 1977).

Techniques previously used to measure CO_2 solubilities include β-track radiography (Holloway et al., 1976; Mysen et al., 1975, 1976; Mysen, 1976; Mysen and Virgo, 1980ab), high temperature mass spectrometry (Rai et al., 1983), vacuum fusion (Pearce, 1964; Faile and Roy, 1966), gas chromatography (Strnad, 1971; Brey, 1976; Brey and Green, 1976; Mysen et al., 1976), differential thermal analysis (Eggler

and Rosenhauer, 1978), and Raman spectroscopy (Verweij et al., 1977; Sharma, 1979; Sharma et al., 1979). As discussed previously (Introduction), infrared spectroscopy offers a major advantage over most of these techniques in that it is species-specific. Infrared spectroscopy can be used to distinguish between molecules of CO_2 and CO_3^{2-} ions dissolved in a glass. It can also discriminate between dissolved carbon and CO_2 present in fluid inclusions, CO_3^{2-} ions contained in quench or alteration phases, and contaminant carbon. Since solubility studies by their nature require the study of vesicular glasses, yet are concerned only with the dissolved CO_2 content of the glasses, this is a very desirable feature. In addition, spot sizes as small as tens of microns in diameter are attainable with the FTIR. This allows the beam to be directed between bubbles or alteration phases, and permits examination of sample heterogeneity. Since fusion of the sample is not required during analysis, the possibility of reaction between species is also eliminated. It is probable that many of the discrepancies found in published CO_2 solubility data are attributable to the problems that infrared spectroscopy eliminates.

Experimental Techniques

Sample Synthesis

The synthesis of CO_2-bearing glass samples is discussed in detail in Chapter 1. For this particular study, powdered silicate starting material of approximate albite composition was synthesized by grinding and mixing Johnson-Matthey Specpure Na_2CO_3, Al_2O_3, and SiO_2 in an agate mortar for 6 hours, followed by melting at 1580°C for 12 hours in air at

1 atm. This decarbonated glass was ground under ethanol for 6 hours and dried at 850°C in air for 2 days to remove any hydrocarbon residue. A microprobe analysis of the decarbonated glass is given in Table 6; the glass is deficient in Na_2O and enriched in SiO_2 relative to stoichiometric albite, probably due to a combination of Na_2O volatilization during decarbonation and drying and SiO_2 contamination during grinding in the agate mortar. It is emphasized that the drying process was necessary to reduce the adsorbed H_2O content of the starting material. The results presented in Chapter 1 suggest that slight deficiencies in Na_2O content could affect CO_2 solubility. It is again noted that less emphasis is placed on the actual values of CO_2 reported than on the pressure and temperature dependence of CO_2 solubility in these glasses. It is doubtful that these characteristics of silicate glasses vary significantly with small changes in Na_2O content.

Bubbles from 5 μm to 100μm in diameter and presumably containing gaseous or liquid CO_2 are evident in the CO_2-saturated glasses. No quench carbonate is visible. The glasses are often yellow or blueish-orange due to the disseminated Ag and the bubbles tend to be present in streaky clusters distributed throughout the glass. The CO_2-saturated samples studied in this report are not zoned, probably due to excess CO_2 present throughout the capsule as a vapor phase at all times during melt equilibration.

The quenched glasses were sectioned by diamond saw, ground into plates 50-250 μm in thickness, polished in a slurry of Al_2O_3 and H_2O, and measured for thickness using a digital-dial indicator. They were placed on metal apertures 50-1000 μm in diameter and examined

Table 6- Average of 5 microprobe analyses of the albite glass used in this part of the study. Microprobe conditions were: 15 kV accelerating voltage; sample current: 5 nA on brass; 40-50 micron beam size. Also given is an analysis of stoichiometric albite.

	Analyzed	Ideal
Na_2O	10.38	11.82
Al_2O_3	20.43	19.44
SiO_2	69.66	68.74
TOTAL	100.47	100.00

microscopically to verify that bubbles were not present in the region of glass exposed by the aperture. In some instances, a few small (~5 μm diameter) bubbles were unavoidable, but based on the similarity of spectra of both bubbled and unbubbled regions of other glasses, these have not affected the measurements presented here.

Infrared Spectroscopy of CO_2-Saturated Glasses

Infrared spectra were obtained for this study on both the Perkin-Elmer 180 Infrared Spectrophotometer and the Nicolet Instruments 60SX Fourier Transform Infrared Spectrometer (FTIR). Both machines yield quantitatively similar results, but the FTIR is quicker and has the advantage of the smaller beam sizes (≥10 μm) previously mentioned. Infrared spectra from the FTIR were obtained using a $HgCdTe_2$ detector, KBr beamsplitter, globar source, a mirror velocity of 1.57 cm/sec., and 1012 to 8096 scans.

Typical spectra are shown in Figure 15, which shows the spectra of both a CO_2-bearing and a CO_2-free albite glass. The CO_2-free glass was synthesized at 1 atm. in air in a vertical quench furnace. The assignments of six absorption bands unique to the CO_2-bearing glass are reviewed: The first, a weak band at ~3710 cm^{-1} is tentatively attributed to a combination of the $\nu_1 + \nu_3$ modes of CO_2 dissolved in the glass in the form of molecular CO_2. The second, a broad absorption band at ~3550 cm^{-1} is attributed to the stretch of hydroxyl groups and is due to water dissolved in the glass (Stolper, 1982a). For reasons discussed previously (Chapter 1), H_2O appears to be an unavoidable consequence of the experimental technique. The sharp band at 2352 cm^{-1} is due to the

Figure 15- The upper box shows the spectra of a CO_2-bearing (top, sample # ABC-53) and CO_2-free (bottom) glass of albite composition, both scaled to a sample thickness of 45 microns. Absorption band assignments are noted. The spectra go offscale at ~1200 cm^{-1} due to the vibrations of the aluminosilicate glass matrix. The absorption band at 2287 cm^{-1} due to molecular $^{13}CO_2$ is highlighted and enlarged in the bottom box.

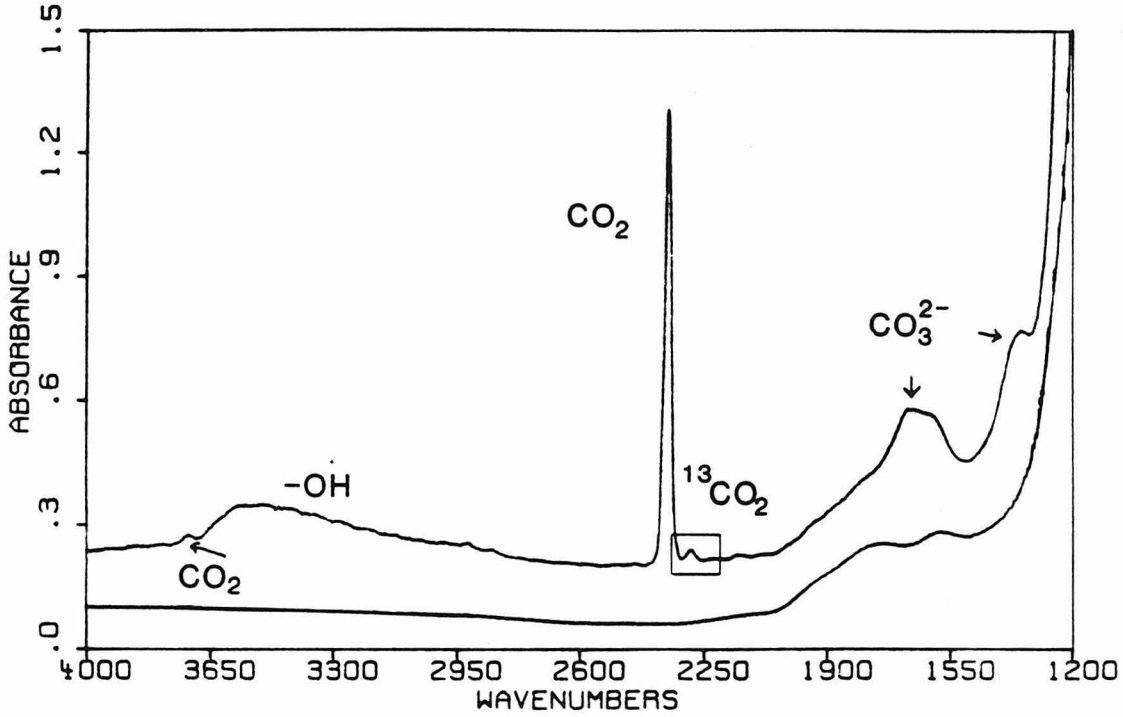
ABSORBANCE
.0
.3
.6
.9
1.2
1.5
4000
3650
3300
2950
2600
2250
1900
1550
1200
WAVENUMBERS
CO_2
CO_3^{2-}
-OH
$^{13}CO_2$
CO_2

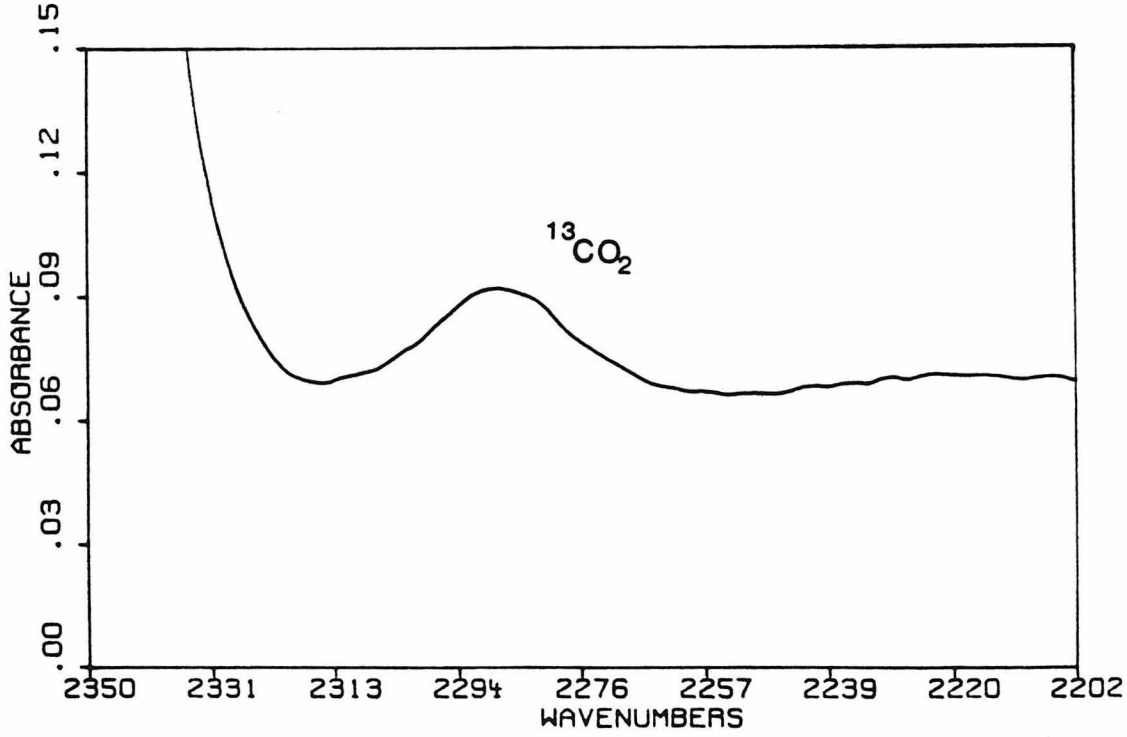
ABSORBANCE
.00
.03
.06
.09
.12
.15
2350
2331
2313
2294
2276
2257
2239
2220
2202
WAVENUMBERS
$^{13}CO_2$

ν_3 mode of CO_2 dissolved in the glass in the form of molecular $^{12}CO_2$. Another weak band at 2287 cm^{-1} is attributed to the ν_3 antisymmetric stretch of molecular $^{13}CO_2$. The absorption bands at 1610 cm^{-1} and 1375 cm^{-1} are attributed to CO_2 dissolved in sodium aluminosilicate glasses in the form of distorted CO_3^{2-} ionic-complexes.

Computer collection of the spectra presented in this chapter and in the following chapters obviated the need for digitizing spectra by hand. To determine the intensity of absorption bands for this portion of the study, the computer collected spectrum of CO_2-free glass was scaled to the thickness of each CO_2-bearing glass and computer subtracted from each spectrum of CO_2-bearing glass. This resulted in a spectrum with a relatively flat background from which the intensity of each absorption band could be simply determined. In the cases of the absorptions at 3710 cm^{-1} and 2287 cm^{-1}, background effects due to the more intense bands at 3550 cm^{-1} and 2352 cm^{-1} were estimated and subtracted by hand. These estimates were straightforward in the case of the band at 2287 cm^{-1}, but less obvious for the band at 3710 cm^{-1}. For these measurements only band heights, rather than the integrated area under bands have been determined.

In silicate glasses saturated with CO_2, the intensity of the band at 2352 cm^{-1} is usually too intense to adequately measure and characterize. This necessitated calibration of the less intense absorption band at 2287 cm^{-1} due to molecular $^{13}CO_2$. The intensity of this band has been calibrated against the intensity of the band at 2352 cm^{-1} in Figure 16, using a set of undersaturated CO_2-bearing sodium aluminosilicate glasses described in Chapter 1. Details regarding each

Figure 16- Intensity of the absorbance band at 2287 cm^{-1} versus the intensity of the absorption band at 2352 cm^{-1}. A line given by $absorbance_{2352} = 38.2\ absorbance_{2287}$ is shown for reference.

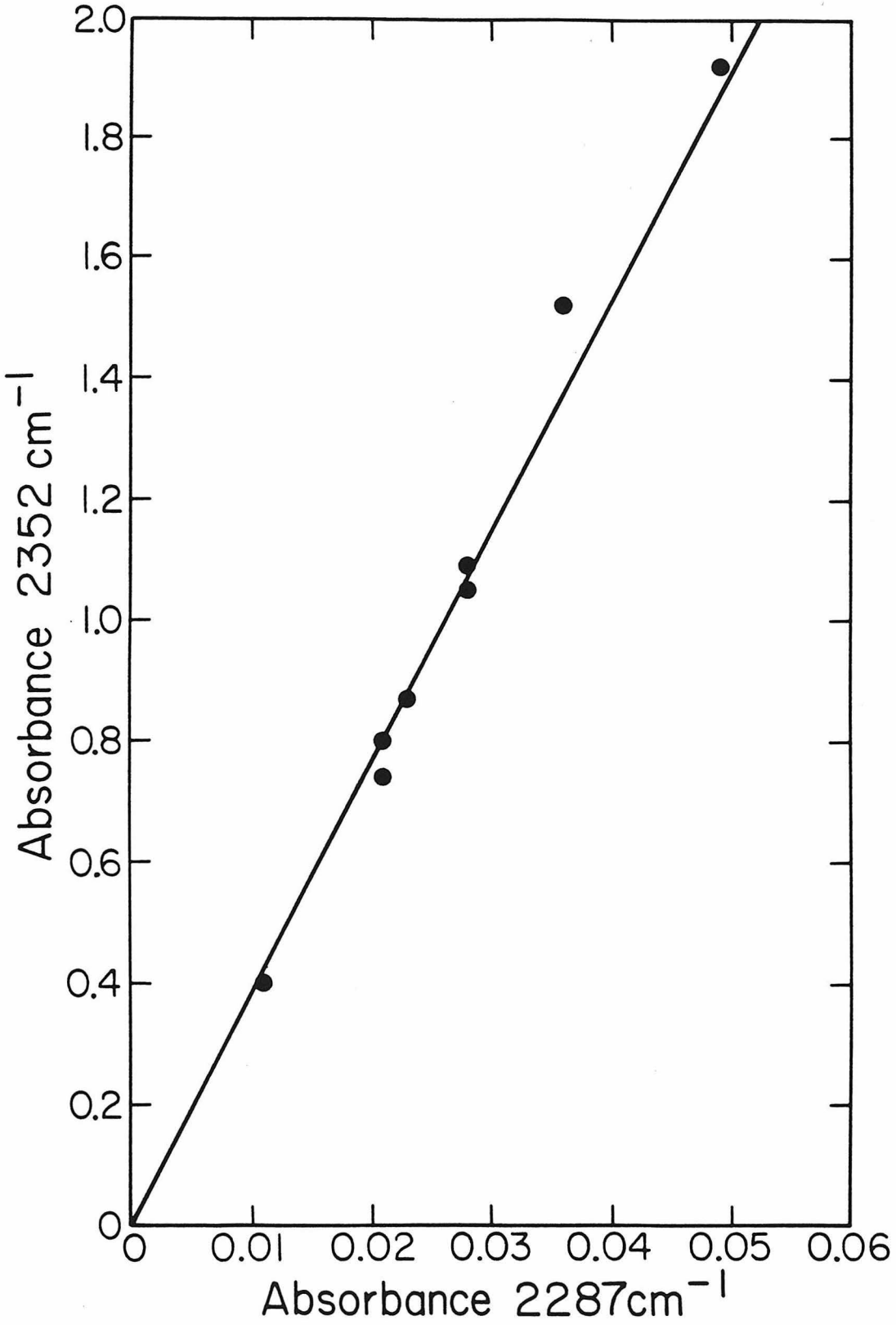
2.0
1.8
1.6
1.4
1.2
1.0
0.8
0.6
0.4
0.2
0
Absorbance 2352 cm⁻¹
0
0.01
0.02
0.03
0.04
0.05
0.06
Absorbance 2287cm⁻¹

of the samples used in the calibration are presented in Table 7. Table 7 demonstrates that absorbance$_{2352}$ = (38.2 ± 2.1) absorbance$_{2287}$. Using this ratio of absorbances and assuming ε_{2352} = 945 ± 45 liter/mole-cm, a value of ε_{2287} = 24.7 ± 1.8 liters/mole-cm is calculated. This value is used for determination of the <u>total</u> dissolved molecular CO_2 content of glasses, not simply dissolved $^{13}CO_2$ and assumes no significant variable fractionation of ^{13}C from experiment to experiment.

The band at ~3710 cm^{-1}, attributed to molecular CO_2 dissolved on the molecular scale in the glasses, could also be used to determine the molecular CO_2 content of these glasses. A preliminary calibration of the band indicates that absorbance$_{2352}$ = (47 ± 6) absorbance$_{3710}$, yielding a molar absorptivity of 20.1 ± 2.7 liters/mole-cm. The molecular CO_2 content of the saturated albite glasses was not determined from the intensity of this band, because the difficulties in background subtraction mentioned previously preclude simple determination of the intensity of this band for most of the samples.

Results

The result of the infrared measurements are presented in Table 8.

Total CO_2 solubility is shown as a function of pressure in Figure 17a. Isothermal CO_2 solubility increases dramatically with pressure over the 15-30 kbar range. There is also a positive correlation between equilibration pressure and the concentration of both molecular CO_2 and CO_3^{2-} at constant temperature (Figures 17b and 17c). At constant pressure, total CO_2 solubility in albite glasses is not a strong function of equilibration temperature, although the results suggest a

Table 7- Samples used in the calibration of the intensity of the absorption band at 2352 cm^{-1} versus the intensity of the absorption band at 2287 cm^{-1}. Sample numbers prefixed ABC are of albite ($NaAlSi_3O_8$) composition, JDC and TJ are of approximate jadeite ($NaAlSi_2O_6$) composition. None of the samples used were saturated with CO_2 except TJ-18.

Sample	Thickness (cm)	Absorbance (2352 cm^{-1})	Absorbance (2287 cm^{-1})	abs_{2352}/abs_{2287}
ABC 53	0.0045	1.09	0.028	38.9
ABC 54	0.0057	0.74	0.021	35.2
ABC 58	0.0075	1.05	0.028	37.5
JDC 103	0.0069	0.87	0.023	37.8
JDC 108	0.0036	0.80	0.021	38.1
JDC 111	0.0113	0.40	0.011	36.4
JDC 112	0.0141	1.52	0.036	42.2
TJ 18	0.0105	1.92	0.049	39.2
AVG.				38.2 ± 2.1^a

[a] 1 standard deviation.

Table 8- Data obtained from CO_2-saturated albite glasses.

Sample	P (kbar)	T (°C)	Duration (min.)	Density[a] (g/l)	Band (cm^{-1})	Abs.	Thickness (cm)	Band (cm^{-1})	Abs.	Thickness (cm)	Band (cm^{-1})	Abs.	Thickness (cm)	Molecular CO_2 (wt.%)	CO_3^{2-}[b] (wt.%)	Total CO_2 (wt.%)	$\frac{CO_2}{CO_3^{2-}}$	H_2O[c] (wt.%)
41	15	1450	65	2445	3516	0.81	0.0118	2287	0.032	0.0052	1597	0.26	0.0118	0.45	0.20	0.65	2.26	0.63
42	15	1525	62	2445	3522	1.17	0.0115	2287	0.069	0.0150	1598	0.38	0.0150	0.34	0.23	0.56	1.47	0.94
37	20	1450	60	2510	3517	0.66	0.0092	2287	0.071	0.0092	1600	0.27	0.0088	0.55	0.27	0.82	2.04	0.64
48	20	1450	60	2510	3520	0.06	0.0052	2288	0.078	0.0052	1600	0.16	0.0052	0.53	0.27	0.80	1.96	0.10
4	20	1525	100	2510	3534	0.53	0.0116	2285	0.084	0.0116	1600	0.37	0.0116	0.51	0.28	0.79	1.82	0.41
5	20	1650	60	2510	3540	0.41	0.0130	2288	0.078	0.0130	1605	0.43	0.0130	0.43	0.29	0.72	1.47	0.28
12	25	1450	60	2530	3552	0.37	0.0095	2286	0.096	0.0095	1610	0.44	0.0095	0.71	0.40	1.11	1.77	0.35
15	25	1525	65	2530	3518	1.10	0.0098	2287	0.090	0.0098	1598	0.46	0.0098	0.65	0.41	1.06	1.58	1.00
36	25	1650	60	2530	3524	0.39	0.0062	2288	0.054	0.0062	1609	0.32	0.0062	0.61	0.45	1.06	1.37	0.56
43	30	1450	60	2535	3514	0.55	0.0092	2287	0.109	0.0092	1615	0.64	0.0092	0.83	0.60	1.44	1.38	0.53
40	30	1525	90	2535	3495	1.17	0.0116	2288	0.120	0.0116	1631	0.93	0.0116	0.73	0.70	1.42	1.04	0.90
39	30	1650	70	2535	3518	0.87	0.0112	2287	0.108	0.0112	1600	0.94	0.0112	0.68	0.73	1.41	0.93	0.69

[a] Densities estimated from Kushiro (1978).

[b] CO_3^{2-} concentrations are expressed as wt.% CO_2.

[c] H_2O contents obtained using the method of Stolper (1982a) and a molar absorptivity of 80 liters/mole-cm.

Figure 17- Total CO_2 (a), molecular CO_2 (b), and CO_3^{2-} (c) concentration versus pressure. The temperature of melt equilibration is listed for each set of runs and is also indicated by triangles (1450°C), circles (1525°C), and squares (1625°C). For clarity, only sample #37 is shown at 1450°C, 20 kbar.

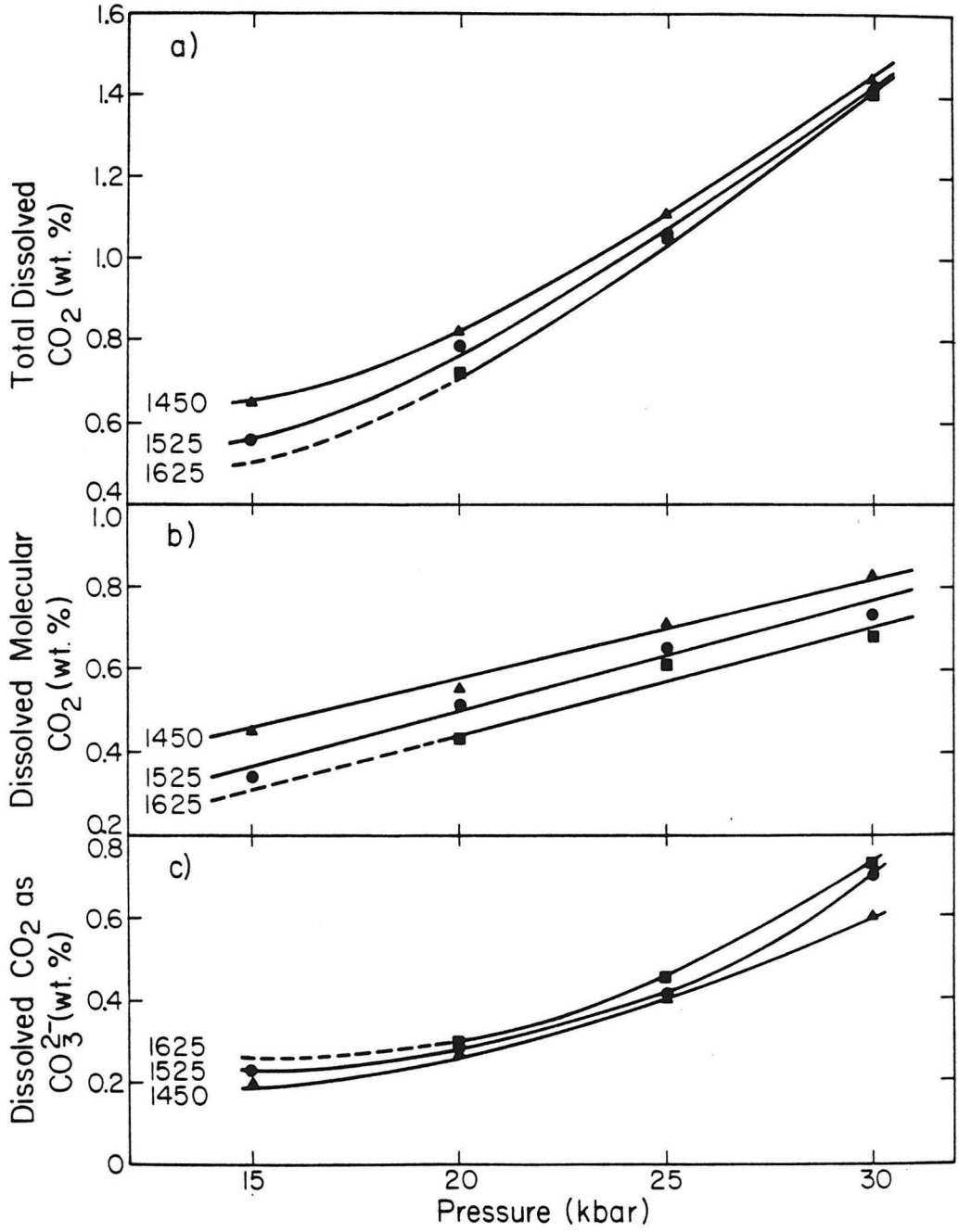
a)
b)
c)
Total Dissolved CO_2 (wt. %)
Dissolved Molecular CO_2 (wt. %)
Dissolved CO_2 as CO_3^{2-} (wt. %)
1450
1525
1625
Pressure (kbar)
15
20
25
30
0
0.2
0.4
0.6
0.8
1.0
1.2
1.4
1.6

slight negative temperature dependence of CO_2 solubility over the 1450-1625°C temperature range (Figure 18a). Within the precision of the analyses, this temperature effect may be negligible, rather than negative. The concentration of molecular CO_2 decreases with increasing temperature at constant pressure; this effect is largely counterbalanced by a positive correlation between equilibration temperature and CO_3^{2-} concentration (Figures 18b and 18c)

Molecular CO_2/CO_3^{2-} ratios are plotted as functions of pressure and temperature in Figures 19a and 19b. The ratio is dependent on both pressure and temperature of melt equilibration and generally decreases both with increasing pressure and increasing temperature. This slight variation is comparable with the range for albite glasses reported in Chapter 1 and is not of the magnitude reported by Mysen (1976).

The water contents of all of the run products are disturbingly high. The possible sources of this water in these nominally anhydrous runs are discussed at length in Chapter 1. The belief that it is unavoidable in piston-cylinder experiments due to a combination of adsorbed water on our starting materials and diffusion of hydrogen into the capsules during run conditions is reiterated. It is doubtful that previous studies of CO_2 solubility using analogous methods of glass preparation have had more success establishing anydrous conditions.

While previous workers have suggested that H_2O would increase the solubility of CO_2 in silicate melts (e.g., Mysen, 1976; Eggler and Rosenhauer, 1978), there is no apparent correlation between H_2O content and CO_2 solubility. It is noted that two glasses equilibrated at the same pressure and temperature (#37 and #48, Table 3) contain different

Figure 18- Total CO_2 (a), molecular CO_2 (b), and CO_3^{2-} (c) concentration versus temperature for the glasses studied. The pressure of melt equilibration for each set of runs is also listed. For clarity, only sample #37 is shown at 1450°C, 20 kbar.

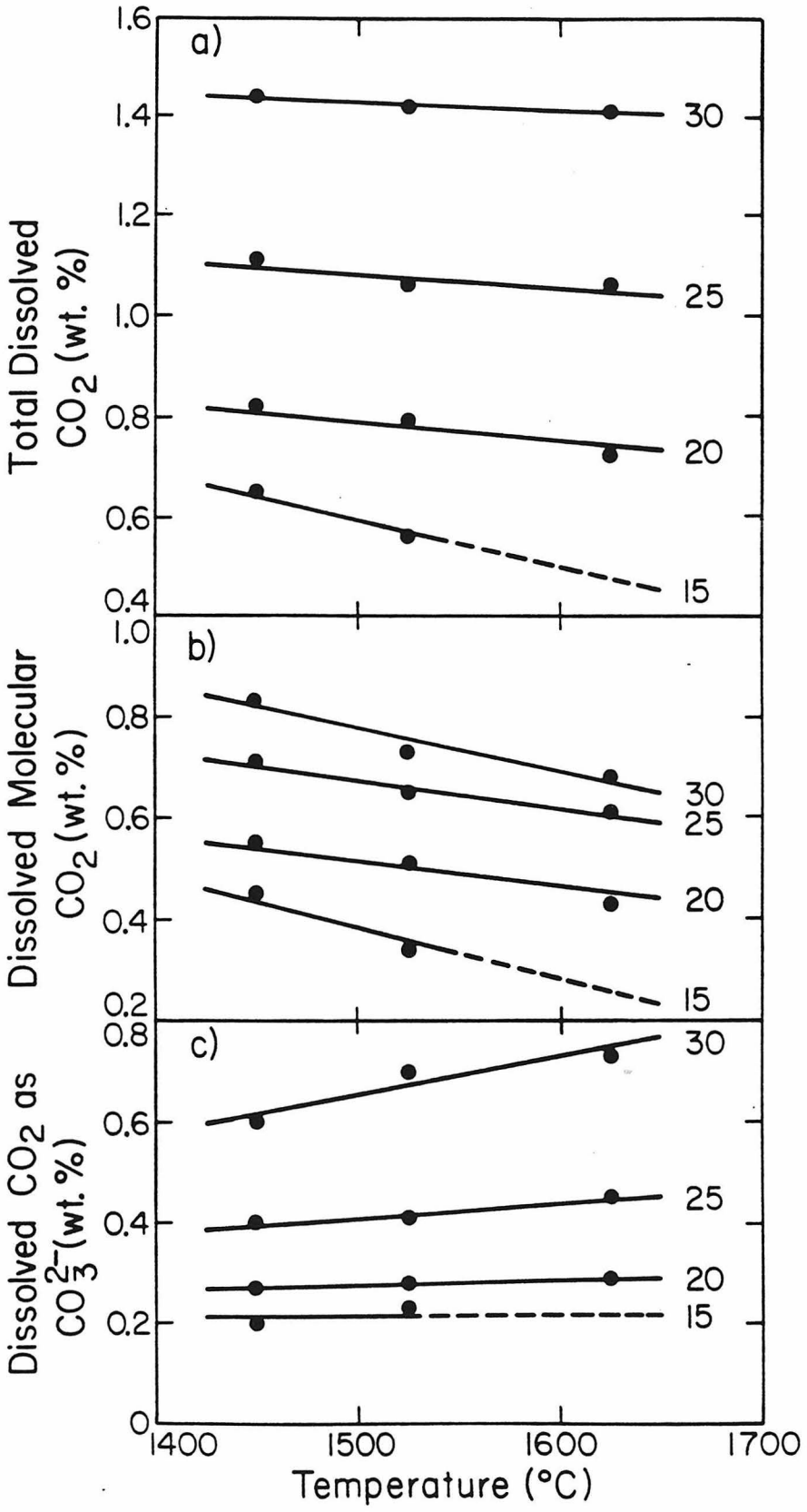
a)
b)
c)
Total Dissolved CO_2 (wt. %)
Dissolved Molecular CO_2 (wt. %)
Dissolved CO_2 as CO_3^{2-} (wt. %)
30
25
20
15
1.6
1.4
1.2
1.0
0.8
0.6
0.4
0.2
0
1400
1500
1600
1700
Temperature (°C)

Figure 19- Molecular CO_2/CO_3^{2-} ratios versus temperature (a) and pressure (b). Temperature is again indicated in (b) by triangles (1450°C), circles (1525°C), and squares (1625°C). The 15 kbar, 1525°C data point might be inconsistent with the rest of the data and is shown by a dashed circle in both figures.

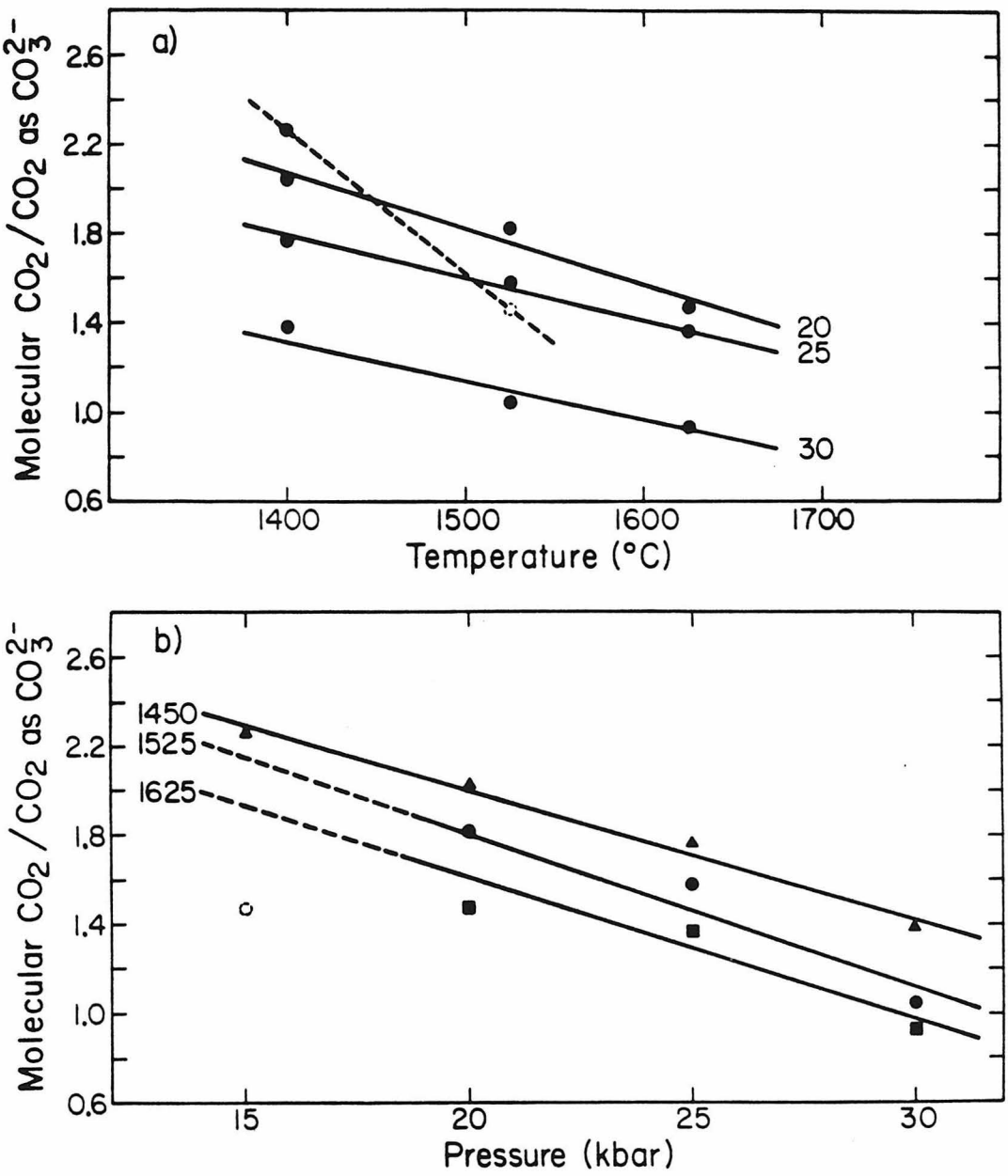
a)
Molecular CO_2/CO_2 as CO_3^{2-}
2.6
2.2
1.8
1.4
1.0
0.6
1400
1500
1600
1700
Temperature (°C)
20
25
30
b)
1450
1525
1625
15
20
25
30
Pressure (kbar)

amounts of dissolved water (0.64 wt.% and 0.10 wt.%, respectively), yet their dissolved molecular CO_2 and CO_3^{2-} contents, and hence their total dissolved CO_2 contents (0.82 wt.% and 0.80 wt.%, respectively), are essentially the same.

Comparison with Previous Results

Mysen et al. (1976), Mysen (1976), Mysen and Virgo (1980b) and Brey (1976) studied the solubility of CO_2 in albite glasses. The first three studies used β-track radiography to find a positive temperature and pressure dependence of CO_2 solubility in the 10-30 kbar; 1450-1750°C ranges. The latter study, on the basis of gas chromatography, inferred a negligible or slightly negative temperature dependence for CO_2 solubility over a comparable range of pressures and temperatures.

The results agree with the Mysen studies in many ways. The absolute CO_2 solubilities are similar to those reported by Mysen (1976). Compare, for example, 1.44 wt.% CO_2 at 30 kbar, 1450°C with Mysen's (1976) 1.6 wt.% CO_2 and Brey's (1976) 2.1 wt. % CO_2 at the same pressure and temperature. The results also confirm the strong positive pressure dependence of CO_2 solubility found by Mysen (1976). Note, however, that there is no evidence for a strong positive temperature dependence of CO_2 solubility found in this study, but there is evidence for a slight negative temperature dependence, in accord with the inference of Brey (1976).

Studies of the temperature dependence of CO_2 solubility in other silicate compositions have also contradicted the data produced by β-track radiography. Rai et al. (1983) used high temperature mass

spectrometry and Sharma (1979) used Raman spectroscopy to find a slight negative temperature dependence of CO_2 solubility in melts of diopside composition at 20 kbar, 1550-1725°C. Brey (1976) found a slight negative temperature dependence on CO_2 solubility in olivine melilite melt at 30 kbar, 1450-1650°C. In addition, although there are no comparable β-track studies, Pearce (1964) used a vacuum fusion technique to find a strong negative temperature dependence of CO_2 solubility in sodium silicate melts at 1 atm. CO_2 pressure. Faile and Roy (1966) also report a negligible temperature dependence of CO_2 solubility in potassium silicate glasses to 10 kbar pressure. While I can make no firm assessment of the reasons for the discrepancies between the results produced by β-track radiography and the results produced by all other techniques (see Rai et al., 1983 or Tingle, 1985), I must again arrive at the conclusion that aspects of the results produced by β-track radiography are suspect.

Conclusions

1. In CO_2-saturated albite glasses equilibrated at constant temperature, both molecular CO_2 and CO_3^{2-} concentrations increase with increasing pressure. The ratio of molecular CO_2 to CO_3^{2-} decreases slightly with increasing pressure.
2. In CO_2-saturated albite glasses equilibrated at constant pressure, the concentration of molecular CO_2 decreases with increasing equilibration temperature while the CO_3^{2-} concentration increases; the net effect is a slight decrease in total CO_2 content with increasing temperature at constant pressure

Chapter 3. The Speciation of Carbon Dioxide in Ca ± Mg Silicate Glasses

The dissolution of CO_2 as both molecular CO_2 and CO_3^{2-} is a characteristic not only of the sodium aluminosilicate glasses discussed in the last two chapters, but of many aluminosilicate glasses dominated by cations with a +1 valence state (e.g., orthoclase glass, Figure 20). Preliminary work has also indicated that natural rhyolitic glasses contain dissolved molecular CO_2 (Figure 21). This could be the consequence of a number of factors discussed below (Chapter 4), but is probably due in large part to similarities in structure between these glasses, all of which are probably nearly fully polymerized (Chapter 1), with monovalent cations providing charge balance for aluminum in the glass framework.

Previous work (e.g., Brey, 1976; Mysen and Virgo, 1980ab; Rai et al., 1983) has indicated that the speciation of dissolved CO_2 in glasses rich in divalent cations (such as Ca^{2+} or Mg^{2+}) is quite different from the speciation of CO_2 in sodium aluminosilicate glasses. This chapter explores these differences in detail.

Synthesis of CO_2-Bearing Glass Standards

Three starting compositions were used: di, $CaMgSi_2O_6$; anc, a calcium aluminosilicate composition near the 1 atm. anorthite-tridymite-wollastonite eutectic with approximately the chemical formula $CaAl_{0.8}Si_{2.9}O_8$; and 519B, natural basaltic glass ALV-519-4-1 from the FAMOUS region of the mid-Atlantic Ridge. The first two compositions were prepared by mixing and grinding appropriate amounts of Johnson-Matthey Specpure $CaCO_3$, SiO_2, and Al_2O_3 or MgO in agate under ethanol; the third was prepared by grinding selected chips of ALV-519-4-1 under

Figure 20- Infrared spectrum of a 39 micron thick piece of orthoclase glass (ORC-3) containing 0.38 wt.% CO_2, as measured into the Pt capsule. Tentative band assignments are shown. The glass was equilibrated at 1700°C and 20 kbar for 1 hour using the techniques described in Chapter 1.

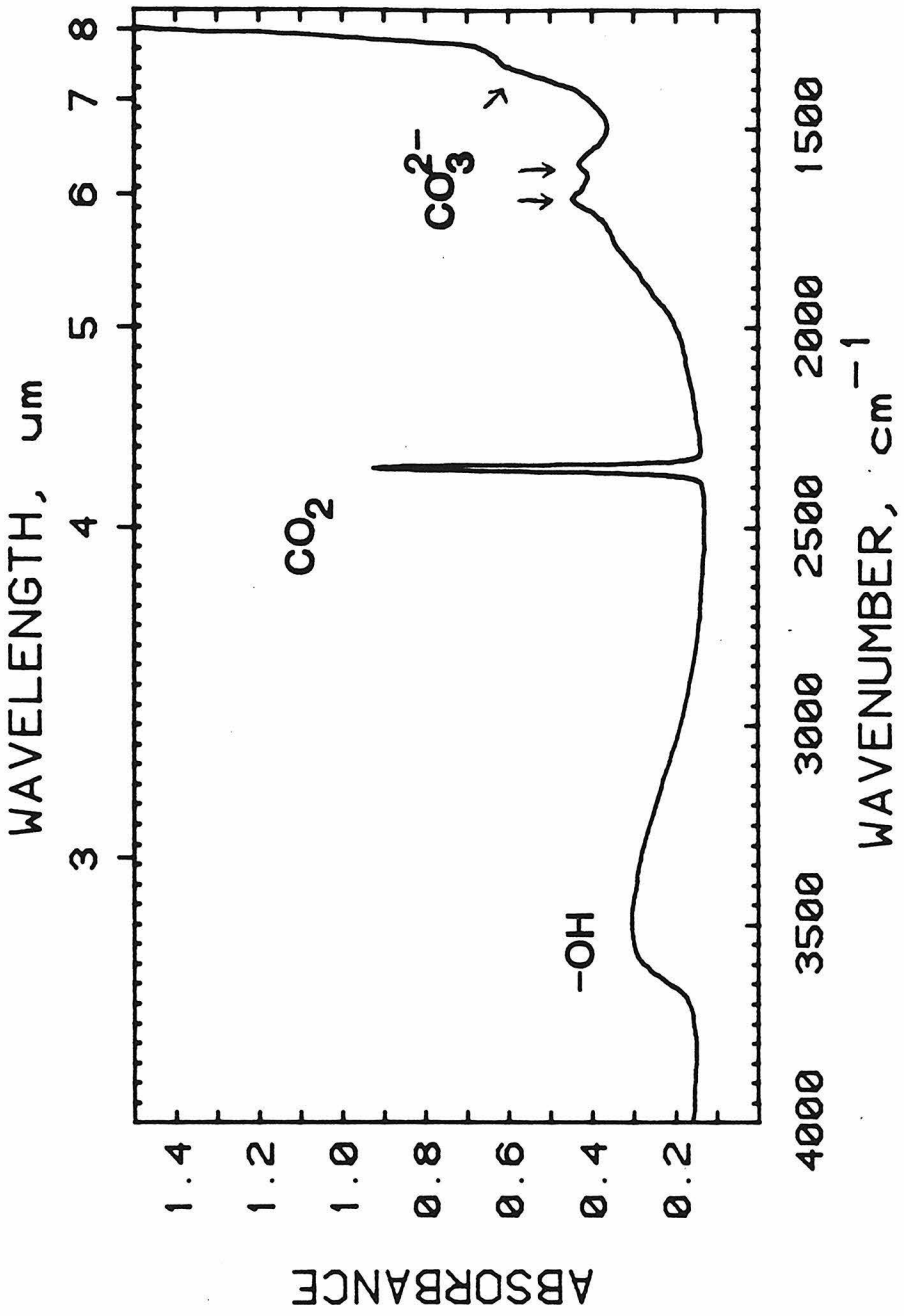
WAVELENGTH, um
3
4
5
6
7
8
4000
3500
3000
2500
2000
1500
WAVENUMBER, cm^{-1}
ABSORBANCE
0.2
0.4
0.6
0.8
1.0
1.2
1.4
CO_2
CO_3^{2-}
-OH

Figure 21- Infrared spectrum of a 33 micron thick piece of rhyolite glass (KS-2) containing 0.43 wt.% CO_2 as measured into the Pt capsule. Tentative band assignments are shown. The glass was equilibrated at 1550°C and 25 kbar for 1 hour using the techniques disussed in Chapter 1.

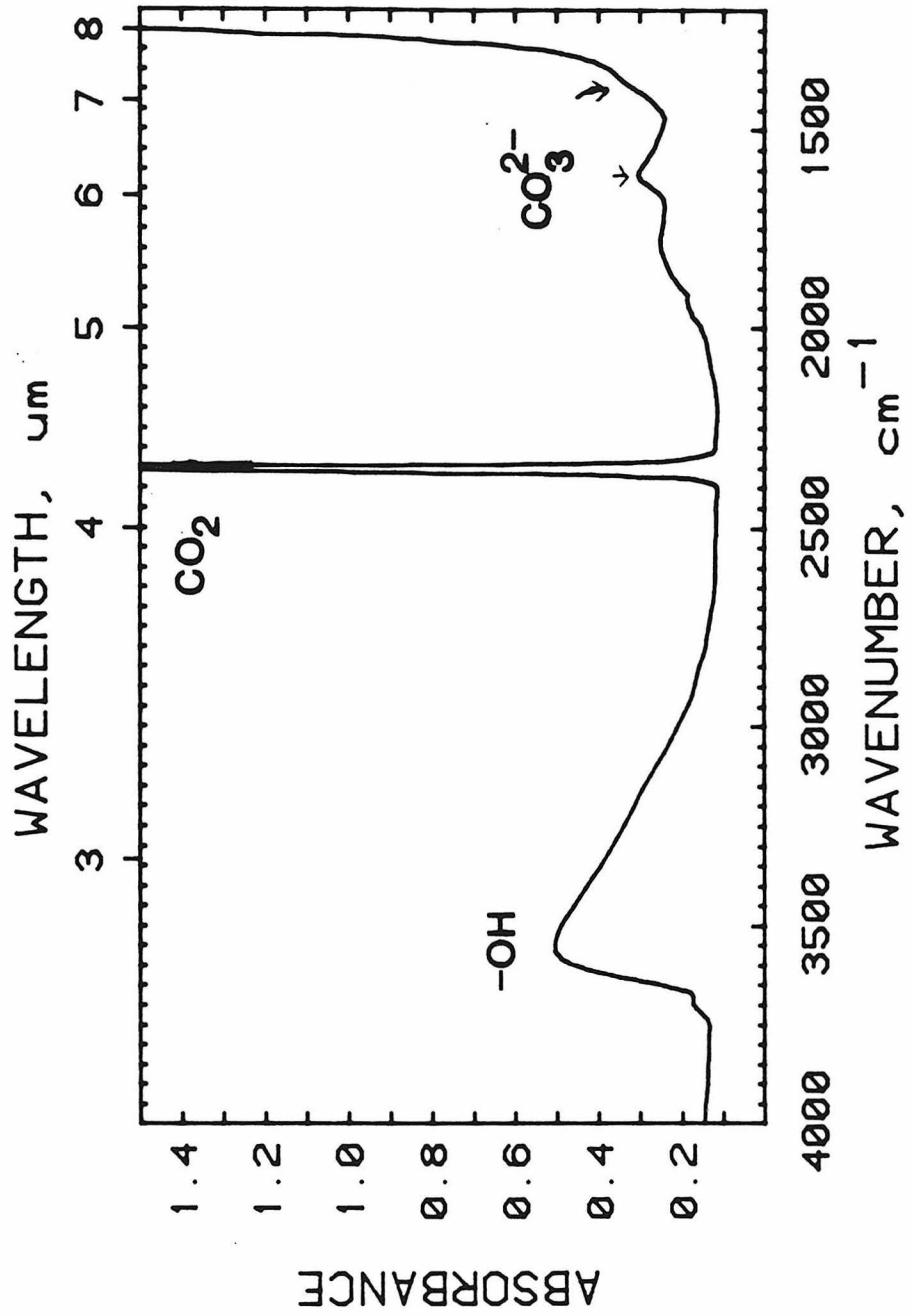
WAVELENGTH, um
3
4
5
6
7
8
4000
3500
3000
2500
2000
1500
WAVENUMBER, cm^{-1}
ABSORBANCE
1.4
1.2
1.0
0.8
0.6
0.4
0.2
CO_2
CO_3^{2-}
-OH

similar conditions. The chips were free of alteration, contained less than 5% phenocrysts by volume, and were ultrasonically cleaned in dilute HCl before grinding. All three compositions were then held at 800-850°C for 12-24 hours: di and anc in air, 519B in a CO_2-H_2 mixture giving an f_{O_2} approximately at the QFM buffer. This heat treatment resulted in decarbonation, dehydration and crystallization or recrystallization of the starting compositions, which were then stored over dessicant.

Major element analyses of one or more glasses of each composition studied were obtained using the MAC-5 electron microprobe with a 15 kV operating voltage, a sample current of 5 nA on brass and a 40-50 micron beam size (Table 9).

Pt capsules used for experiments with the 519B composition had been pre-doped with Fe to reduce Fe loss from the 519B melts during run conditions. To pre-dope the capsules, they were filled with glass of 519B composition and held for 24 hours at 1580°C and the QFM buffer at 1 atm. The silicate glass was removed using HF and these capsules were reloaded with silicate and $Ag_2C_2O_4$. This technique effectively eliminated loss of Fe (Table 9).

In all cases, the melts quenched to glass. None of the synthetic glasses was saturated with CO_2 vapor and no bubbles or inclusions were noted. Some high pressure runs were done without added silver oxalate in order to synthesize CO_2-free glasses. Anhydrous, decarbonated glasses of each composition were also synthesized at 1 atm. on Pt loops: anc and di at 1450°C in air, 519B at 1315°C at the QFM buffer. The infrared spectra of these glasses did not differ from the spectra of glasses synthesized at high pressure without added $Ag_2C_2O_4$.

Table 9- Microprobe analyses of glass compositions used for piston-cylinder runs. The 519B analysis given is of glass run in an Fe-doped capsule (519B-5). Ideal analyses of the anc and dic compositions and an analysis of natural 519B glass are also included. Microprobe techniques are described in the text.

	ANC	Ideal	DIC	Ideal	519B	Natural[a]
Na_2O	--	--	--	--	2.30	2.13
MgO	--	--	17.52	18.62	10.76	10.15
Al_2O_3	14.22	14.40	--	--	15.83	16.44
SiO_2	61.67	62.35	55.07	55.49	47.77	49.07
K_2O	--	--	--	--	0.10	0.07
CaO	23.02	23.25	25.68	25.89	11.40	11.65
TiO_2	--	--	--	--	0.73	0.74
Cr_2O_3	--	--	--	--	0.10	0.03
MnO	--	--	--	--	0.16	0.16
FeO[b]	--	--	--	--	8.52	8.86
TOTAL	98.91	100.00	98.27	100.00	97.67	99.45
DENSITY (g/l)	2590		2820		2790	

[a]Glass analysis from Bryan and Moore (1977)

[b]All Fe reported as FeO.

Two synthetic glasses provided by Dr. S. Sharma were also used in this study: a $CaMgSi_2O_6$ + CO_2 glass (Di #89; Sharma et al., 1979) and a $Ca_2MgSi_2O_7$ + CO_2 glass (Ak #51; Rai et al., 1983). $CaCO_3$ was used as a CO_2 source for both runs, which were saturated with CO_2-rich vapor.

Results

Band Assignments and Intensities

Figure 22 shows the spectra of both a CO_2-bearing and a CO_2-free glass of anc composition. Three absorption bands are observed in the CO_2-bearing anc glass that are not present in the CO_2-free sample. Both spectra go offscale at approximately 1200 cm^{-1} due to vibrations of the aluminosilicate glass matrix. In Figure 23, a portion of the spectrum of a CO_2-bearing anc glass after subtraction of the CO_2-free anc glass spectrum is shown. This spectrum is overlain by the spectrum of $NaAlSi_2O_6$ + CO_2 glass discussed in Chapter 1. The three absorption bands evident in the $NaAlSi_2O_6$ + CO_2 glass spectrum were shown to be characteristic of all $NaAlSi_2O_6$-SiO_2-CO_2 glasses.

The spectrum of the anc + CO_2 glass (Figures 22 and 23) has absorption bands at 1515 cm^{-1} and 1435 cm^{-1}. These bands are considered to be analogous to the bands in the spectrum of $NaAlSi_2O_6$ + CO_2 glass (Figure 23) at 1610 cm^{-1} and 1375 cm^{-1}. Like the latter bands, the bands in the anc + CO_2 spectrum are always approximately equal in intensity regardless of total dissolved CO_2 content or total dissolved H_2O (Figure 24).

Recall that the bands at 1610 cm^{-1} and 1375 cm^{-1} in the $NaAlSi_2O_6$ + CO_2 spectrum were assigned to the ν_3 antisymmetric stretch of distorted

Figure 22- Infrared spectra of ANC-10 (solid), containing 0.61% dissolved CO_2, and a CO_2-free anc glass synthesized at 1 atm (ANC-BL, dashed). Both spectra have been scaled to 42 microns sample thickness. Aluminosilicate vibrations cause the spectra to go offscale at ~1200 cm^{-1}.

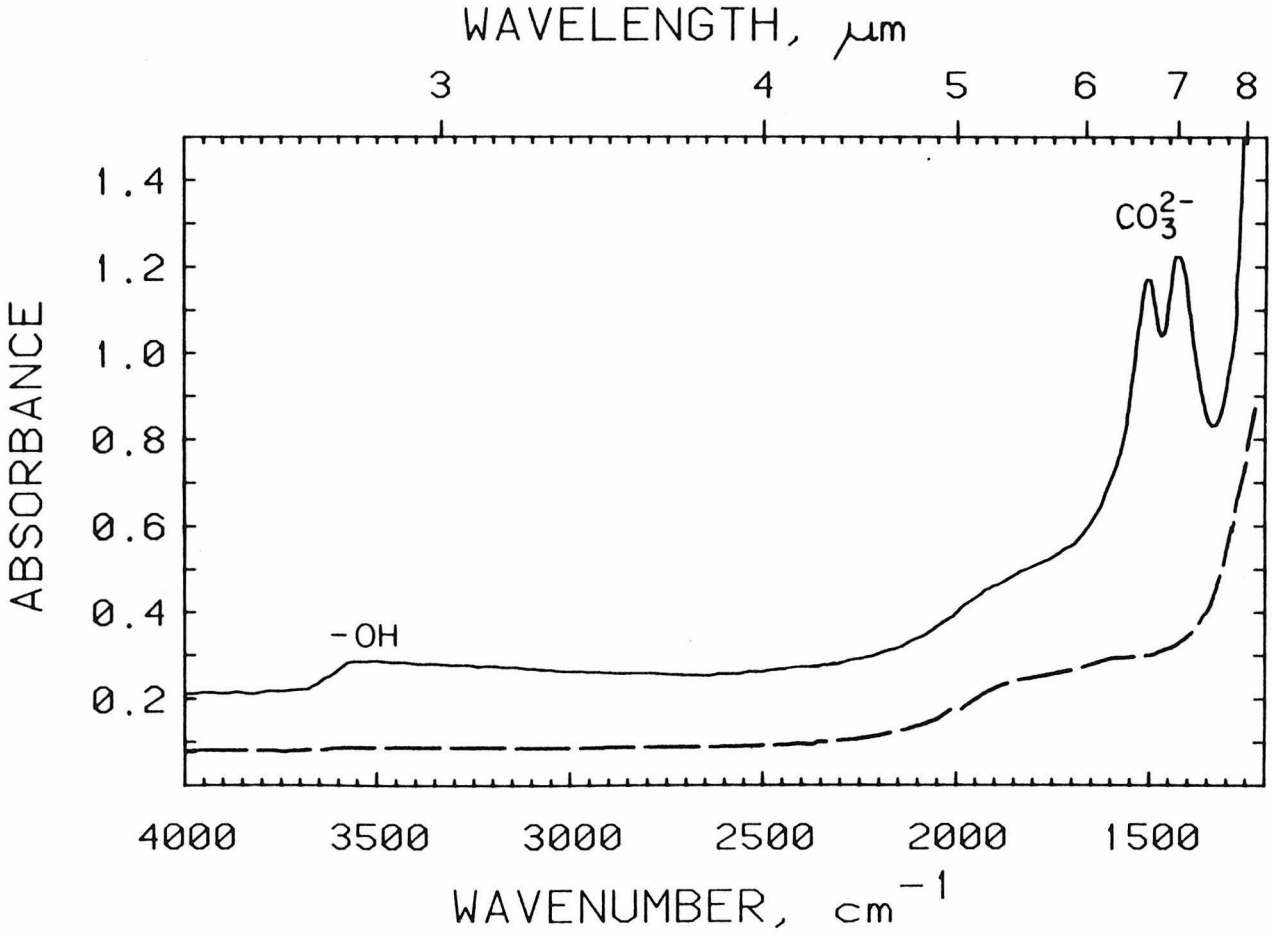
WAVELENGTH, μm
3
4
5
6
7
8
ABSORBANCE
1.4
1.2
1.0
0.8
0.6
0.4
0.2
CO_3^{2-}
-OH
4000
3500
3000
2500
2000
1500
WAVENUMBER, cm^{-1}

Figure 23- Background subtracted spectra of ANC-9 glass (dashed) containing 0.12 wt.% dissolved CO_2 and a jadeite composition glass (solid, JDC-84) containing 0.80 wt.% dissolved CO_2 as measured by infrared spectroscopy.

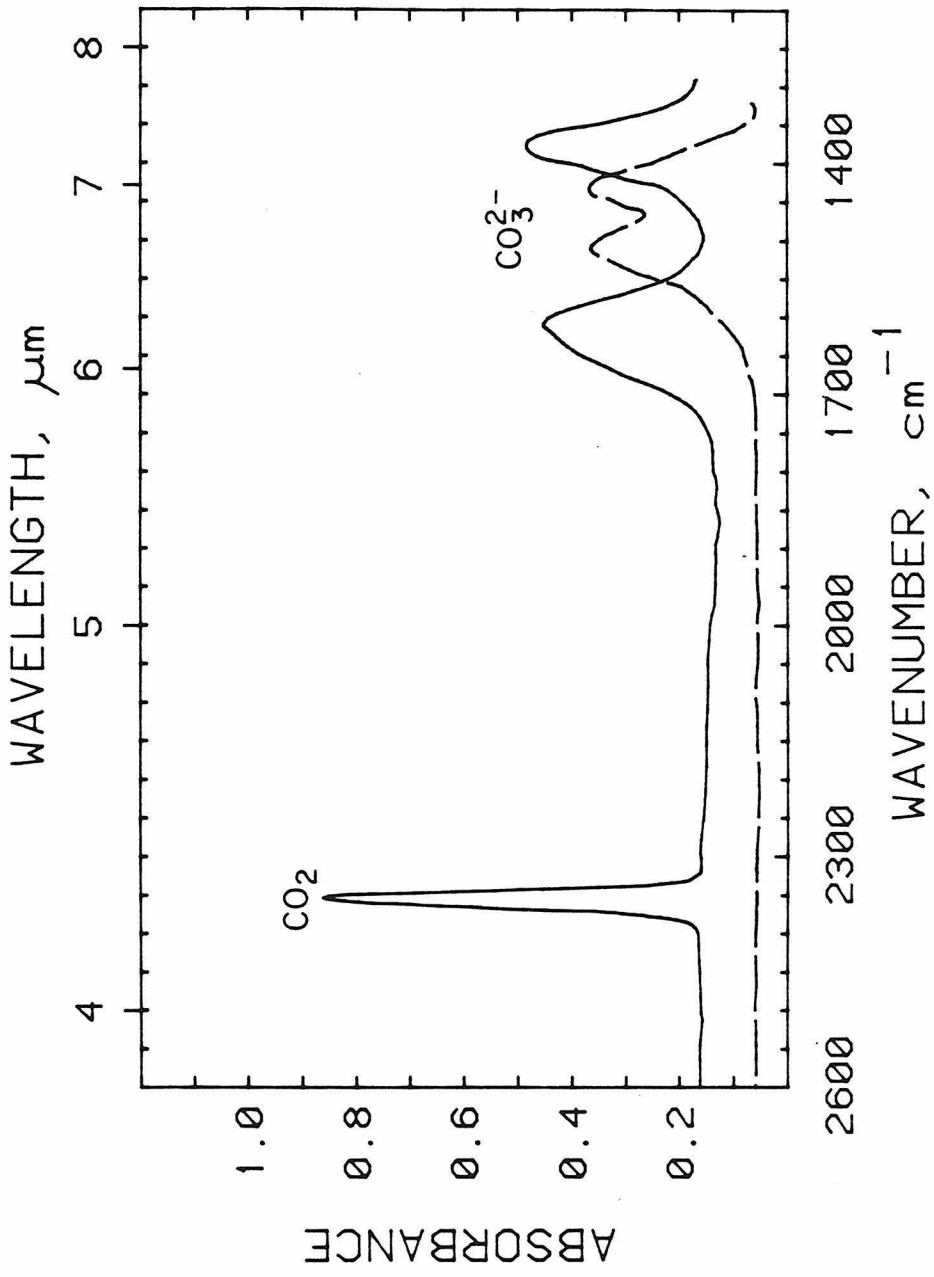
WAVELENGTH, μm
4
5
6
7
8
WAVENUMBER, cm⁻¹
2600
2300
2000
1700
1400
ABSORBANCE
1.0
0.8
0.6
0.4
0.2
CO2
CO3 2-

Figure 24- Intensity of the carbonate absorption band at 1515 cm^{-1} versus the intensity of the carbonate absorption band at 1435 cm^{-1} for synthetic Ca ± Mg silicate glasses. Open circles are data from glasses of anc composition; filled circles are di composition; filled squares are 519B composition.

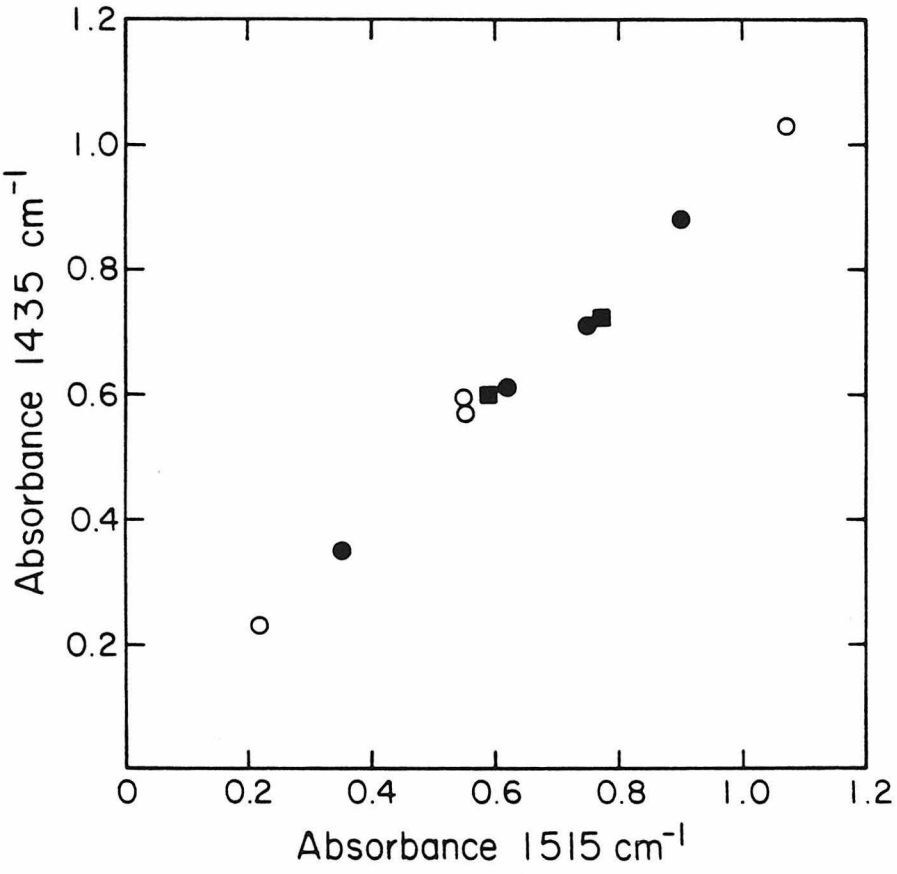
1.2
1.0
0.8
0.6
0.4
0.2
0
0.2
0.4
0.6
0.8
1.0
1.2
Absorbance 1435 cm⁻¹
Absorbance 1515 cm⁻¹

Na-carbonate ionic complexes. The bands at 1515 cm^{-1} and 1435 cm^{-1} in the spectrum of anc + CO_2 glass are also assigned to the antisymmetric stretch of distorted CO_3^{2-} groups. Similar assignments have been made previously in some infrared (Brey and Green, 1975) and Raman (Sharma , 1979; Sharma et al., 1979; Mysen and Virgo, 1980ab) studies of Ca ± Mg-bearing glasses. However, in some studies of CO_2-bearing Ca-rich silicate glasses, the high energy band at 1515 cm^{-1} has either not been identified (Mysen et al., 1975, 1976; Eggler et al., 1979) or has been attributed to a second structural site for CO_3^{2-} in the glass that differs from that of the CO_3^{2-} producing the low-energy band (Rai et al., 1983). It is reiterated that this splitting mimics to within a few wavenumbers the splitting observed in the infrared spectrum of scapolite, a mineral that contains distorted CO_3^{2-} groups. Note that Ca^{+2} is associated with the CO_3^{2-} groups in scapolite (Papike and Stephenson, 1966; Chamberlain et al., 1985).

Figure 25 shows infrared spectra typical of synthetic CO_2-bearing glasses of anc, di and 519B compositions. All display absorption bands centered at ~1515 cm^{-1} and ~1435 cm^{-1} despite the compositional differences between glasses. The same splitting is observed in the diopside and akermanite glasses provided by Dr. S. Sharma (Sharma, 1979; Sharma et al., 1979; Rai et al., 1983). Figures 26 and 27 show that the same doublet is observed in natural basaltic glasses, although the intensities are more than an order of magnitude lower. It is likely that the distinctive splitting of the carbonate band observed in all of these glasses is characteristic of metal-carbonate ionic-complexes in which the metal cation is Ca (and/or Mg), based on the striking contrast

Figure 25- Infrared spectra, from 2000 cm^{-1} to 1200 cm^{-1}, of 519B-6, DIC-8, and ANC-10. Sample thicknesses are noted in Table 10.

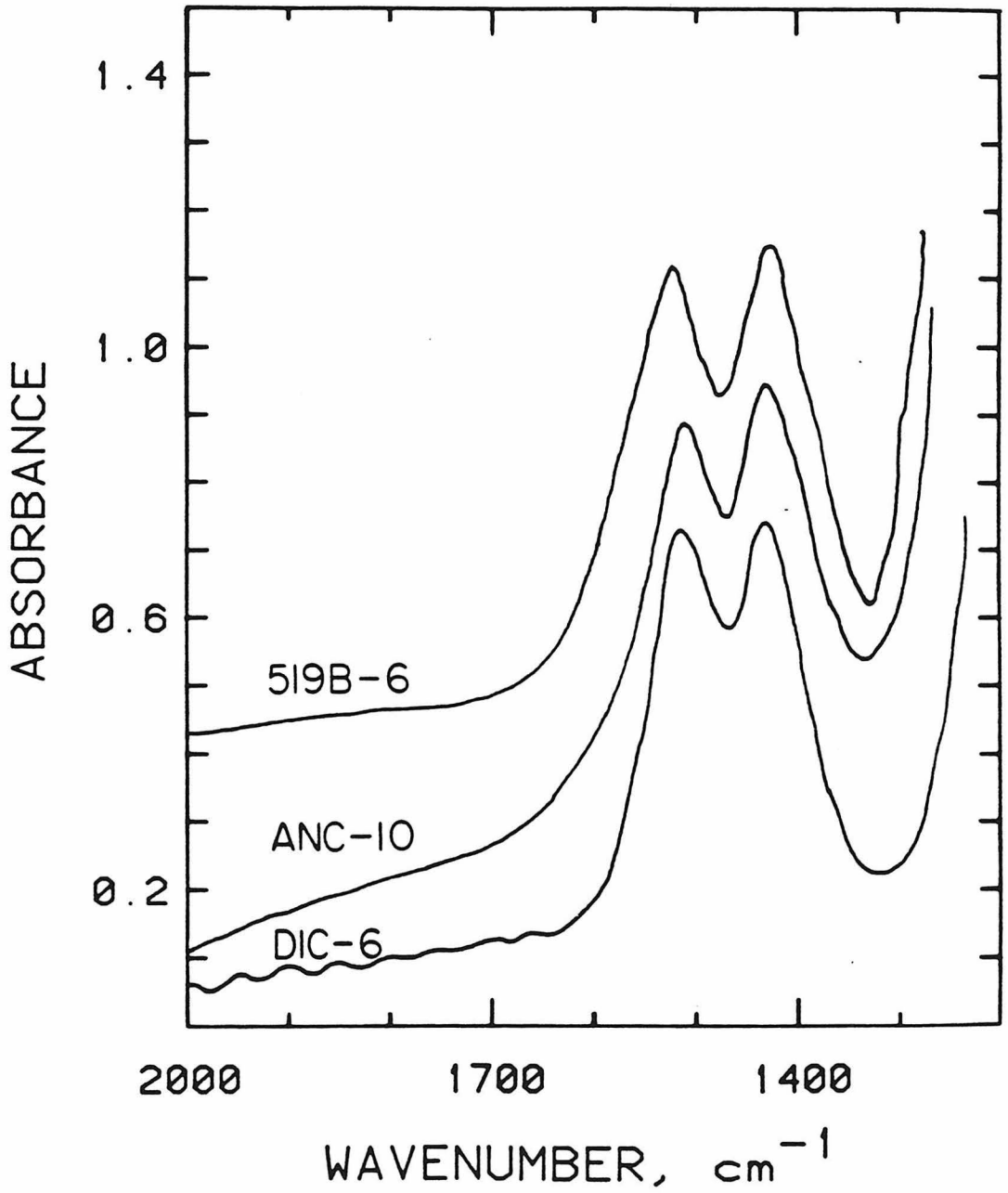
1.4
1.0
0.6
0.2
ABSORBANCE
519B-6
ANC-10
DIC-6
2000
1700
1400
WAVENUMBER, cm⁻¹

Figure 26- Infrared spectrum, from 2000 cm^{-1} to 1200 cm^{-1}, of a 150 micron thick piece of basaltic glass TT152 29-1 from the Juan de Fuca Ridge. Absorption bands at 1515 cm^{-1} and 1435 cm^{-1} due to dissolved carbonate are evident.

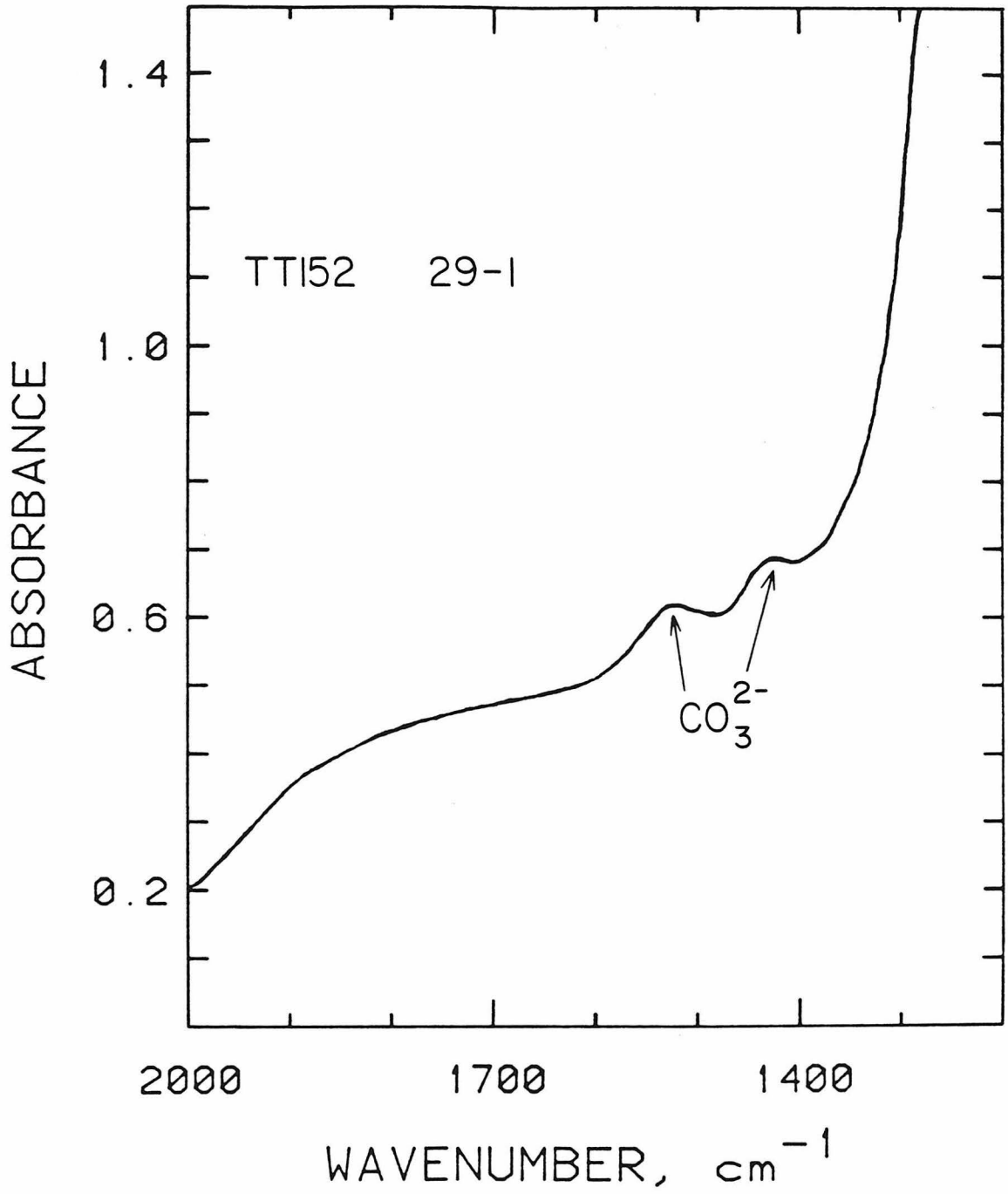
1.4
1.0
0.6
0.2
ABSORBANCE
TT152 29-1
CO_3^{2-}
2000
1700
1400
WAVENUMBER, cm^{-1}

Figure 27- Background subtracted infrared spectra, from 1700 cm^{-1} to 1350 cm^{-1} of synthetic glass 519B-6 (top, 59 microns sample thickness) and natural glass ALV519-4-1 (bottom, scaled to 1470 microns sample thickness). Both the natural and synthetic glass have similarly shaped spectra.

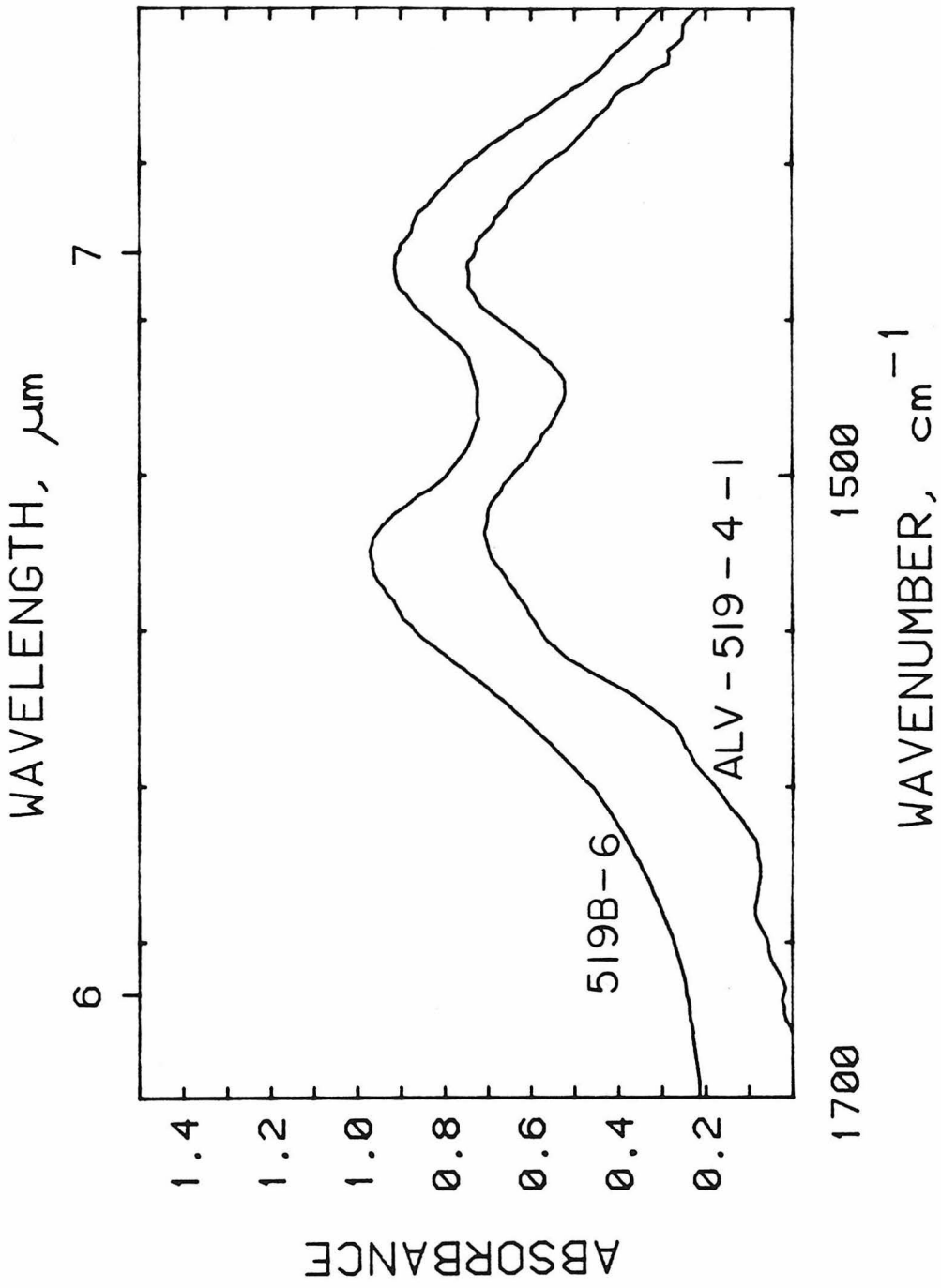
WAVELENGTH, μm
6
7
1700
1500
WAVENUMBER, cm⁻¹
ABSORBANCE
0.2
0.4
0.6
0.8
1.0
1.2
1.4
519B-6
ALV-519-4-1

with the splitting of this band in sodium aluminosilicate glasses. This may reflect specific distinctions between Na and Ca (or Mg) cations or more general distinctions between mono- and divalent cations associated with carbonate groups. In either case, it is concluded that the local environments of the carbonate groups dissolved in all of these Ca ± Mg glasses are similar to the extent sensed by infrared spectroscopy, despite the wide range of silicate composition that they span. It is also noted that the doublets in the synthetic and natural basalt spectra shown in Figures 26 and 27 are slightly broader at their base and split slightly more than in the simpler compositions, possibly reflecting either the participation of minor Na in carbonate complexes or a wider range of local environments for carbonate in more complex compositions. The splitting of the ν_3 band in the systems studied here also appears independent of Al-concentration, in contrast to the conclusion for Na-aluminosilicate glasses in Chapter 1, in which the presence of Al appears to be essential for the degree of splitting observed.

Another important difference between the infrared spectra of the Ca ± Mg-bearing glasses studied here and the $NaAlSi_2O_6$-SiO_2-CO_2 glasses studied in Chapter 1 is also illustrated in Figure 23. The sharp band at 2352 cm^{-1} in the spectrum of the $NaAlSi_2O_6$ + CO_2 glass was attributed in Chapter 1 to the ν_3 antisymmetric stretch of molecular CO_2. This molecular CO_2 was concluded to be homogeneously dissolved on the molecular level and not present in fluid inclusions. No molecular CO_2 was detected in any of the glasses reported on here, based on the absence of an absorption band at 2352 cm^{-1}. If the molar absorptivity

for the 2352 cm^{-1} band in sodium aluminosilicate glasses is used, none of the synthetic or natural glasses studied here contains more than 25 ppm molecular CO_2 and most must contain less than 10 ppm. This once again contrasts with the conclusions of Mysen et al. (1975, 1976) based on studies of KBr pellets. The likely reasons for the spurious identification of molecular CO_2 in those early studies is also discussed in Chapter 1.

No bands attributed to C-H vibrations such as those expected for dissolved methane were observed in any of the natural or synthetic glasses. Surprisingly, no bands attributed to methane were detected in the diopside glass provided by Dr. S. Sharma despite the great thickness of the sample (0.039 cm), and the relatively high concentration of methane (0.27 wt.%) that was determined by high temperature mass spectrometry (Rai et al., 1983). If the extinction coefficient or molar absorptivity for the C-H stretch band at ~3000 cm^{-1} is of the order of 500 liters/mole-cm, similar to the value for solid methane (Chapados and Cabana, 1972) or the value for methane contained in melanophlogite (~200 liters/mole-cm), a clathrate-type framework silicate (spectrum obtained by Professor G. Rossman from a sample referenced in Cooper and Dunning, 1972), an intense absorption band would have been expected for the high reported methane concentration. Graphite was observed in the diopside glass sent by Dr. Sharma, so the methane found by Rai et al. (1983) in the diopside glass might be produced by reaction during heating of the sample. Alternatively, the extinction coefficient for methane in silicate glasses could be anomolously low, rendering it undetectable.

Table 10 lists the band locations and intensities for all of the infrared spectra obtained during this study. Three different intensities are listed for the carbonate bands for each sample: the total area under the doublet, the intensity of the 1515 cm^{-1} band above background, and the intensity of the 1435 cm^{-1} band above background. Ideally, it might have been best to deconvolve the doublet into two bands and measure the deconvolved intensities. However, since all of the bands have essentially identical shapes, this was not regarded as necessary.

Band Intensity Calibrations

The intensities of the 1515 cm^{-1} band, the 1430 cm^{-1} band and the integrated area under both bands are plotted versus total dissolved CO_2 content in Figures 28a, b and c. Total CO_2 contents are based on the amounts of silver oxalate loaded into the capsules. The accuracy of some of these total CO_2 contents has been confirmed via the deuteron beam measurements made on some of these glasses (Table 11). The band intensities increase regularly with total CO_2 for all compositions and indicate that molar absorptivities and integrated molar absorptivities are roughly independent of composition over the range of compositions reported here. The molar absorptivity is essentially constant below 0.8 wt.% CO_2. At high total CO_2 contents these trends begin to curve, suggesting that molar absorptivities decrease with increasing CO_2 content at high total CO_2 contents. These deviations from constant molar absorptivity may indicate that CO_3^{2-} groups dissolved in the glasses are interacting electrostatically with one another at high

Table 10- Infrared data obtained for synthetic Ca ± Mg glasses in this study. Run conditions of glass syntheses are also included.

Sample	P (kbar)	T (°C)	Duration (min.)	Loaded CO_2 (wt.%)	Thickness (cm)	Band (cm^{-1})	Intensity (abs.)	H_2O[a] (wt.%)	Band (cm^{-1})	Intensity (abs.)	Band (cm^{-1})	Intensity (abs.)	Area[b] (cm^{-1})
ANC-BL	c	1450	480	0.00	0.0145	3550	0.02	0.02		d		d	d
ANC-7	20	1450	60	0.96	0.0057	3525	0.12	0.31	1525	1.07	1445	1.13	197.22
ANC-9	20	1450	60	0.12	0.0061	3530	0.09	0.17	1510	0.22	1425	0.23	37.26
ANC-10	20	1550	60	0.61	0.0042	3520	0.07	0.19	1510	0.55	1435	0.58	102.26
ANC-11	20	1550	60	0.38	0.0068	3545	0.13	0.22	1510	0.55	1430	0.58	99.30
DIC-BL	c	1450	480	0.00	0.0083	3520	0.02	0.03		d		d	d
DIC-6	15	1625	60	1.29	0.0037	3515	0.03	0.09	1515	0.90	1440	0.88	149.87
DIC-7	15	1625	60	0.32	0.0050	3505	0.02	0.04	1520	0.35	1440	0.35	60.28
DIC-8	15	1625	60	0.51	0.0055	3520	0.03	0.06	1515	0.62	1440	0.61	104.53
DIC-9	15	1625	60	0.63	0.0051	3550	0.02	0.05	1515	0.75	1435	0.71	126.33
519B-BL	c	1315	480	0.00	0.0126	d	d	d		d		d	d
519B-5	20	1550	60	0.87	0.0033	3505	0.09	0.29	1525	0.59	1425	0.60	116.06
519B-6	20	1550	15	0.54	0.0059	3550	0.05	0.09	1525	0.77	1435	0.72	145.26

[a]Water analyses done using the method of Stolper (1982a) and a molar absorptivity of 60 liters/mole-cm for the infrared absorption band at 3550 cm^{-1}. Densities are given in Table 9.
[b]Total area under carbonate doublet.
[c]1 atm.
[d]Below detection limit.

Figure 28- Intensities of the 1515 cm^{-1}(a) and 1435 cm^{-1}(b) bands and the integrated intensity under both bands (c) versus wt.% CO_2 loaded into the capsules for synthetic glasses from this study. All intensities are normalized to 100 microns sample thickness. Open circles are data from glasses of anc composition, filled circles are di composition, and filled squares are 519B composition. Best fit lines for ε=375 liters/mole-cm and ε^*=69500 liters/mole-cm^2 are shown, assuming a density of 2735 g/liter, and are constrained by the origin.

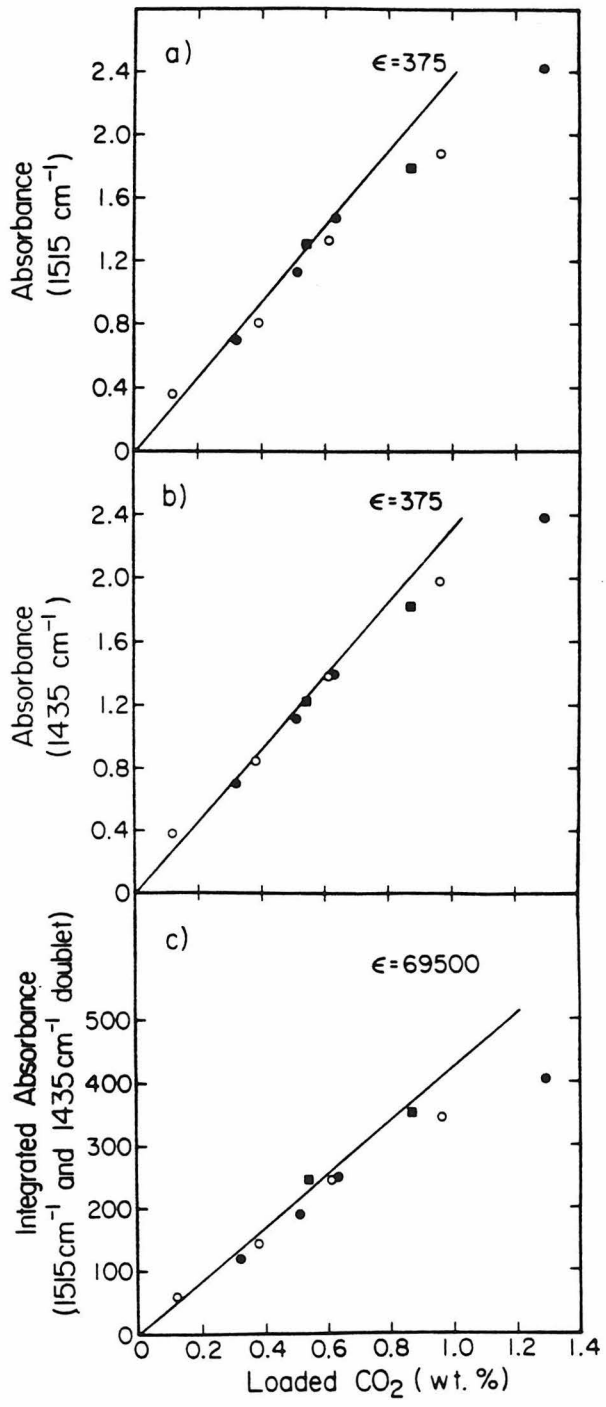
a)
ε=375
Absorbance (1515 cm⁻¹)
b)
ε=375
Absorbance (1435 cm⁻¹)
c)
ε=69500
Integrated Absorbance (1515 cm⁻¹ and 1435 cm⁻¹ doublet)
Loaded CO2 (wt. %)

Table 11- Comparison of loaded CO_2 (wt.%) with CO_2 (wt.%) analyzed using the $^{12}C(d,p_0)^{13}C$ nuclear reaction. Analysis conditions given in Appendix 1.

SAMPLE	LOADED CO_2 (wt.%)	ANALYZED CO_2 (wt.%)
ANC-BLANK	0.00	0.01
ANC-9	0.12	0.12
ANC-10	0.61	0.58
ANC-11	0.38	0.35

concentrations or that carbon loss through Pt capsules (Watson et al., 1982; Chapter 1) is more severe in C-rich experiments. It is emphasized that the deviation from linearity in Figure 28 occurs at total CO_2 contents much higher than in most natural basaltic glasses and will not affect the quantitative measurement of dissolved CO_2 contents of such samples.

Molar absorptivities of 375 ± 20 liters/mole-cm were determined by the method of least squares (Albarade and Provost, 1977) for the absorption bands at both 1515 cm^{-1} and 1435 cm^{-1}, excluding sample DIC-6, which contains 1.29 wt. % dissolved CO_2. An integrated molar absorptivity of 69500 ± 3000 liters/mole-cm^2 was determined for the total area under the doublet. These values are illustrated in Figure 28 and should only be used for Ca ± Mg glasses containing $\leq$0.80% CO_2 by weight. It is noted that these extinction coefficients are much higher than those we determined for the carbonate bands in sodium aluminosilicate glasses. The premises on which this calibration is based are again emphasized: the total CO_2 contents of the synthetic glasses are accurately known and all of the C is dissolved as carbonate that contributes to the observed doublet. At present, there is no reason to doubt these statements; indeed, the linearity of Figures 28a-c at low concentrations lends them strong support.

Conclusions

1. The CO_2 dissolved in both natural and synthetic Ca ± Mg glass compositions is dissolved essentially entirely as carbonate. This carbonate is probably in the form of distorted ionic-complexes

associated with Ca^{2+} and/or Mg^{2+}, and is spectroscopically different from carbonate dissolved in sodium aluminosilicate glasses. No more than 25 ppm (by weight) molecular CO_2 is dissolved in these glasses.

2. Carbon dioxide analysis of both natural and synthetic Ca ± Mg silicate glasses is possible using infrared spectroscopy.

Chapter 4. Thermodynamic Considerations

There have been two approaches used to understand the thermodynamics of volatile solution in silicate glasses. The first is a macroscopic empirical approach used in the case of CO_2 by Spera and Bergman (1980). While this type of treatment can account for many aspects of the behavior of volatiles in glasses, it neither takes into account nor explains molecular level processes occurring during volatile solution. The second approach, used most recently in the case of water by Stolper (1982b), uses the statistical thermodynamics of molecular level equilibria to understand macroscopic processes. The latter type of treatment is more amenable for analysis of the data generated by infrared spectroscopy and is the approach taken in this chapter.

Speciation of Carbon Dioxide in Silicate Melts

The results presented in Chapter 3 indicate that CO_2 in basaltic and Ca ± Mg glasses dissolves predominately as carbonate. This has been suggested previously (Brey and Green, 1975; Brey, 1976; Mysen et al., 1975, 1976; Mysen and Virgo, 1980ab; Eggler and Rosenhauer, 1978; Eggler et al., 1979; Sharma, 1979; Sharma et al., 1979; Rai et al., 1983), although early infrared studies concluded that significant molecular CO_2 is also dissolved in comparable glass compositions (Mysen et al., 1975, 1976). The results contrast with the results for glasses in the $NaAlSi_2O_6$-SiO_2-CO_2 system reported in Chapter 1, which contain <u>both</u> dissolved carbonate and molecular CO_2. In this section, I speculate on the causes of the apparently strong compositional dependence of carbon dioxide speciation in silicate glasses.

It must be emphasized that although the spectroscopic measurements are on CO_2-bearing glasses quenched from melts, the principal interest of this study is the behavior of CO_2-bearing melts. Throughout this chapter, I will assume that the speciation of CO_2 that has been measured in glasses accurately reflects that of the melts from which they were quenched. Support for this assumption comes from numerous comparisons between the properties of melts and glasses at 1 atm (e.g., Taylor et al., 1980; Seifert et al., 1981; Okuno and Marumo, 1982; Aines et al., 1983) and from the fact that the speciation of water in glasses quenched from melts does not appear to be affected by quenching provided that quenching is done rapidly (Stolper et al., 1983).

Since the type of thermodynamic treatment used here has been used to understand the dissolution of water (Stolper, 1982b), the case of water is briefly reviewed. Water, like carbon-dioxide, dissolves in silicate glasses and melts both in molecular form and as ions (hydroxyl in the case of water and carbonate in the case of carbon dioxide) produced by reaction between the molecular species and oxygen atoms of the silicate melt (Stolper, 1982a). The homogeneous equilibrium between melt species has been described as follows for water-bearing melts:

$$H_2O(\text{molecular}) + O^{2-} = 2OH^-, \qquad (2)$$

with an equilibrium constant:

$$K_1 = \frac{(a^m_{OH^-})^2}{(a^m_{O^{2-}})\ (a^m_{H_2O,mol})}, \qquad (3)$$

where a^m refers to the activity of each of the melt species. At very low concentrations of dissolved water, the concentration of unreacted oxygen is essentially the same as in anhydrous melt, because it has not decreased either by dilution with molecular water or by extensive conversion to hydroxyl groups, and $a^m_{O}2-$ can be treated as constant. The activities of hydroxyl and molecular water can be approximated by their mole fractions (Stolper, 1982b) and therefore:

$$\frac{(X^m_{OH})^2}{(X^m_{H_2O,mol})} \simeq (a^m_O 2-)\ (K_1) \simeq \text{constant} . \qquad (4)$$

Therefore, at low total water concentrations the concentration of molecular water in melts is expected to be proportional to the square of the concentration of hydroxyl groups. This is related to the oft-quoted "square-root" relationship between the fugacity of water in melts and its mole fraction at low total water contents (Stolper, 1982b).

A similar treatment can be applied to the equilibrium between molecules of CO_2 and carbonate in melts. The homogeneous equilibrium between melt species can be described with the following sort of reaction:

$$CO_2(\text{molecular}) + O_r = CO_3^{2-} , \qquad (5)$$

where O_r represents a reactive oxygen. This reaction has an equilibrium constant given by:

$$K = \frac{(a^m_{CO_3^{2-}})}{(a^m_{O_r})\,(a^m_{CO_2,mol})} . \qquad (6)$$

CO_2 solution is envisioned as the mixing of CO_2 molecules with C-free silicate melt species. These react according to reaction (5), producing carbonate, until the equilibrium constant K is satisfied.

It is likely that not all oxygens in silicate melts are equally reactive with molecular CO_2 to produce carbonate. Thus, for each distinguishable type of oxygen in the melt, a reaction such as (5) can be written, each having its own value of K (equation 6). Many of the oxygen species in silicate melts may be effectively inert with respect to CO_2. K in equation (6) would be approximately zero for these oxygen species. For purposes of discussion, it will be assumed that one reaction of the form of equation (5) is dominant and thus that O_r in equation (5) refers to a subset of the oxygens in the melt (e.g., to the bridging, non-bridging, or free oxygens in the sense of Toop and Sammis, 1962). Thus $a^m_{O_r}$ will be less than 1 for CO_2-free melts and will probably vary with the silicate composition of the melt.

The relationships between the activities of molecular CO_2, carbonate, various types of oxygen atoms in the melt, and melt composition are not obvious and are not likely to be simple. In this discussion, the melt is envisioned to be a mixture of CO_2 molecules, carbonate groups, and oxygen atoms, analogous to the model developed by Stolper (1982b) for molecular water, hydroxyl groups, and oxygen atoms in hydrous melts. In the latter case, an ideal mixture of these species was assumed, giving activities equal to mole fractions. In the case of

a mixture of CO_2 molecules, carbonate groups, and oxygen atoms, the fact that the each species has a different size complicates the relationship between activity and composition even for ideal (in the sense that all configurations are energetically equivalent) mixtures. In these situations, volume fractions have greater significance than mole fractions (Flory, 1944; 1953, Chapter XII; Guggenheim, 1952, Chapter X). For the simple analysis given here, however, it will be assumed that activity equals mole fraction for each species, keeping in mind that this is only an approximation. Mole fraction in this context refers to the number of moles of a particular mixing species in the mixture over the total number of species. For example, for a melt consisting of 1 mole of CO_2 molecules, 3 moles of CO_3^{2-} groups, and 1 mole of $NaAlSi_2O_6$ (6 moles of O), $X_{CO_2,mol} = 0.1$ and $X_{CO_3^{2-}} = 0.3$.

If only low total CO_2 contents are considered, such that $a^m_{O_r}$, the activity of the reactive oxygen species, can be treated as approximately constant and the activities of the carbon-bearing species can be approximated by their mole fractions, equation (6) can be approximated by:

$$\frac{(X^m_{CO_3^{2-}})}{(X^m_{CO_2,mol})} \simeq (a^m_{O_r})\,(K) \simeq \text{constant} . \qquad (7)$$

The observation that for each sodium aluminosilicate composition there is an approximately linear relationship between the concentration of molecular CO_2 and carbonate up to ~1% total CO_2 (Figures 11, 12, and 13) is thus precisely what we would expect based on homogeneous

equilibrium between melt species. In Ca ± Mg-bearing systems, $X^m_{CO_2,mol}$ is effectively zero.

Although the CO_2/CO_3^{2-} ratio increases as silica increases along the $NaAlO_2$-SiO_2 join, it is not clear whether this should be attributed to decreasing soda and alumina or to increasing silica. The experiments on silicate compositions that lost sodium during extended drying at 800°C (ab-X, jd-X, and eu-X, Chapter 1) point to a major role for the sodium concentration. Even the relatively minor soda losses experienced by these compositions (resulting in slightly peraluminous bulk compositions) result in dramatic increases in the ratio of molecular CO_2 to carbonate in the glasses. Indeed, this was the first indication that these compositions were depleted in soda.

The observed variations in speciation with melt composition in the sodium aluminosilicate glasses can consequently be readily rationalized in terms of equations (6) and (7). Suppose that the equilibrium constant K in equation (6) does not vary over the range of compositions that we have studied. It is then clear from equation (7) that at low total dissolved CO_2 contents, the ratio of CO_3^{2-} to molecular CO_2 would increase with increasing soda content, provided that the basicity of the melt (i.e., the activity of reactive oxygens, $a^m_{O_r}$), increases with increasing soda content. This would be the case, for example, if CO_2 molecules reacted primarily with non-bridging oxygens or free oxygens (Toop and Samis, 1962; Pearce, 1964; Wagner, 1975), since in both cases the concentrations of these oxygens are expected to be correlated with Na_2O content.

Is this effect likely to be the entire explanation of why no molecular CO_2 was detected in any of the Ca ± Mg silicate glasses reported on here? That is, do the Ca ± Mg melts studied here simply have much higher concentrations of reactive oxygens (higher $a_{O_r}^m$) than the sodium aluminosilicate melts? In some instances, this is probably true (Binsted et al., 1985). However, another way to alter the ratio of carbonate to molecular CO_2 in melts is to change the value of K as defined in equation (6) with the silicate chemistry of the melt. Consider the possibility that the reaction of CO_2 with oxygen atoms associated with sodium cations has a much lower value of K than the reaction of CO_2 with structurally analogous oxygen atoms associated with calcium cations. In other words, suppose that calcium carbonate ion-complexes are stabilized relative to unreacted CaO and CO_2 to a greater extent than are sodium carbonate complexes relative to unreacted NaO^- and CO_2. If this were the case, then it might be expected, as is in fact observed (Brey, 1976; Mysen and Virgo, 1980ab), that as the silicate composition varies from albite to anorthite, for example, the ratio of carbonate to molecular CO_2 would increase. However, simple thermodynamic considerations regarding the variation in the K for equation (6) from Na- to Ca- and Mg-bearing glasses are ambiguous. (Compare Spera and Bergman (1980) to Holloway (1981).)

At this point, I cannot say with confidence whether the absence of molecular CO_2 in the Ca ± Mg glasses is due to high $a_{O_r}^m$ in these glasses, to variations in K for equation (6) from Na- to Ca ± Mg-rich systems and as functions of other compositional variables, or to some combination of these effects. Nor can it be determined from the data

whether the differences are cation-specific or reflect more general differences between systems rich in monovalent cations and systems rich in divalent cations. It will be possible to definitively address these issues only by detailed study of carbonate to molecular CO_2 ratios as functions of melt composition.

As it is written, reaction (5) does not explicitly take into account the changes in the speciation of the C-free aluminosilicate matrix of the melt that accompany formation of carbonate (e.g. changes in degree of polymerization, etc.) However, a linear relationship between $X^m_{CO_3^{2-}}$ and $X^m_{CO_2,mol}$ for sodium aluminosilicate melts is expected to hold at low total CO_2 contents for each silicate composition regardless of the details of the reactions describing the molecular CO_2-carbonate-oxygen interactions. The linearity results from the fact that one carbon dioxide molecule is converted into one carbonate group and from the approximation that the activities of the oxygen species are constant. For example, a linear relationship would also be expected to hold at low CO_2 concentrations if reaction (5) were replaced by:

$$CO_2(\text{molecular}) + 2O^- = CO_3^{2-} + O^\circ, \qquad (8)$$

where O^- and O° refer to non-bridging and bridging oxygens, respectively, in the sense of Toop and Samis (1962). This is the kind of reaction proposed by Eggler and Rosenhauer (1978) for the production of carbonate groups in diopside and other basic melt compositions.

At high total dissolved CO_2 contents the relationship between the concentration of molecular CO_2 and carbonate for all melt compositions

is expected to deviate from linearity when the approximations that a_{O_r} in equation (6) or that a_{O^-} and a_{O° in the equivalent expression for equation (8) are constant break down. Under these circumstances, it would be expected that the molecular CO_2/carbonate ratio would begin to increase with increasing total CO_2, as in the case of the solution of water, where the ratio of molecular water to the square of the hydroxyl concentration eventually begins to increase as water content increases (Stolper, 1982b). Just where the expected deviation from linearity would become noticeable is unclear, but it must be at >1% total CO_2 in the compositions that have been studied (Figures 11 and 28). If a reaction such as that described in equation (8) describes the molecular level interactions between molecular CO_2 and carbonate in sodium aluminosilicate melts, the linear relationship could extend to relatively high total CO_2 contents. In such a case, the activity of the major species O° might be changed little by the addition of small amounts of carbonate and the activity of O^-, a minor species, might be buffered by interactions with other C-free melt species and change very little even after substantial molecular CO_2 has been converted to CO_3^{2-}. This will be true for any carbonate-producing reaction involving relatively minor oxygen species whose concentrations might be essentially buffered by the concentrations of major species not greatly affected by the addition of carbonate or molecular CO_2.

The thermodynamic treatment presented here is consistent with some aspects of the bulk thermodynamic treatment of Spera and Bergman (1980) and, in fact, explains why part of their treatment is successful. Spera and Bergman (1980) analyzed available data on the pressure and

temperature dependence of CO_2 solubility in silicate melts using a thermodynamic model of CO_2-bearing silicate melts in which the activity of CO_2 dissolved in the melt was assumed to be proportional to the mole fraction of total dissolved CO_2. The results presented in Chapter 1 also suggest that the relationship between activity and composition in CO_2-bearing melts can be approximated as linear. This follows from the fact that the activity of CO_2 in the melt can be assumed to be roughly equal or proportional to the mole fraction of dissolved <u>molecular</u> CO_2, which is in turn approximately proportional to total dissolved CO_2 because carbonate and molecular CO_2 contents are proportional. The results can thus explain why Spera and Bergman's "ideal" model for the relationship between a_{CO_2} and the mole fraction of total dissolved CO_2 is so successful at explaining phase equilibrium data.

Spera and Bergman (1980) also used available solubility data to determine $\bar{V}_{CO_2}$, the partial molar volume of CO_2 in silicate melts, for a number of melts including albite, jadeite, and nepheline. Recall that most of the dissolved CO_2 in albite is molecular CO_2, whereas most in nepheline is expected to be carbonate. Spera and Bergman (1980) found $\bar{V}_{CO_2}$ to be essentially identical for these melts despite the difference in their speciation. This observation suggests that the volume change accompanying reactions such as (5) and (8) are minor and is consistent with the observation that CO_2 speciation is only weakly dependent on pressure.

Solubility of CO_2 in silicate melts

In addition to accounting for changes in the speciation of CO_2 with melt composition, the thermodynamic approach used here can rationalize changes in the solubility of CO_2 in silicate melts with changing pressure, temperature, and silicate composition. The equilibrium between silicate melt and CO_2-bearing vapor can be modelled by the following heterogeneous equilibrium:

$$CO_2^{vapor} = CO_2^{melt}(molecular) \ . \qquad (9)$$

The difference between the volume of CO_2 in the vapor and the partial molar volume of CO_2 in the melt (e.g., Spera and Bergman, 1980) requires that with increasing pressure at constant temperature, the concentration of molecular CO_2 dissolved in a CO_2-saturated melt of constant silicate composition should increase. This is in accord with the observations in Chapter 2 for albitic melt (Figure 17b). Entropy considerations further dictate that with increasing temperature at constant pressure, the lefthand side of reaction (9) should be favored and the concentration of molecular CO_2 dissolved in a melt of constant silicate composition should decrease, again in agreement with the results (Figure 18b) for albitic melt.

The results shown in Figure 19 might suggest that the value of K increases slightly, or that reaction (5) favors the formation of CO_3^{2-} with both increasing temperature and pressure. These effects are small and again suggest that the volume and entropy changes associated with reaction (5) are small. Recall that at constant pressure and

temperature, the activity of reactive oxygen (equation 7) has been treated as constant at low total dissolved CO_2 concentrations. It is noted in the last section that at some high total dissolved CO_2 content, $a^m_{O_r}$ will decrease, causing the ratio of carbonate to molecular CO_2 to decrease. The small, but systematic changes in the molecular CO_2/CO_3^{2-} ratio observed under vapor-saturated conditions are attributed to changes in the value of the equilibrium constant K (equations 6 and 7) as functions of pressure and temperature coupled with possible changes in $a^m_{O_r}$ as total dissolved CO_2 content varies.

The total solubility of CO_2 is the sum of the dissolved molecular CO_2 and carbonate. Its dependence on pressure and temperature can only be evaluated by considering the effects of pressure and temperature on both reactions (5) and (9). Thus, the sum of the negative temperature dependence of molecular CO_2 solubility for albitic melt and the positive temperature dependence of the ratio of CO_3^{2-} to molecular CO_2 for albitic melt is a slight negative temperature dependence of the total CO_2 solubility. A similar competition between decreasing solubility of molecular H_2O and increasing OH/H_2O ratios with increasing temperature (Stolper et al., 1983) may explain the slight negative temperature dependence of total water solubility in melts (Karsten et al., 1982). The positive pressure dependence of both molecular CO_2 solubility and the ratio of CO_3^{2-} to molecular CO_2 (except perhaps at low pressure and high temperature, Figure 19b), assures a positive correlation between pressure and total CO_2 solubility. A likely consequence of these considerations is a correlation between both the pressure and temperature dependence of CO_2 solubility and melt composition. For

instance, in the case of molten SiO_2, which probably dissolves CO_2 nearly entirely as molecular CO_2 (see below), the decrease in CO_2 solubility with increasing temperature can be expected to be more dramatic than the decrease observed for molten albite. Likewise, the increase in total CO_2 solubility in silica melt with increasing pressure can be expected to be less dramatic than for albitic or jadeitic melts.

There is no evidence for abrupt changes in CO_2 solubility or speciation with changing pressure and temperature (as suggested by Mysen et al., 1976 and Holloway et al., 1976) over the ranges of pressure and temperature studied here. Since abrupt changes in melt polymerization (i.e., $a^m_{O_r}$) might be expected to result in abrupt changes in the ratio of molecular CO_2 to CO_3^{2-} (equation 7), it is concluded that no evidence for abrupt changes in melt structure exists in the data presented here.

Reaction (9) has an equilibrium constant:

$$K_{CO_2} = \frac{a^m_{CO_2,mol}}{a^v_{CO_2}} = \frac{a^m_{CO_2,mol}}{f_{CO_2}/f^o_{CO_2}} \sim \frac{X^m_{CO_2,mol}}{f_{CO_2}/f^o_{CO_2}}, \qquad (10)$$

where $a^m_{CO_2,mol}$ and $a^v_{CO_2}$ refer to the activities of molecular CO_2 in the melt and CO_2 in the vapor. The fugacity of CO_2 in the vapor is f_{CO_2} and of CO_2 in pure CO_2 vapor is $f^o_{CO_2}$. The standard state for CO_2 in the vapor is pure CO_2 vapor at pressure and temperature; i.e., $a^v_{CO_2}$ is 1 at all pressures and temperatures for pure CO_2 vapor and less than one if the vapor contains other constituents. The standard state for molecular CO_2 in the melt is a fictive form of pure CO_2 at pressure and

temperature such that the activity coefficient of molecular CO_2 in the melt approaches 1 as its concentration approaches zero. The reciprocal of K_{CO_2} can thus be regarded as a Henry's law constant and the approximation given in equation (7) ($a^m_{CO_2,mol} \sim X^m_{CO_2,mol}$) will be strictly true as long as Henry's law holds.

If K_{CO_2} is only weakly dependent on melt composition for melts near the $NaAlO_2$-SiO_2 join, this would mean that the mole fraction of molecular CO_2 ($X^m_{CO_2,mol}$) would be similar in all melts equilibrated with pure CO_2 vapor at a given pressure and temperature. The total CO_2 solubility is the sum of CO_2 dissolved as molecular CO_2 and carbonate; therefore, since the amount of dissolved carbonate at constant $X^m_{CO_2,mol}$ increases from silica to jadeite (Figure 11), it should be anticipated from the results that CO_2 solubility should also increase in this order. This is precisely what is observed (Mysen, 1976).

This form of thermodynamic treatment also suggests that it should be possible, given the measured solubility of CO_2 in one melt composition at a given pressure and temperature, to use our CO_2 speciation data to calculate the solubility of CO_2 in other melt compositions at the same pressure and temperature. The speciation data suggest that the ratio of the solubility of total CO_2 in albite melts to that in jadeite melts should be ~0.54. Mysen (1976) reported that this ratio ranged from 0.65 at 1625°C and 20 kbar to 0.90 at 1450°C and 10 kbar. The agreement is considered to be satisfactory given the possible uncertainties in Mysen's measurements and the absolute CO_2/CO_3^{2-} measurements presented here. This analysis also suggests that pure silica liquid would dissolve CO_2 essentially entirely as molecular CO_2;

the solubility of CO_2 will then be ~70% of that in albite melt, assuming that at saturation $X^m_{CO_2,mol}$ is the same in all melts. Based on the data from Chapter 2, this suggests a solubility of 0.46 wt.% CO_2 in metastable silica melt at 20 kbar, 1625°C and 0.99 wt.% at 30 kbar, 1625°C. The results of Boettcher (1984) on phase equilibria in the system SiO_2-CO_2-H_2O also suggest a non-trivial solubility of CO_2 in silica melts.

Water versus CO_2 speciation

There are some important differences between the behavior of water and carbon dioxide in silicate melts that can be evaluated in light of the previous discussion of homogeneous equilibria in melts. In contrast to the case of carbon dioxide, the speciation of water in melts shows very little dependence on silicate composition. For example, variations in the proportions of molecular water and hydroxyl groups between melts on the $NaAlSi_2O_6$-SiO_2 join or between these and melts on the $CaAlSi_2O_8$-SiO_2 join appear to be minor (L.A. Silver and E. Stolper, unpublished results), whereas CO_2 speciation varies dramatically over this composition range. Likewise, total water solubility is only weakly dependent on silicate composition, whereas carbon dioxide solubility is strongly dependent on melt composition (Mysen et al., 1975, 1976; Mysen, 1976; Mysen and Virgo, 1980ab; Eggler and Rosenhauer, 1978).

Mono- and divalent cations probably play roles in the solubility mechanisms of water in the silicate melts in which they are present. However, these roles appear to be minor compared to those that they play in the case of CO_2 solubility, where such cations seem to be essential

for the formation of carbonate groups and where energetic differences between different metal-carbonate complexes may dominate both the speciation and solubility behavior of CO_3^{2-} in melts. In other words, all of the oxygens in silicate melts can be regarded as nearly equally available for reaction with water molecules via equation (2). Although the OH groups formed by such a reaction may be associated with the Na, Ca, etc. in melts that contain such cations, these metal hydroxide complexes seem to be energetically similar. The result is that variations in K_1 in equation (4), which is an expression of the variation in the free energy differences between these species in the melt, are minor, and K_1 values of .1-.3 seem to satisfy most hydrous systems. In contrast, it seems likely that only certain types of oxygens are available for reaction with CO_2 molecules in equation (5). Thus, even if K in equation (6) is constant for a series of melts, the carbonate to molecular CO_2 ratio can vary from melt to melt due to variations in the activity of the reactive oxygen species ($a^m_{O_r}$) in equation (6). In addition, the energetics of the reaction (i.e., the stability of the carbonate complex relative to the left hand side of equation (5)) may depend dramatically on the cations present in the melt; that is, K for reaction (5) may be strongly dependent on the mono- and divalent cations that are present and perhaps on other compositional factors. The strong composition dependence of CO_2 speciation and solubility in melts may thus be viewed as a combination of the variations in concentrations of "reactive" oxygen species (i.e., $a^m_{O_r}$ in equation (6)) and of the equilibrium constants of the homogeneous

equilibria governing the interactions between CO_2 and CO_3^{2-} (i.e., K in equation (6)) with melt composition.

Conclusions

1. The speciation of CO_2 in silicate melts is controlled by the homogeneous equilibria between CO_2 molecules, carbonate groups, and oxygen atoms in the melts. The approximately linear relationship between molecular CO_2 and carbonate concentrations in sodium aluminosilicate melts can be readily understood by considering the thermodynamics of such equilibria. The strong dependence of the molecular CO_2 to carbonate ratio can also be accounted for if the melts are considered to contain several different oxygen species, only some of which react with molecular CO_2 to produce carbonate. The observed compositional dependence of the molecular CO_2 to CO_3^{2-} ratio in sodium aluminosilicate melts is consistent with the hypothesis that soda concentration is the major factor controlling the availibility of oxygens for reaction with molecular CO_2 to form carbonate and that the carbonate is dissolved as sodium carbonate complexes. The lack of dissolved molecular CO_2 in Ca ± Mg melts is consistent with an increased stability of the carbonate ion in melts with a greater concentration of divalent cations and/or a higher concentration of reactive oxygens.
2. Observed variations in total CO_2 solubility with both melt composition and the pressure and temperature of melt equilibration can be understood using the measured species concentrations and a simple thermodynamic model. The approximately linear relationship

between the activity of CO_2 in melts and the mole fraction of total dissolved CO_2 that has been proposed by Spera and Bergman (1980) can also be readily understood using the results.

3. The strong dependence of CO_2 speciation on melt composition contrasts with the speciation of water in glasses.

4. The results demonstrate that infrared spectroscopic measurements of species concentrations in glasses provide a direct approach to developing a quantitative understanding of the molecular level interactions involved in the solubility of CO_2 in silicate melts and of the thermodynamic properties and phase equilibria of CO_2-bearing silicate melts.

Chapter 5. The Concentration of Dissolved Carbon Dioxide in Natural Basaltic Glasses

Although there is considerable uncertainty about the concentrations of dissolved carbon in oceanic basalt glasses (Delaney et al., 1978; Harris, 1981; Harris and Anderson, 1983; Byers et al., 1983, 1984, 1985; Pineau and Javoy, 1983; Des Marais and Moore, 1984; Mattey et al., 1984; Sakai et al., 1984) and much speculation about the nature of the dissolved carbon (Brey and Green, 1975; Mysen et al., 1975; Eggler et al., 1979), there is general agreement that carbon dioxide plays an important role in the evolution of oceanic basalts. The carbon dioxide-rich vesicles and vapors exsolved from these magmas are the critical evidence for this (Moore et al., 1977; Moore, 1979; Gerlach and Graeber, 1985; Greenland et al., 1985). These vapor compositions are probably the result of the limited solubility of CO_2 relative to water in basaltic melts at low pressures and have implications for the understanding of eruptive processes (Gerlach and Graeber, 1985; Greenland et al., 1985), the oxidation state of magmas (Mathez, 1984) and the carbon budget of the oceans and atmospheres (Berner et al., 1983). At deeper levels, heterogeneities in the CO_2 contents of the source regions of basalts may correlate with heterogeneities in the concentrations of other incompatible elements and in isotopic ratios (Schilling et al., 1980; Harris, 1981), and may strongly influence the phase equilibria of these source regions and the petrochemistry of their melting products (Eggler, 1973, 1974, 1978; Wyllie, 1979)

CO_2 dissolved as both molecular CO_2 (Mysen et al., 1975) and carbonate (CO_3^{2-}) (Mysen et al., 1975; Brey and Green, 1975; Eggler, 1978; Eggler et al., 1979) as well as CO (Byers et al., 1983, 1984) and hydrocarbons (Harris and Anderson, 1983; Byers et al., 1983, 1984) have

all been suggested to be dissolved in MORB (mid-ocean ridge basalt) or MORB-like glasses. The structural sites of these dissolved species, even if they are present in basaltic glasses, are matters of speculation. Furthermore, since vesicular CO_2, carbonaceous material (either as graphite, carbynes, hydrocarbons or amorphous matter located in microcracks and on vesicle walls (Mathez and Delaney, 1984)) and carbonate alteration (Pineau and Javoy, 1983) are widespread in basaltic glasses, measurements of the absolute concentrations of dissolved C (or CO_2) have been difficult.

Infrared spectra have consequently been obtained for a series of natural submarine basaltic glasses (Table 12) in an effort to resolve this problem. Spectroscopic techniques used are the same as those discussed in Chapter 2. Major element analyses of the glasses are listed in Table 13. Also listed is the name of the scientist from whom each sample was received, the location and depth of the ocean floor from which it was collected, and notes on the crystal and vesicle content of each sample.

Density measurements were made on each natural glass with a Berman balance using toluene as a reference liquid and are listed in Table 13. For sample sizes greater than 5 mg, a precision of ±0.2% is estimated, based on the reproducibility of measurements of a quartz standard. This contrasts with a precision of ±2% given in Stolper (1982a) and is revised as the consequence of author error. Unknown uncertainties in the densities of natural glasses are contributed by the variable phenocryst and vesicle contents of the samples. These uncertainties are presumed to be minor both because the samples were

Table 12- Infrared data obtained for the natural basaltic glasses used in this study.

Sample	Thickness (cm)	Band (cm^{-1})	Intensity (abs.)	H_2O[a] (wt.%)	Band (cm^{-1})	Intensity (abs.)	Band (cm^{-1})	Intensity (abs.)	Area[b] (cm^{-1})
ALV-519-4-1	0.0210	3540	0.34	0.17	1520	0.085	1440	0.084	14.35
ALV-906-R3	0.0160	3550	0.17	0.11	1520	0.125	1430	0.126	21.60
ALV-918-R1	0.0180	3545	0.29	0.17	1515	0.061	1450	0.054	8.73
ALV-923-R6	0.0155	3540	0.18	0.13	1525	0.039	1430	0.040	6.75
ALV-981-R23	0.0196	3535	0.26	0.14	1520	0.168	1435	0.160	28.68
TT152-21	0.0126	3535	0.44	0.37	1525	0.078	1440	0.075	12.23
TT152 29-1	0.0150	3525	0.29	0.21	1530	0.081	1445	0.082	13.76
TT152 37	0.0159	3550	0.36	0.24	1530	0.082	1430	0.081	12.42
TT152 43-19	0.0181	3545	0.28	0.16	1525	0.090	1440	0.092	14.94
KN54-2-2	0.0196	3530	0.66	0.37	1525	0.149	1430	0.134	22.12
RAMA 26-1	0.0151	3530	0.69[c]	1.31	1520	0.025	1430	0.026	2.65
TR123 4D-20	0.0185	3550	0.21	0.12	1535	0.053	1435	0.062	9.28
HU81-017 6-11	0.0145	3540	0.38	0.29	1515	0.037	1435	0.037	5.26
LOIHI BENTH-2[d]	0.0146	3530	0.88	0.64		e		e	e
K12-40	0.0117	3530	0.15	0.14	1515	0.061	1430	0.064	10.06
K1697	0.0109	3550	0.27	0.26	1520	0.021	1400	0.028	3.01

[a]Water analyses done using the method of Stolper (1982a) and a molar absorptivity of 60 liters/mole-cm for the infrared absorption band at 3550 cm^{-1}. Densities are given in Table 13.

[b]Total area under carbonate doublet.

[c]Sample thickness 0.0058 cm for H_2O measurement only.

[d]Two separate pieces run, results agree within 5%.

[e]Below detection limit.

Table 13- Major element analyses, densities, depths of eruption and dredge sites of natural basaltic glasses studied. Estimates of vesicle and phenocryst contents and the name of the donor of each sample are also included.

	ALV519 4-1	ALV906 R3	ALV918 R1	ALV923 R6	ALV981 R23	TT152 STA21-35	TT152 STA29-1	TT152 STA37	TT152 STA43-19	KN54- 2-2	RAMA 26-1	TR123 40-20	HU81-017 STA6-11	LOIHI BENTH-2	K12-40	K1697
Na_2O	2.13	2.91	2.61	2.26	3.05	2.63	2.58	2.79	2.35	3.45	3.15	2.42	2.69	2.45	2.15	2.23
MgO	10.15	8.15	8.04	8.29	8.52	7.11	7.25	6.32	8.01	7.78	7.73	9.25	6.39	6.65	8.79	6.80
Al_2O_3	16.44	15.56	15.13	15.64	16.92	13.71	14.39	13.72	15.10	17.05	17.05	18.11	13.40	13.74	15.51	13.60
SiO_2	49.07	49.83	50.38	50.34	49.70	50.92	49.91	50.98	50.46	52.14	50.06	46.78	51.19	47.95	49.29	52.60
K_2O	0.07	0.07	0.10	0.07	0.05	0.16	0.15	0.23	0.10	0.21	0.33	0.03	0.21	0.44	0.05	0.41
CaO	11.65	11.49	12.02	12.61	11.05	10.88	11.77	10.75	12.45	10.35	10.11	10.90	10.48	11.99	12.03	6.80
TiO_2	0.74	1.31	1.32	1.21	1.25	2.02	1.72	1.93	1.42	1.57	1.16	0.82	2.09	2.53	1.02	2.50
Cr_2O_3	0.03	0.10	—	—	0.07	—	—	—	—	—	0.07	0.07	—	0.13	—	—
MnO	0.16	0.14	0.16	0.18	0.15	0.19	0.18	0.18	0.16	—	0.17	0.08	0.22	0.33	0.19	—
FeO[a]	8.86	9.41	9.47	9.53	8.70	12.56	11.04	11.95	9.94	8.72	7.62	9.78	11.94	11.97	12.49	10.90
TOTAL	99.30	98.97	99.37	99.78	99.56	100.08	98.99	98.85	99.99	101.27	97.45	98.24	98.61	98.18	101.54	95.84
Source of Analysis:	b	c	d	d	c	e	e	e	e	f	c	c	e	g	h	i
Phenocrysts:[j]	m	s	m	s	s	m	m	m	n	s	s	p	m	m	m	p
Vesicles:[j]	m	m	s	n	s	s	s	p	s	s	n	m	m	m	m	s
Density (g/l):	2790	2830	2810	2770	2790	2840	2810	2820	2830	2760	2730	2870	2680	2850	2800	2810
Donated by:	W.B. Bryan	D. Muenow	S. Newman	S. Newman	H. Craig	J. Delaney	J. Delaney	J. Delaney	J. Delaney	W.B. Bryan	S. Newman	J.G. Schilling	J. Delaney	H. Craig	D. Muenow	D. Harris
Location:	Mid-Atlant. Ridge	East Pacific Rise	East Pacific Rise	East Pacific Rise	East Pacific Rise	Juan de Fuca Ridge	Juan de Fuca Ridge	Juan de Fuca Ridge	Juan de Fuca Ridge	Cayman Trough	Mariana Trench	Mid-Atlantic Ridge	Juan de Fuca Ridge	Loihi	Galapagos Spreading Center	Kilauea
Depth (m):	2710	2614	2635	2540	2600	2410-2520	2310 2360	2235-2240	2282	4795		1950	2600	1106-1130	2650	2960

[a] All Fe reported as FeO.
[b] Bryan and Moore (1977).
[c] This study. Microprobe conditions: 15 kV accelerating voltage; sample current: 5 nA on brass; 40-50 micron beam size.
[d] Newman et al. (1983).
[e] J.R. Delaney, pers. comm.
[f] W.B. Bryan, pers. comm.
[g] Hawkins and Melchior (1984).
[h] Byers et al. (1984).
[i] Harris (1981).
[j] n = none; m = minor (<1%); s = some (1% - 5%); p = prevalent (>5%).

generally poor in these constituents and no unusually high or low densities were recorded.

Results

Figures 26 and 27 show that carbon dioxide dissolved as carbonate can be readily detected in submarine basaltic glasses via infrared spectroscopy. By measuring the intensity of the carbonate band, the concentration of CO_2 dissolved as carbonate can be determined using Beer's law and the value of molar absorptivity derived in Chapter 3 (Figure 28). Carbonate concentrations (expressed as ppm CO_2 by weight) determined in this way for natural basaltic glasses are listed in Table 14; values based on the total area under the doublet as well as on the individual band intensities of the 1515 cm^{-1} and 1430 cm^{-1} bands are given along with the average of these three values. The intensity of the 1515 cm^{-1} band is the easiest to determine and is probably the most reliable of the individual values tabulated in Table 14. No absorption bands attributable to any other C-bearing species (e.g., molecular CO_2, CO, hydrocarbons) have been detected in natural basaltic glases; I conclude that the carbonate concentration corresponds to the <u>total</u> dissolved carbon content. Also tabulated are dissolved water contents based on the intensity of the 3550 cm^{-1} band (Table 12). No correlation is observed between the dissolved H_2O and CO_2 contents or between depth of magmatic eruption and total dissolved CO_2 content (Figures 29 and 30).

The infrared technique that has been developed contrasts in important ways from most of the other techniques in current use for the

Table 14- Total dissolved CO_2 concentrations (in ppm by weight) in natural basaltic glasses, based on the intensities of the infrared absorption bands at 1515 cm^{-1} and 1435 cm^{-1} and the integrated intensity under both bands. The means of these determinations are given and are also given as C concentrations (also in ppm by weight).

Sample	CO_2 1515 cm^{-1} (ppm)	CO_2 1435 cm^{-1} (ppm)	CO_2 area (ppm)	CO_2 avg. (ppm)	C avg. (ppm)
ALV-519-4-1	171	168	156	165	45
ALV-906-R3	325	326	304	318	87
ALV-918-R1	142	126	110	126	34
ALV-923-R6	108	109	100	106	29
ALV-981-R23	363	344	335	347	95
TT152 STA 21	257	246	218	240	65
TT152 STA 29-1	227	228	208	221	60
TT152 STA 37	216	212	177	202	55
TT152 STA 43-19	207	211	186	199	54
KN54-2-2	325	291	261	292	80
RAMA 26-1	72	74	41	62	17
TRI23 4D-20	118	137	111	122	33
HU81-017 STA 6-11	112	111	86	103	28
LOIHI BENTH-2	a	a	a	a	a
K12-40	220	229	196	215	59
K1697	81	108	63	84	23

[a]Below detection limit.

Figure 29- Dissolved CO_2 (ppm) versus dissolved H_2O (wt.%) for all natural basaltic glasses studied. Sample locations are labelled. Data are given in Tables 12 and 14.

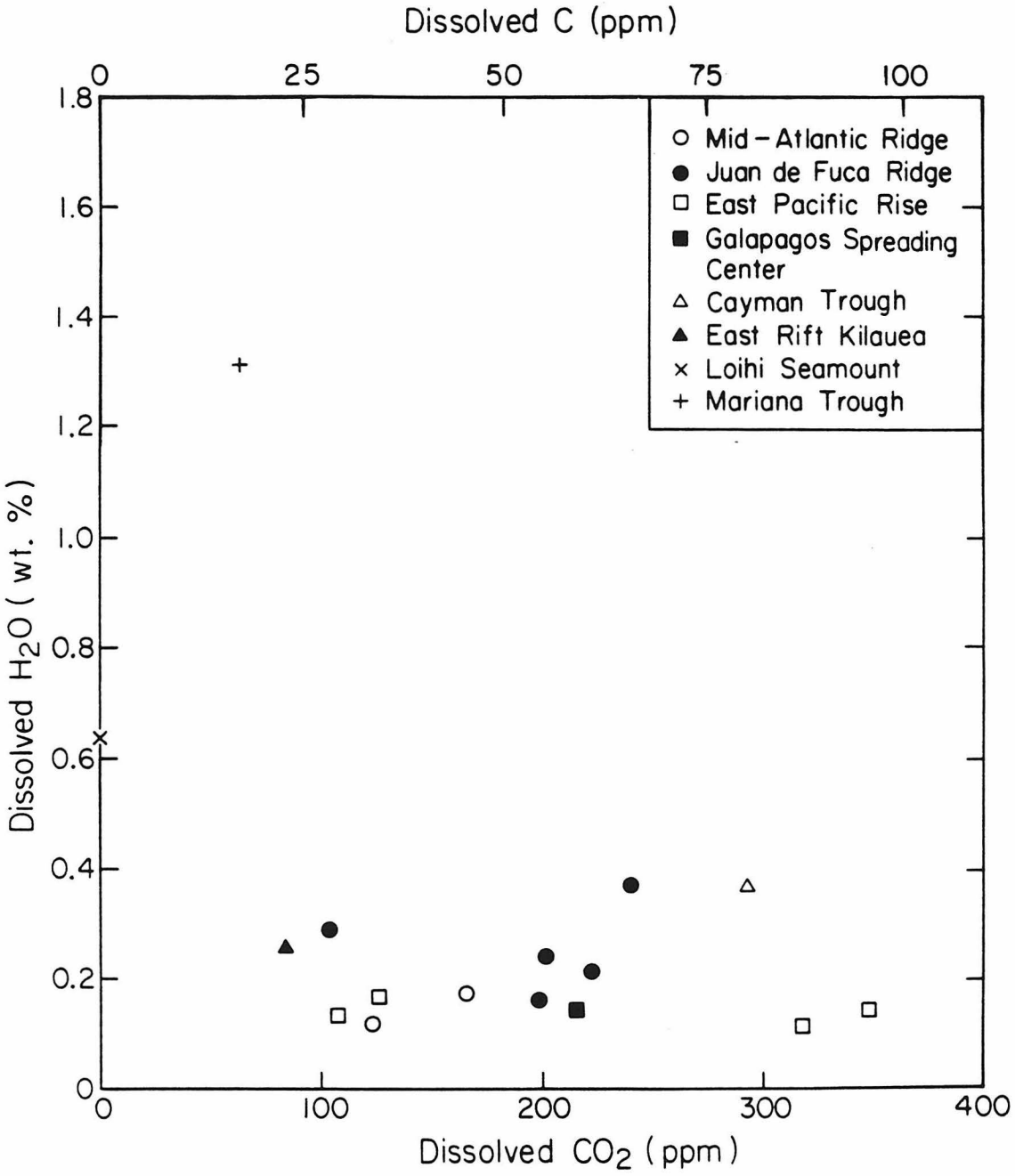
Dissolved C (ppm)
0
25
50
75
100
1.8
1.6
1.4
1.2
1.0
0.8
0.6
0.4
0.2
0
Dissolved H_2O (wt. %)
0
100
200
300
400
Dissolved CO_2 (ppm)
Mid – Atlantic Ridge
Juan de Fuca Ridge
East Pacific Rise
Galapagos Spreading Center
Cayman Trough
East Rift Kilauea
Loihi Seamount
Mariana Trough

Figure 30- Dissolved CO_2 (wt.%) versus depth of eruption (where available) for all the natural basaltic glasses studied. Error bars indicate uncertainties in eruption depth. Sample locations are labelled. Rama 26-1, KN54-2-2, and Loihi Benth-2 are not included.

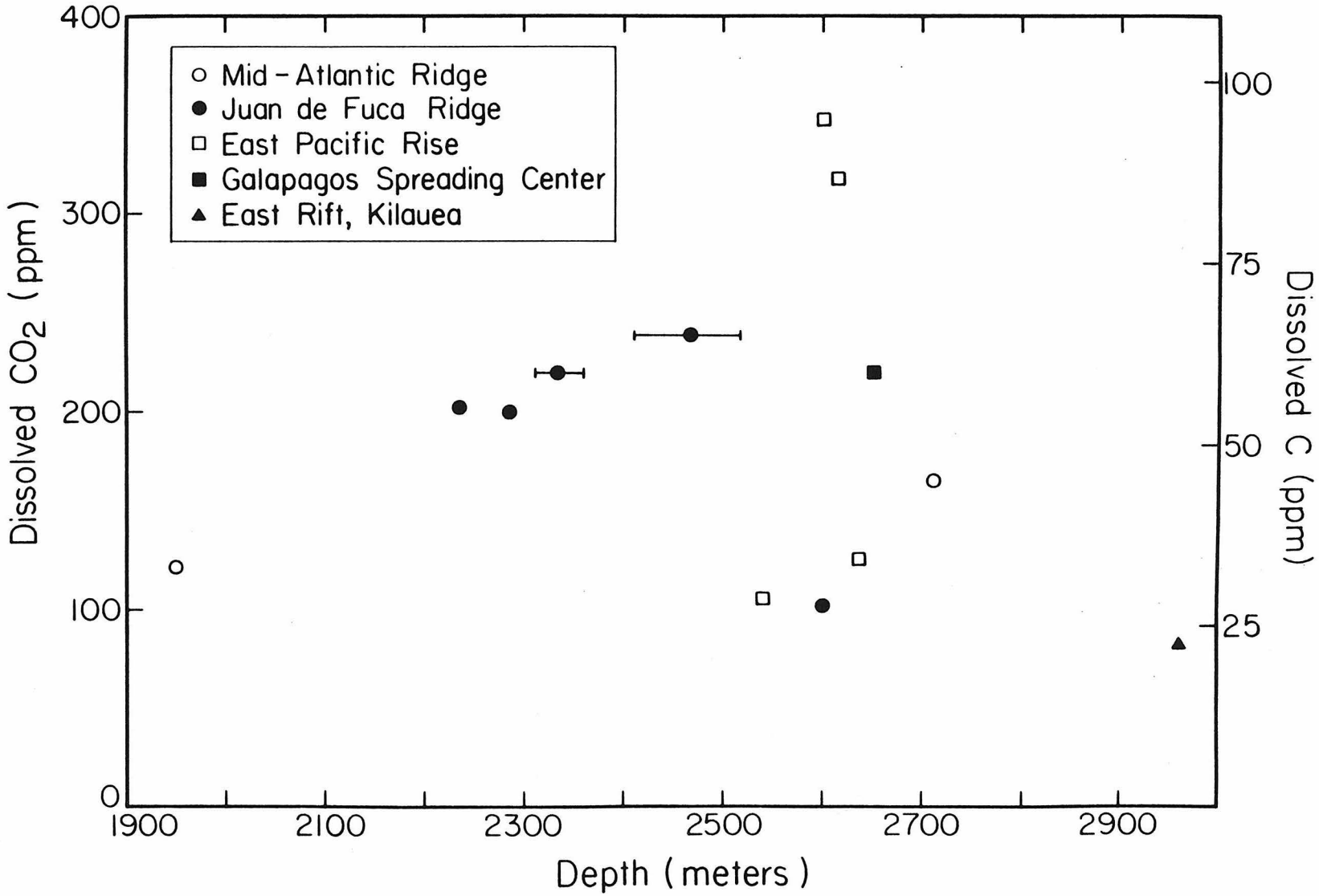
Mid - Atlantic Ridge
Juan de Fuca Ridge
East Pacific Rise
Galapagos Spreading Center
East Rift, Kilauea
Dissolved CO_2 (ppm)
Dissolved C (ppm)
Depth (meters)
400
300
200
100
0
100
75
50
25
1900
2100
2300
2500
2700
2900

measurement of carbon contents of glasses. First, it is species specific; it probes only for carbon dissolved in a particular form, in this case, carbonate. This species specific nature may not be advantageous if there are forms of dissolved carbon that are not detectable via infrared analysis (e.g., CO_4 groups). However, on balance, this is an advantage since it discriminates between dissolved and extraneous forms of carbon (e.g., CO_2-rich vesicles or crystalline carbonate alteration). Second, this technique has excellent spatial resolution. With modern instrumentation, "spot" sizes as small as a few tens of microns or better can be analyzed. This allows sample homogeneity to be examined and allows vesicle- and crystal-free regions of glass to be studied. Third, it minimizes contributions from surface contamination (Barker and Torkelson, 1975), since the samples are highly polished shortly before analysis and because it is likely that adsorbed carbon species would have a distinctive infrared signature. Finally, the technique is non-destructive. Consequently, the analyst is not concerned with total extraction as in most vaporization techniques and there is no danger of reaction among various species during analysis.

It is emphasized again that no molecular CO_2 was observed in any of the spectra of natural basaltic glasses. In general, analyses were performed on vesicle-free regions, but in some cases a few bubbles were in the light path. Even in these latter cases, no absorptions due to gaseous CO_2 were observed. Presumably the vesicles are CO_2-rich and the absence of a molecular CO_2 band in these cases probably reflects either the very low CO_2 content of a single bubble or the fact that vesicles more than several microns in size are not well sampled by the infrared

beam (e.g., the light may be diffracted around the vesicle). It is noted, however, that significant molecular CO_2 is not contained in submicroscopic vesicles or clusters of vesicles. If molecules of CO_2 were present in this form, they would have been readily detected by infrared spectroscopy, since CO_2 molecules absorb at wavelengths of light (4-5 μm) longer than the diameter of such vesicles or clusters.

The accuracy of the analyses is dependent on the calibration shown in Figure 28. The molar absorptivities are estimated to be accurate to better than ±15%; the availability of a wider range of standards might improve this. The precision (i.e., the reproducibility) of these analyses is on the order of < ±5-6% based on repeated analyses of selected specimens. However, there are discrepancies (Table 14) of up to ±15% between analyses of total CO_2 for each sample by the three different intensity measurements listed in Table 12. Below 100 ppm dissolved CO_2, these discrepancies can be as large as ±30%. This is a real limitation of this technique since the bands are very broad and become difficult to discriminate from the silicate background when they are less intense than ~0.04 absorbance units using the PE 180 spectrophotometer. This precision at low absorbances may be improved with further development of the FTIR.

Many analyses of CO_2 in ocean-floor basaltic glasses have been reported in the literature. A comparison between the analyses presented here and literature values for the same samples is shown in Table 15. Although it is not always clear, most previous authors have also tried to determine <u>dissolved</u> CO_2 contents; the analyses of dissolved CO_2 given here are always lower than the values in the literature and in some

Table 15- Comparison of CO_2 contents determined in this study with values determined in the literature. References are noted.

Sample	"Dissolved" CO_2 (ppm by weight) This study	Literature	Reference
ALV-519-4-1	165	447	Sakai et al., 1984
		230	Des Marais and Moore, 1984
ALV-981-R23	347	645	Pineau and Javoy, 1983
		436	D.J. Des Marais, pers. comm.
K1697	84	300	Harris, 1981
		310	Harris and Anderson, 1983
K12-40	215	1100	Byers et al., 1984

cases the deviations are substantial. For example, Pineau and Javoy (1983) report 645 ppm CO_2 as dissolved carbon in sample ALV-981-R23 as compared to 347 ± 52 (±15%) ppm CO_2 by this analysis. However, Pineau and Javoy's analysis includes the contents of vesicles under 10 microns in diameter, some alteration carbonate, and graphite, which may account for the differences between analyses. Likewise, Sakai et al. (1984) report 447 ppm CO_2 in ALV-519-4-1 as compared to 165 ± 25 ppm. Sakai et al.'s analysis is dependent on their estimation of the contribution of CO_2 filled vesicles to their analysis of CO_2. However, there is no simple explanation of the discrepancy between the value presented here and that of Des Marais and Moore (1984) for the same sample since they took great pains to eliminate CO_2 from surfaces and vesicles; do note, however, that they could not conclusively rule out a contribution from vesicles in their highest temperature combustion. Harris (1981) and Harris and Anderson (1983) use a vacuum fusion technique to arrive at an analysis of 300 ppm CO_2 for sample K1697. The analysis here yields 84 ± 25 ppm CO_2. This difference might again be attributed to vesiculation, as noted by Harris (1981). Although I again have no explanation, the results are also consistently lower than those given by either Byers et al. (1983, 1984) or Mattey et al. (1984) for comparable basaltic glasses (compare 1100 ppm CO_2 in K12-40 analyzed by Byers et al. (1984) with 215 ± 32 ppm in this study). While I can make no definitive assessment of all of the reasons for these possible discrepancies, it is again emphasized that the technique used here avoids CO_2 in vesicles and the problems of C contamination that have plagued previous studies. It is also true that for some problems total CO_2, including that in vesicles

and perhaps even on surfaces, may be more relevant (e.g., pre-eruptive C content); in these cases the analyses presented here may be of limited value since they only measure the dissolved carbonate content.

Despite the analyses of K1697 and ALV-519-4-1, the results are most consistently similar to those of Harris (1981), Harris and Anderson (1983) and Des Marais and Moore (1984). However, there is no evidence for the correlation between dissolved CO_2 content and depth of eruption that they proposed, and it is concluded that no such general relationship exists (Figure 30). In localized geographic regimes such as the Juan de Fuca Ridge (samples TT152-21, 29-1, -37, -43) there is a hint of such a relationship, but explanations other than the pressure dependence of solubility are easy to formulate. Given all of the factors contributing to the actual CO_2 content of submarine basalts [e.g., Moore, 1977; Moore et al., 1979; Des Marais and Moore, 1984), a simple relationship between depth of eruption (pressure of quenching) and CO_2 content would be surprising.

Conclusions

1. Based on the calibration of the infrared technique using synthetic samples containing known amounts of dissolved CO_2 presented in Chapter 3, submarine basalt glasses contain from 0-400 ppm dissolved CO_2, all as carbonate. No general correlation is observed between carbonate content and dissolved water content or depth of magmatic eruption.

Conclusions

The experiments presented in this study have not lead to a complete understanding of the solution mechanisms of CO_2 in silicate glasses; the individual conclusions summarized at the end of each chapter represent only an initial effort. Obviously, no one technique can yield all the necessary data. Infrared spectroscopy, as used in this study, is probably limited by an inability to distinguish subtle changes in the aluminosilicate framework of glasses that result from CO_2 dissolution.

Despite this, a number of fundamental conclusions have been reached via this study:

Infrared spectroscopy is a useful beam technique for studying the speciation and concentration of dissolved CO_2 in both synthetic and natural glasses. The infrared technique offers some advantages over other CO_2 analysis techniques, most importantly its species specific nature.

CO_2 dissolves as both molecular CO_2 and CO_3^{2-} in silicate glasses. The relative proportions of the two species vary significantly as a function of silicate composition; the most important compositional variables appear to be the concentration and valence state of the dominant cation in the glass. This influence can only be confirmed with more extensive work in simple synthetic systems (e.g., $NaAlSi_3O_8$-$CaAl_2Si_2O_8$-CO_2) and better knowledge of the structure of silicate glasses. In silicate glasses where both species are present, the relative proportions of molecular CO_2 and CO_3^{2-} also vary, though less significantly, with the pressure and temperature of melt equilibration and probably, at some high total dissolved CO_2 content, with total dissolved CO_2.

In addition, the solubility of CO_2 in molten albite as a function of pressure and temperature has been determined. The concentration and speciation of CO_2 in natural basalt glass has also been studied.

Carbon dioxide is clearly a major component of both volcanic gasses and many volcanic glasses and is apparently an important constituent of many basic and ultrabasic magma types. These observations have prompted extensive study of the effects of CO_2 on phase equilibria in an attempt to understand the effects of CO_2 on melt behavior. The results of these studies have been used to infer the structural changes that occur in melts as CO_2 is added and, ultimately, have been used to construct bulk thermodynamic models. This type of empirical treatment has given little insight into processes occurring on the molecular level.

Even if incomplete, the data presented in this thesis demonstrate the superior power of both infrared spectroscopy and the statistical thermodynamics approach for understanding solution mechanisms. The beginnings of a thermodynamic model of volatile solution are presented in this study; this model correctly accounts for some aspects of the behavior of CO_2-melt interaction (i.e., solubility relations, changes in CO_2 speciation as a function of silicate composition and the pressure and temperature of melt equilibration). The model takes into account observable processes occurring on the molecular level which the contrasting treatment can only infer. Little has been concluded in this dissertation regarding the reasons why CO_2 effects silicate phase equilibria. The data presented here should ultimately be an integral part of future efforts to understand the effects of CO_2 on natural systems.

Appendix 1. Measurement of the Carbon Content of Silicate Glasses Using the $^{12}C(d,p_0)^{13}C$ Nuclear Reaction

Beam techniques such as infrared spectroscopy have several advantages over bulk techniques for the analysis of C in geological materials. Beam techniques are non-destructive, the beam may be aimed at specific sites in the sample to avoid some of the contaminants that complicate the interpretation of bulk analytic techniques, and sample homogeneity may be checked. However, infrared spectroscopy may also fail to detect forms of dissolved carbon that are of interest. Electron microprobe techniques have also been used for the qualitative analysis of low level C in silicate glasses (Mathez and Delaney, 1984), but quantitative results are difficult to obtain for a variety of reasons, including the rapid attentuation of low energy X-rays and problems with surface contamination (Goldstein et al., 1976). More significantly, sample currents required for the analysis of C result in mobility of sodium in silicate glasses. Sodium is present in many geologically relevant glasses in relatively high concentrations. Since the mechanism of C dissolution in these glasses is apparently intimately associated with Na_2O (Chapter 1), electron microprobe techniques must be used with caution. Even if sodium mobility under the electron beam can be minimized, care must be taken to avoid mobilization of the carbon itself.

In this appendix, I describe the use of the $^{12}C(d,p_0)^{13}C$ nuclear reaction for the absolute measurement of dissolved C in a series of C-rich, synthetic silicate glasses. This beam technique avoids most of the problems encountered during analysis of low-level C contents by electron microprobe and by bulk analysis. It has been used previously for the analysis of C in metals (Cookson, 1979), lunar samples (Filleux

et al., 1979), minerals (Oberhauser et al., 1983; Mathez et al., 1984), and meteorites (Heymann et al., 1985). Here the usefulness of the nuclear technique is demonstrated by the measurement of the C content of a variety of the synthetic silicate glasses used in this study.

Experimental Procedure

The C analyses were performed using a collimated, 0.25 mm^2, 1.4 MeV deuteron beam from the Caltech EN tandem Van de Graaf accelerator and a 500 mm^2 silicon detector placed at an angle of 160° to the beam. Samples were doubly polished, mounted on tantalum holders with superglue, and coated with a ~50 Å gold or gold-palladium layer. During analysis, the samples were held under vacuum (10^{-7} torr) using silicone-based diffusion oil and were in close proximity to an LN_2 coldfinger. The glasses luminesced under deuteron bombardment, facilitating beam placement.

The principles of C analysis by nuclear reaction have been reviewed previously (Cookson, 1979; Filleux et al., 1979; Oberhauser et al., 1983; Mathez et al., 1984). Some features merit review. Deuterons impinging on the surface of the sample lose energy with increasing depth (x) as they penetrate the sample (Figure 31). At an energy ultimately determined by the cross-section of the $^{12}C(d,p_0)^{13}C$ reaction, the deuterons no longer react to produce ^{13}C. Similarly, protons emitted by the reaction lose energy as they leave the glass; their ultimate energy as seen by the detector is determined both by the energy of the reactive deuteron and the characteristic stopping power $((\frac{dE}{dx})_p)$ of the glass as expressed by:

Figure 31- Representation of the energetics of the nuclear reaction as deuterons impinge on the glass surface. $E_{d_0} > E_d$ and $E_{p_{max}} > E_p$. (After Filleux et. al., 1977)

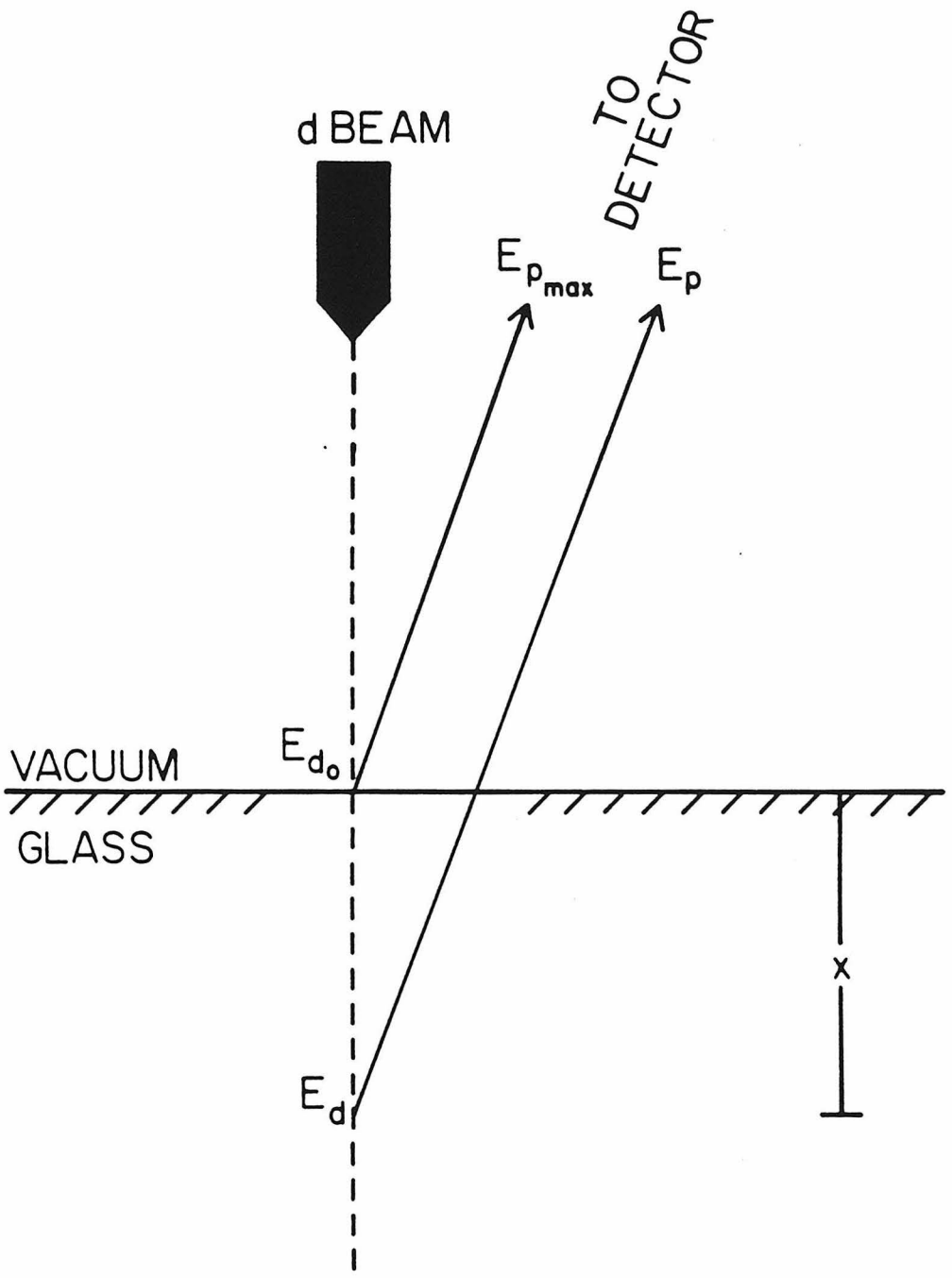
d BEAM
TO DETECTOR
$E_{p_{max}}$
E_p
VACUUM
GLASS
E_{d_o}
E_d
x

$$E_p = E_{p_{max}} + 0.6\ (E_d - E_{d_o}) + x \sec 20^0 \left(\frac{dE}{dx}\right)_p \qquad (11)$$

where $E_{p_{max}}$ is the maximum proton energy, E_{d_o} is the deuteron energy at the surface, E_d is the deuteron energy at depth x, and 20° = 180° - 160°, where 160° is the angle between incoming deuterons and outgoing protons. The highest energy deuterons (E_{d_o}) thus react at the surface of the glass (x=0); these reactions result in the highest energy protons ($E_{p_{max}}$) at the detector. As defined here, $\left(\frac{dE}{dx}\right)_p$ is negative. In principle, use of the relationship permits depth versus concentration profiling by monitoring the number of protons emitted from a sample as a function of proton energy. 1.4 MeV deuterons were chosen for their large cross-section, which allows us to reduce irradiation times to a mean of 10 minutes. This deuteron energy should also reduce the sensitivity of the method to surface contamination, but the spectra are clearly resolvable into a surface and volume component, shown schematically in Figure 32.

Each glass spectrum was fit as a linear combination of the spectrum of a blank glass of the same composition (or SiO_2 glass) and of calcite ($CaCO_3$) from the Hilton deposit, San Diego, Calif., weighted by $\left(\frac{dE}{dX}\right)_p$ (Anderson and Ziegler, 1977). This allowed calibration of the integrated intensity of the volume component versus C content. A spectrum of calcite was obtained after every 4 to 6 glass irradiations, to minimize errors due to variations in charge integration. The absolute accuracy of this method is estimated to be ±5% total C.

Figure 32- Idealized depiction of proton energy versus protons counted for a thin surface layer (dotted), a thick target (dashed), and a thick target with a thin surface contaminant layer (solid). (After Filleux et. al., 1977)

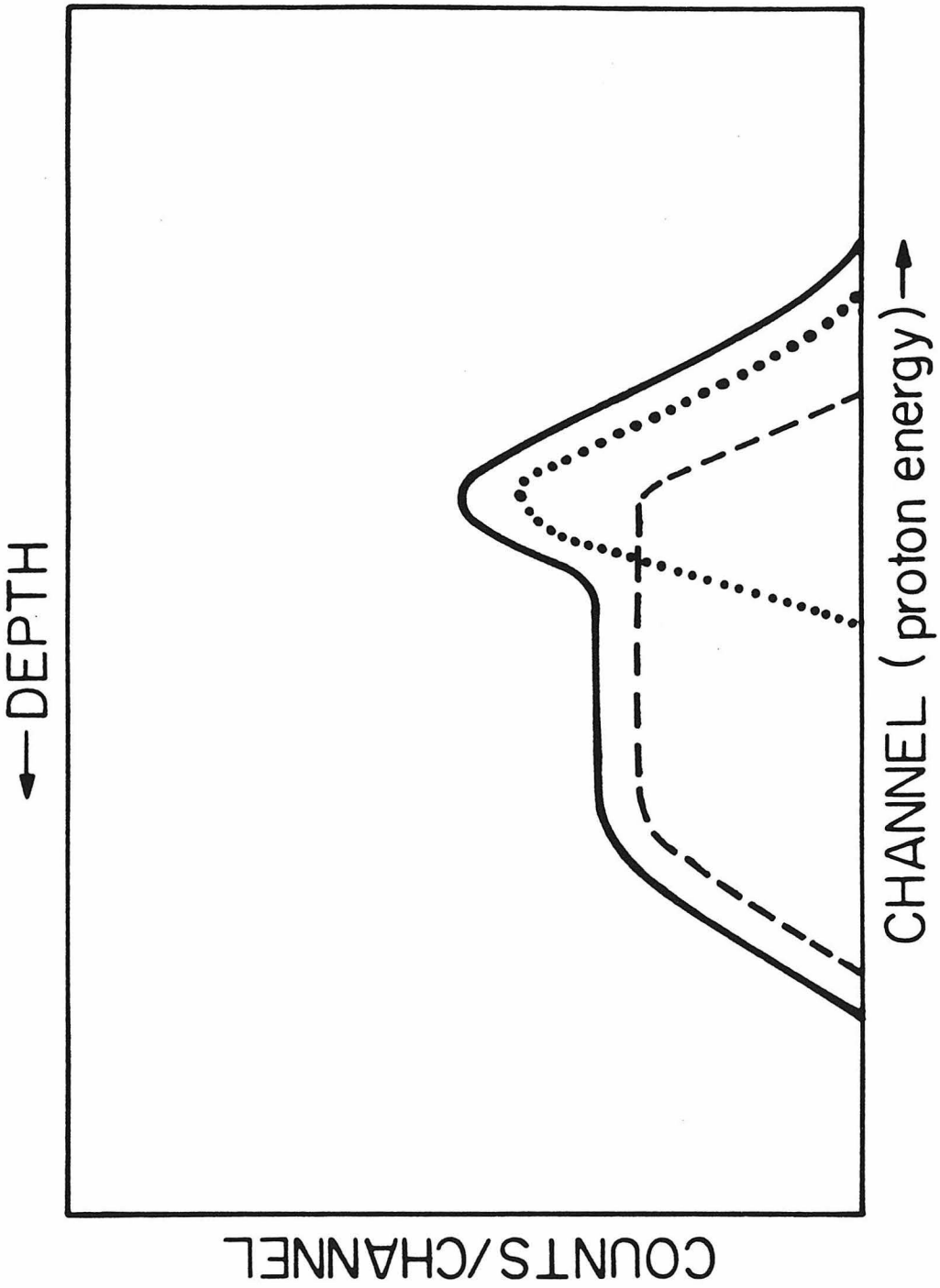
COUNTS/CHANNEL
CHANNEL (proton energy)→
←DEPTH

Results

Figure 33 shows the proton spectra for an $NaAlSi_3O_8$ glass containing 0.19 wt.% dissolved C. The peak due to the $^{12}C(d,p_0)^{13}C$ reaction is noted, as are peaks due to resonant O reactions and Rutherford backscattering edges from deuteron scattering on the Na, Al, and Si in the glass. The increase in intensity of the C peak with increasing dissolved C content is shown in Figure 34. Note that no surface component is visible in these spectra, which were obtained during 10 minute runs. During 30 minute irradiations, the surface component slightly increases in intensity with time due to deposition of C on the glass. No change is observed in the volume component, implying no significant loss of C from the samples and confirming the ability to distinguish between the surface and volume components. The fit of a spectrum of $NaAlSi_2O_8$ + CO_2 glass as a linear combination of the spectra of $CaCO_3$ and SiO_2 glass is shown in Figure 35.

Tables 2 and 11 list the C analysis of each glass (expressed as wt. % CO_2) accompanied by the amount of C originally loaded into each glass; the results are shown graphically in Figure 36. Considering both the ±10% uncertainty in loaded C content and the ±5% uncertainty in the C analyses, the amount of loaded C is adequately reproduced. Analyses of these glasses and natural basaltic glasses containing <300 ppm C tend to be inadequate; preliminary work with glasses containing C at less than these levels has yielded inconsistent results. Experience indicates that four factors are probably responsible: a) a surface C film on the samples was not adequately removed before analysis; b) these experiments were not performed under ultra-high (10^{-9} torr) vacuum conditions;

Figure 33- Spectrum of ABC-53. Resonant $^{16}O(d,p)$ reaction peaks and the deuteron Rutherford backscattering edges due to Na, Al, and Si are noted. Irradiation time is approximately 10 minutes.

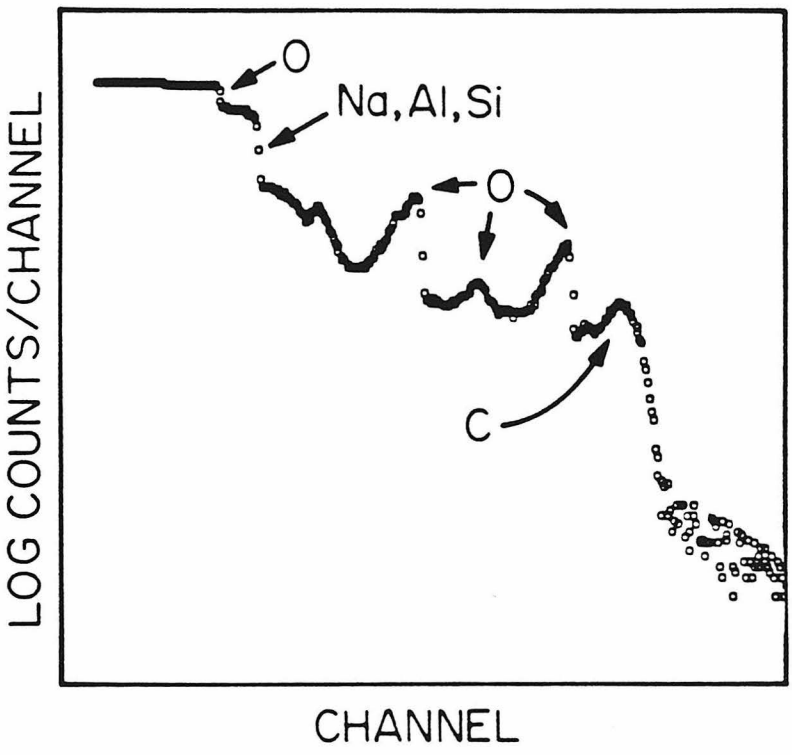
O
Na, Al, Si
O
C
LOG COUNTS/CHANNEL
CHANNEL

Figure 34- C reaction peaks for SiO_2 (Q), silicon (S), and $NaAlSi_2O_8$ glasses containing 0.085 (1), 0.049 (2), and 0.19 (3) wt.% dissolved C.

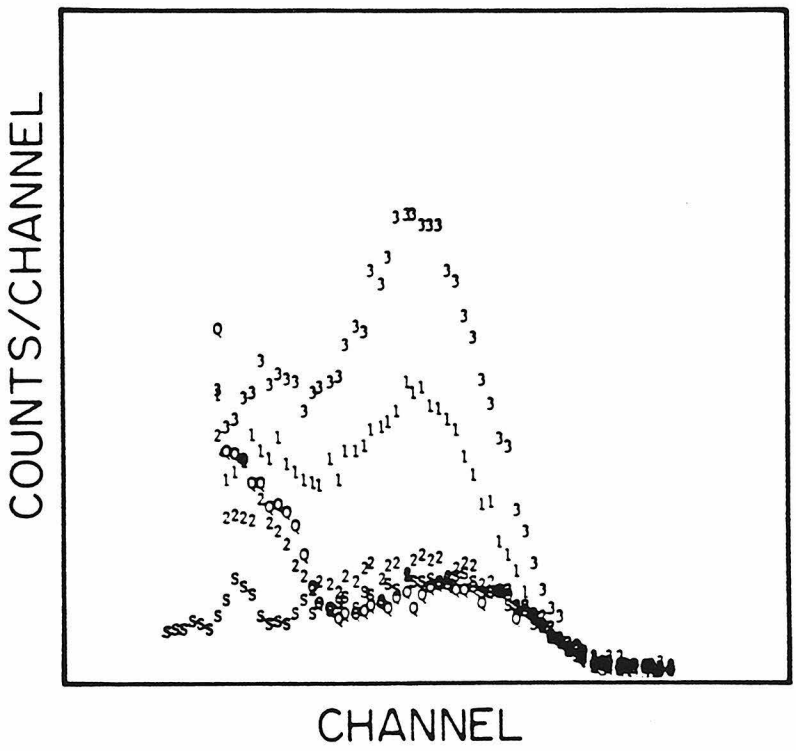
COUNTS/CHANNEL
CHANNEL

Figure 35- $NaAlSi_2O_8$ + CO_2 glass spectrum fitted as a linear combination of SiO_2 and $CaCO_3$ spectra.

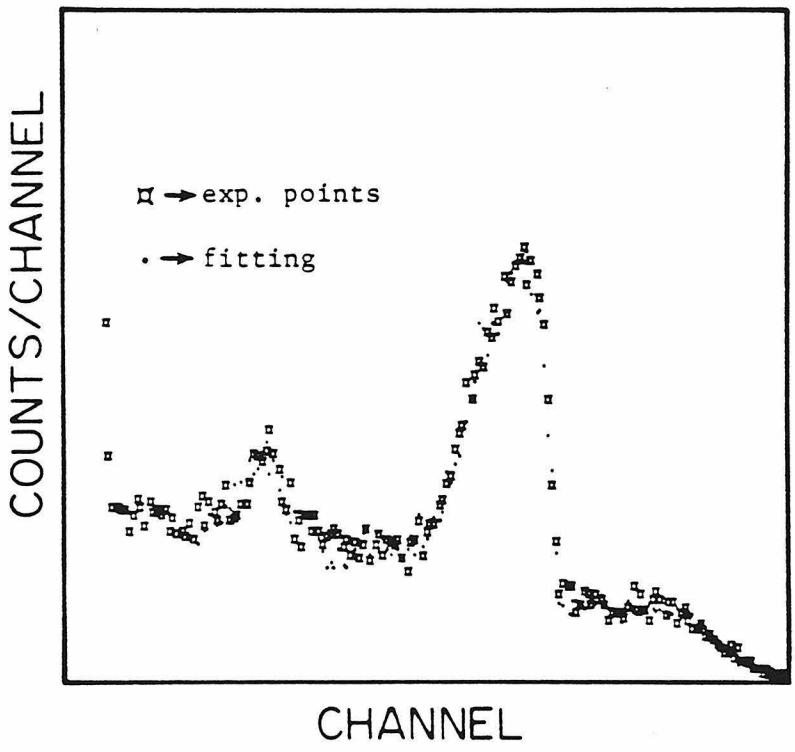
COUNTS/CHANNEL
exp. points
fitting
CHANNEL

Figure 36- Analyzed C versus loaded C for all glasses analyzed.

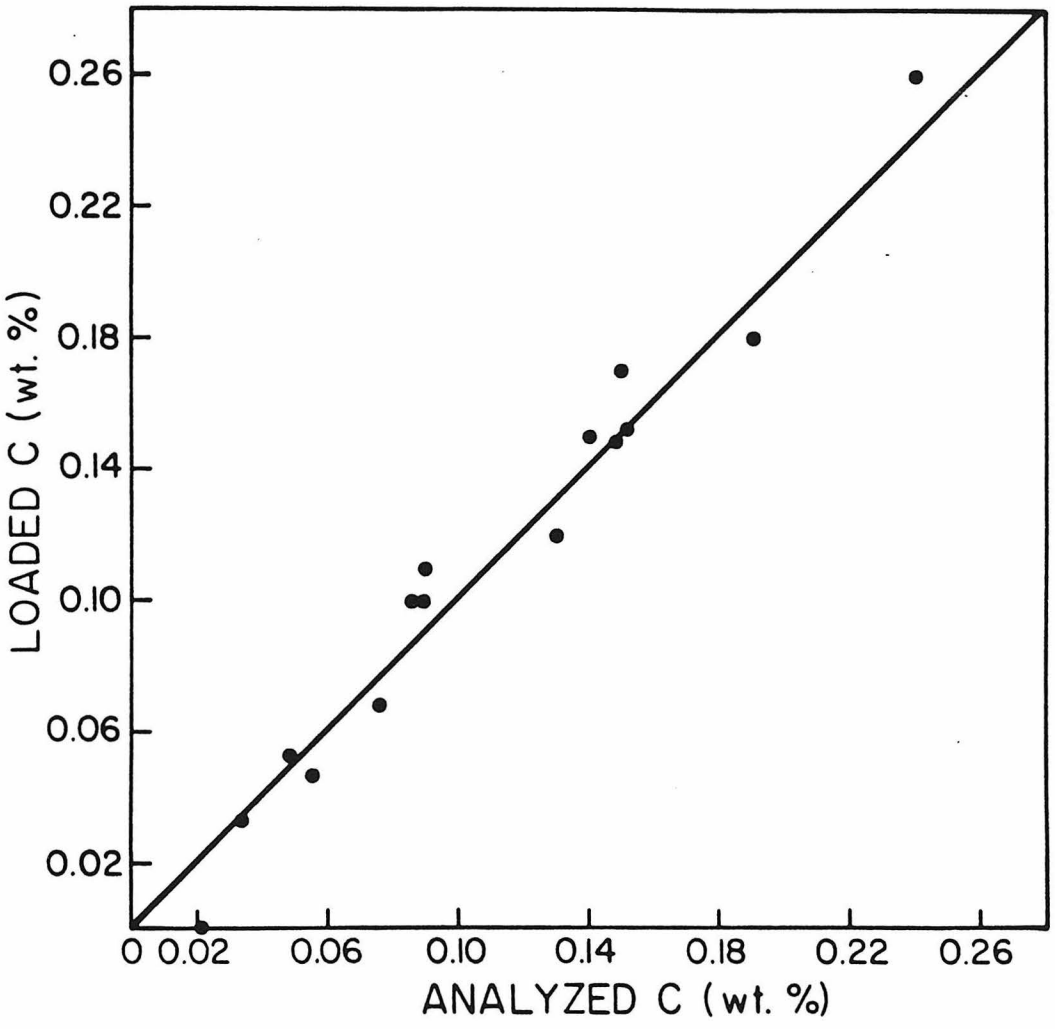
0.26
0.22
0.18
0.14
0.10
0.06
0.02
LOADED C (wt. %)
0 0.02
0.06
0.10
0.14
0.18
0.22
0.26
ANALYZED C (wt. %)

observable surface contaminant C becomes significant relative to dissolved C at low levels of dissolved C, making deconvolution of the volume component in Figure 34 quite difficult; c) the presence of contaminant C in microcracks in the glass generated during polishing cannot be ruled out; and d) run times (10 minutes) were not long enough. All four of these factors can be eliminated and it is clear that this method is a useful technique for low-level C analyses in natural glasses.

Conclusions

1. The $^{12}C(d,p_0)^{13}C$ nuclear reaction is a useful, non-destructive technique for the analysis of C in geologically relevant glasses. The method is unencumbered by many of the problems associated with other beam techniques, although more care in sample handling is necessary for adequate low-level (<300 ppm) C analyses. The use of a collimated 100 micron diameter beam is eventually possible, accompanied by run times of reasonable length.

References

Aines RD, Silver LA, Rossman GR, Stolper E, Holloway JR (1983) Direct observation of water speciation in rhyolite at temperatures up to 850°C. Geol Soc Am Abstr with Prog: 15, 512

Albarede F, Provost A (1977) Petrological and geochemical mass-balance equations: an algorithm for least-squares fitting and general error analysis. Comp Geosc. 3: 309-326

Anderson HH, Ziegler JF (1977) Hydrogen Stopping Powers and Ranges in All Elements. New York, Pergamon Press

Barker C, Torkelson BE (1975) Gas adsorption on crushed quartz and basalt. Geochim Cosmochim Acta 39: 212-218

Berner RA, Lasaga AC, Garrels RM (1983) The carbonate-silicate geochemical cycle and its effect on atmospheric carbon dioxide over the last 100 million years. Am J Sci 283: 641-683

Binsted N, Greaves GN, Henderson CMB (1984) An EXAFS study of glassy and crystalline phases of compositions $CaAl_2Si_2O_8$ (anorthite) and $CaMgSi_2O_6$ (diopside). Contrib Mineral Petrol 89: 103-109

Boettcher AL (1984) The system SiO_2-H_2O-CO_2: melting, solubility mechanisms of carbon, and liquid structure to high pressures. Am Mineral 69: 823-833

Boettcher AL, Windom KE, Bohlen SR, Luth RW (1981) Low-friction, anhydrous, low- to high-temperature furnace sample assembly for piston-cylinder apparatus. Rev Sci Instrum 52: 1903-1904

Boettcher AL, Burnham C. Wayne, Windom KE, Bohlen SR (1982) Liquids, glasses, and the melting of silicates to high pressures. J Geol 90: 127-138

Boettcher AL, Guo Q, Bohlen S, Hanson B (1984) Melting in feldspar-bearing systems to high pressures and the structures of aluminosilicate liquids. Geol 12: 202-204

Brey G (1976) CO_2 solubility and solubility mechanisms in silicate melts at high pressures. Contrib Mineral Petrol 57: 215-221

Brey G, Green DH (1975) The role of CO_2 in the genesis of olivine melilitite. Contrib Mineral Petrol 49: 93-103

Brey G, Green DH (1976) Solubility of CO_2 in olivine melilitite at high pressures and the role of CO_2 in the earth's upper mantle. Contrib Mineral Petrol 55: 217-230

Bryan WB, Moore JG (1977) Compositional variations of young basalts in the Mid-Atlantic Ridge rift valley near lat. 36°49'N. Geol Soc America Bull 88: 556-570

Byers CD, Muenow DW, Garcia MO (1983) Volatiles in basalts and andesites from the Galapagos Spreading Center, 85° to 86°W. Geochim Cosmochim Acta 47: 1551-1558

Byers CD, Christie DM, Muenow DW, Sinton JM (1984) Volatile contents and ferric-ferrous ratios of basalt, ferrobasalt, andesite, and rhyodacite glasses from the Galapagos 95.5°W propagating rift. Geochim Cosmochim Acta 48: 2239-2246

Byers CD, Garcia MO, Muenow DW (1985) Volatile in pillow rim glasses from Loihi and Kilauea volcanoes, Hawaii. Geochim Cosmochim Acta 49: 1887-1896

Chamberlain CP, Docka JA, Post JE, Burnham CW (1985) Scapolite: alkali atom configurations, antiphase domains, and compositional variations. Am Mineral 70: 134-140

Chapados C, Cabana A (1972) Infrared spectra and structures of solid CH_4 and CD_4 in phases I and II. Can J Chem 50: 3521-3533

Cookson JA (1979) The production and use of a nuclear microprobe of ions at MeV energies. Nuc Inst Meth 165: 477-508

Cooper JF, Dunning GE (1972) Melanophlogite from Mount Hamilton, Santa Clara County, California. Am Mineral 57: 1494-150

Delaney JR, Muenow DW, Graham DG (1978) Abundance and distribution of water, carbon and sulfur in the glassy rims of submarine pillow basalts. Geochim Cosmochim Acta 42: 581-594

Des Marais DJ, Moore JG (1984) Carbon and its isotopes in mid-oceanic basaltic glasses. Earth Planet Sci Lett 69: 43-57

Duyckaerts G (1959) The infrared analysis of solid substances - a review. Analyst 84: 201-214

Eggler DH (1973) Role of CO_2 in melting processes in the mantle. Carnegie Inst Washington Yearb 72: 457-467

Eggler DH (1974) Effect of CO_2 on the melting of peridotite. Carnegie Inst Washington Yearb 73: 215-224

Eggler DH (1978) The effect of CO_2 upon partial melting of peridotite in the system of Na_2O-CaO-Al_2O_3-MgO-SiO_2-CO_2 to 35 kb, with an analysis of melting in a peridotite-H_2O-CO_2 system. Am J Sci 278: 305-343

Eggler DH, Rosenhauer M (1978) Carbon dioxide in silicate melts: II. Solubilities of CO_2 and H_2O in $CaMgSi_2O_6$ (diopside) liquids and vapors at pressures to 40 kb. Am J Sci 278: 64-94

Eggler DH, Mysen BO, Hoering TC, Holloway JR (1979) The solubility of carbon monoxide in silicate melts at high pressures and its effect on silicate phase relations. Earth Planet Sci Lett 43: 321-330

Faile SP, Roy DM (1966) Solubilites of Ar, N_2, CO_2 and He in glasses at pressures to 10 kbars. J Am Ceramic Soc 49: 638-643

Filleux C, Tombrello TA, Burnett DS (1977) Direct measurement of surface carbon concentrations. Proc Lunar Sci Conf 8th: 3755-3772

Fine G, Stolper E (1985a) The speciation of carbon dioxide in sodium aluminosilicate glasses. Contrib Mineral Petrol 91: 105-121

Fine G, Stolper E (1985b) Carbon dioxide in basaltic glasses: Concentrations and speciation. Earth Planet Sci Lett (in press)

Fine G, Johnson T, Stolper E (1985a) The solubility of carbon dioxide in molten albite. Am Mineral (submitted)

Fine G, Stolper E, Mendenhall MH, Livi RP, Tombrello TA (1985b) Measurement of the carbon content of silicate glasses using the $^{12}C(d,p_0)^{13}C$ nuclear reaction. In: JT Armstrong (ed) Microbeam Analysis-1985. San Francisco Press: pp. 241-245

Flory PJ (1944) Thermodynamics of heterogeneous polymers and their solutions. Jour Chem Phys 12: 425-438

Flory PJ (1953) Principles of polymer chemistry. Cornell U Press

Gerlach TM, Graeber EJ (1985) Volatile budget of Kilauea volcano. Nature 313: 273-277

Goldstein JI (1976) Practical Scanning Electron Microscopy. New York, Plenum Press

Greenland LP, Rose WI, Stokes JB (1985) An estimate of gas emissions and magmatic gas content from Kilauea volcano. Geochim Cosmochim Acta 49: 125-130

Guggenheim EA (1952) Mixtures. Oxford U Press

Harris DM (1981) The concentration of CO_2 in submarine tholeiitic basalts. J Geol 89: 689-701

Harris DM, Anderson Jr. AT (1983) Concentrations, sources, and losses of H_2O, CO_2 and S in Kilauean basalt. Geochim Cosmochim Acta 47: 1139-1150

Hawkins J, Melchior J (1983) Petrology of basalts from Loihi Seamount, Hawaii. Earth Planet Sci Lett 66: 356-368.

Heymann D, Vis R, van der Stap C (1985) Carbon concentration mapping in a surface of the Allende meteorite. Abst. Lunar Sci. Conf. 16th: 348-349

Holland TB (1980) The reaction albite = jadeite + quartz determined experimentally in the range 600-1200°C. Am Mineral 65: 129-134

Holloway JR (1981) Volatile interactions in magmas. In: RC Newton, A Navrotsky, BJ Wood (eds) Thermodynamics of minerals and melts. Springer-Verlag, New York: 273-293

Holloway JR, Mysen BO, Eggler DH (1976) The solubility of CO_2 in liquids on the join $CaO-MgO-SiO_2-CO_2$. Carnegie Inst Washington Yearb 75: 626-630

Karsten JL, Holloway JR, Delaney JR (1982) Ion microprobe studies of water in silicate melts: Temperature dependent water diffusion in obsidian. Earth Planet Sci Lett 59: 420-428

Kushiro I (1975) On the nature of silicate melt and its significance in magma genesis: regularities in the shift of the liquidus boundaries involving olivine, pyroxene, and silica minerals. Am J Sci 275: 411-431

Kushiro I (1978) Viscosity and structural changes of albite ($NaAlSi_3O_8$) melt at high pressures. Earth Planet Sci Lett 41: 87-90

Lacy ED (1963) Aluminum in glasses and in melts. Phys Chem Glasses 4: 234-238

Livi RP, Mendenhall MH, Tombrello TA, Fine G, Stolper E (1984) High sensitivity carbon content analyses of geological materials using 1.4 MeV deuterons. Proc Int Symposium on Nuclear Accelerator Physics (Laboratori Nazional di Legarno, Italy)

Mathez EA (1984) Influence of degassing on oxidation states of basaltic magmas. Nature 310: 371-375

Mathez EA, Delaney JR (1981) The nature and distribution of carbon in submarine basalts and peridotite nodules. Earth Planet Sci Lett 56: 217-232

Mathez EA, Blacic JD, Berry J, Maggiore C, Hollander M (1984) Carbon abundances in mantle minerals determined by nuclear reaction analysis. Geophys Res Lett 11: 947-950

Mattey DP, Carr RH, Wright RP, Pillinger CT (1984) Carbon isotopes in submarine basalts. Earth Planet Sci Lett 70: 196-206

McKeown DA, Waychunas GA, Brown GE (1984) Na and Al environments in some minerals and a series of glasses within the Na_2O-Al_2O_3-SiO_2 system. Geol Soc Am Abstr with Prog 16: 589

Moore JG (1979) Vesicularity and CO_2 in mid-ocean ridge basalt. Nature 282: 250-253

Moore JG, Batchelder JN, Cunningham CG (1977) CO_2-filled vesicles in mid-ocean basalt. J Volcan Geotherm Res 2: 309-328

Mysen BO (1976) The role of volatiles in silicate melts: solubility of carbon dioxide and water in feldspar, pyroxene and feldspathoid melts to 30 kb and 1625°C. Am J Sci 276: 969-996

Mysen BO (1977) The solubility of H_2O and CO_2 under predicted magma genesis conditions and some petrological and geophysical implications. Rev Geophys Space Phys 15: 351-361

Mysen BO, Arculus RJ, Eggler DH (1975) Solubility of CO_2 in natural nephelinite, tholeite and andesite melts to 30 kb pressure. Contrib Mineral Petrol 53: 227-239

Mysen BO, Eggler DH, Seitz MG, Holloway JR (1976) Carbon dioxide in silicate melts and crystals: Part I. Solubility measurements. Am J Sci 276: 455-479

Mysen BO, Virgo D (1980a) Solubility mechanisms of carbon dioxide in silicate melts: A Raman spectroscopic study. Am Mineral 65: 885-899

Mysen BO, Virgo D (1980b) The solubility behavior of CO_2 in melts on the join $NaAlSi_3O_8$-$CaAl_2Si_2O_8$-CO_2 at high pressures and temperatures: A Raman spectroscopic study. Am Mineral 65: 1166-1175

Nakamoto K (1978) Infrared and Raman spectra of inorganic and coordination compounds, third edition. John Wiley and Sons, New York

Navrotsky A, Peraudeau G, McMillan P, Coutures JP (1982) A thermochemical study of glasses and crystals along the joins silica-calcium aluminate and silica-sodium aluminate. Geochim Cosmochim Acta 46: 2039-2047.

Newman S, Finkel RC, MacDougall JD (1983) ^{230}Th-^{238}U disequilibrium systematics in oceanic tholeiites from 21°N on the East Pacific Rise. Earth Planet Sci Lett 65: 17-33

Oberheuser G, Kathrein H, Demortier G, Gonska H, Freund F (1983) Carbon in olivine single crystals analyzed by the $^{12}C(d,p)^{13}C$ method and by photoelectron spectroscopy. Geochim Cosmochim Acta 47: 1117-1129

Okuno M, Marumo F (1982) The structures of albite and anorthite melts. Mineral Jour Japan 11: 180-196

Papike JJ, Stephenson NC (1966) The crystal structure of mizzonite, a calcium- and carbonate-rich scapolite. Am Mineral 51: 1014-1027

Pearce ML (1964) Solubility of carbon dioxide and variation of oxygen ion activity in soda-silica melts. J Am Ceramic Soc 47:342-347

Pineau F, Javoy M (1983) Carbon isotopes and concentrations in mid-oceanic ridge basalts. Earth Planet Sci Lett 62: 239-257

Rai CS, Sharma SK, Muenow DW, Matson DW, Byers CD (1983) Temperature dependence of CO_2 solubility in high pressure quenched glasses of diopside composition. Geochim Cosmochim Acta 47: 953-958

Russell JD (1974) Instrumentation and techniques. In: VC Farmer (ed) The infrared spectra of minerals. Mineral Soc London Mon 4: pp. 11-25

Sakai H, Des Marais DJ, Ueda A, Moore JG (1984) Concentrations and isotope ratios of carbon, nitrogen and sulfur in ocean-floor basalts. Geochim Cosmochim Acta 48: 2433-2442

Schilling JG, Bergeron MB, Evans R (1980) Halogens in the mantle beneath the North Atlantic. Phil Trans Royal Soc London Series A 297: 147-178

Seifert FA, Mysen BO, Virgo D (1981) Structural similarity of glasses and melts relevant to petrological processes. Geochim Cosmochim Acta 45: 1879-1884

Sharma SK (1979) Structure and solubility of carbon dioxide in silicate glasses of diopside and sodium melilite compositions at high pressures from Raman spectroscopic data. Carnegie Inst Washington Yearb 78: 532-537

Sharma SK, Hoering TC, Yoder HS (1979) Quenched melts of ackermanite composition with and without CO_2-- Characterization by Raman spectroscopy and gas chromotography. Carnegie Inst Washington Yearb 78: 537-542

Spera FJ, Bergman SC (1980) Carbon dioxide in igneous petrogenesis: I. Aspects of the dissolution of CO_2 in silicate liquids. Contrib Mineral Petrol 74: 55-66

Stolper E (1982a) Water in silicate glasses: An infrared spectroscopic study. Contrib Mineral Petrol 81: 1-17

Stolper E (1982b) The speciation of water in silicate melts. Geochim Cosmochim Acta 46: 2609-2620

Stolper E, Silver LA, Aines RD (1983) The effects of quenching rate and temperature on the speciation of water in silicate glasses. EOS, Trans Am Geophys Union 64: 339

Strnad Z (1971) Determination of the solubility of carbon dioxide at various partial pressures in soda-silica melts using gas chromatography. Phys Chem Glasses 12: 152-155

Taylor M, Brown GE, Jr, Fenn PM (1980) Structure of mineral glasses - III. $NaAlSi_3O_8$ supercooled liquid at 805°C and the effects of thermal history. Geochim Cosmochim Acta 44: 109-117

Tingle TN (1985) An evaluation of absolute carbon concentrations measured by the beta track technique. EOS Trans Am Geophys Union 66: 423

Tomlinson JW (1953) Some aspects of the constitution of liquid oxides. In: Physical chemistry of melts. London Inst Min Metall pp. 22-33

Toop GW, Samis CS (1962) Activities of ions in silicate melts. Trans Met Soc AIME 224: 878-887

Tuddenham WM, Lyon RJP (1960) Infrared techniques in the identification and measurement of minerals. Anal Chem 32: 1630-1634

Verweij H, Van den Boom H, Breemer RE (1977) Raman scattering of carbonate ions dissolved in potassium silicate glasses. J Am Ceram Soc 60: 529-534

Wagner C (1975) The concept of basicity of slags. Met Trans 6B: 405-409

Watson EB, Sneeringer MA, Ross A (1982) Diffusion of dissolved carbonate in magmas: Experimental results and applications. Earth Planet Sci Lett 61: 346-358

White WB (1974) The carbonate minerals. In: WC Farmer (ed) The infrared spectra of minerals. Mineral Soc London Mon 4: 227-284

Wong J, Angell CA (1976) Glass structure by spectroscopy. Marcel Dekker, Inc.

Wyllie PJ (1979) Magmas and volatile components. Am Mineral 64: 469-500.